Final Report

MASH TL3 Evaluation of the CRTS Barrier

Prepared for: **Barrier Systems, Inc.**

Owner: **Lindsay Corporation**

Prepared by: **Chuck A. Plaxico**

ROADSAFE LLC
P.O. BOX 312
CANTON, ME 04221

April 25, 2016

TABLE OF CONTENTS

LIST OF FIGURES

LIST OF TABLES

LIST OF APPENDICES

INTRODUCTION

The Concrete Reaction Tension System (CRTS) Quickchange Moveable Barrier (QMB) is a longitudinal barrier composed of 3.28-ft (1 m) long concrete segments linked by pin-and-hinge connections to form a free-standing barrier installation. The barrier is designed to be moved laterally from one traffic lane to another with a special purpose barrier transfer machine that is capable of transferring the barrier while under tension. This system has been deployed both nationally and internationally since 2000. To facilitate the transfer process, a special element called a variable length barrier (VLB) is intermittently included along the length of the barrier. The VLB is equipped with a hydraulic cylinder that allows it to passively change length to accommodate lateral transfer of the barrier from lane to lane. Under high-speed loading, such as in vehicular impact, the hydraulic cylinder will "lock" preventing extension of the VLB. These VLB elements are only used as needed, for example in curves, and are typically spaced at distances of 56.8 ft (17 m) or greater.

The system was initially tested to National Cooperative Highway Research Program (NCHRP) Report 350 for Test Level 3 (TL3) and received eligibility for use on Federal-Aid projects on June 27, 2000 (see FHWA Letter HSA-B69).[Ross93; *FHWA00*] The system was also successfully tested according to the test procedures and criteria specified in the American Association of State Highway and Transportation Officials (AASHTO) *Manual for Assessing Safety Hardware* (*MASH*) for Test Level 3 (TL3) conditions.[*AASHTO09*; *Alberson16*] The MASH tested system included two VLB elements: one VLB was positioned at 1.5 m downstream from the impact point and a second VLB was positioned 56.8 ft (17 m) further downstream.

Although the system meets the current crash testing standards, its performance at impact locations other than those tested is unknown. Like other free-standing concrete barriers (e.g., portable concrete barriers), the ends of the CRTS system are not restrained; therefore, the tension in the system during an impact arises due to the inertia of system elements upstream and downstream of the impact location. As the impact point gets closer and closer to either end of the system, there are fewer system elements to provide tension. The purpose of this study is to use finite element analysis (FEA) to further evaluate the crash performance of the barrier as a function of impact point, relative to both the leading and trailing ends of the barrier.

OBJECTIVE

One objective of this study was to define the critical length of the system required to achieve minimum barrier deflection when the system is impacted at its midpoint under MASH Test 3-11 conditions (i.e., 5,000-lb pickup impacting at 60 mph and 25 degrees). In other words, to determine how long the system needs to be, such that any further increase in length will not result in a further reduction of system deflection (i.e., length where maximum lateral deflection becomes constant). The second objective was to evaluate the crash performance of a critical-length system as a function of impact location relative to the leading and trailing ends of the system, based on MASH Test 3-11 impact conditions and criteria.

The scope included (1) developing finite element analysis (FEA) models of the CRTS, (2) validating the model based on comparison with a full-scale crash test performed under

MASH Test 3-11 conditions, (3) using the validated FEA model to evaluate crash performance of the CRTS versus impact location on the system. In particular, the evaluation was concerned with barrier performance as the impact location on the barrier gets nearer to the leading and the trailing ends of the system. In addition to impact performance, the maximum lateral deflection of the barrier was also of interest since it is used in determining *working width*, which is a metric used by roadside safety engineers to determine applicability and placement of safety hardware for given site conditions.

APPROACH

A finite element model of the CRTS barrier system was developed and validated through comparison with results from full-scale crash test No. 690900-LTS2 using the procedures outlined in NCHRP Web-Document 179. All analyses were conducted using the non-linear, explicit finite element code, LS-DYNA version MPP_s_R8.0.0 Revision 95309. The validated model was then used to evaluate the performance of the system for impacts at several locations approaching the leading and trailing ends of the barrier, including impact at barrier segments 18, 28, 38, 58 and 85 from the leading end; and for impact at barrier segments 18, 28, 38, and 58 from the trailing end. Two barrier system cases were evaluated:

- Case 1 – 170 CRTS barrier segments with no VLB elements included in the barrier system.
- Case 2 – 168 CRTS barrier segments and two (2) VLB elements, consistent with the crash tested system. One VLB was positioned at 1.5 m downstream of the impact point and a second VLB was positioned at 17 m further downstream.

The results of the analyses were evaluated to assess structural capacity, occupant risk and vehicle stability according to criteria specified in MASH. The occupant risk metrics were computed from acceleration data and angular rate data collected at the center of gravity of the vehicle.

FE MODEL DEVELOPMENT OF THE CRTS AND 18" VLB

The finite element model of the CRTS system was developed based on the construction drawings provided in Appendices A and B. A 557.8 feet (170 m) section of the barrier was developed for use in the study (consistent with full-scale crash test 690900-LTS2). The model included a total of 170 barrier segments, including 168 CRTS segments and two 18-inch VLB segments. The degree of material and geometric fidelity included for each individual segment was dependent upon its location relative to the impact point. It was determined from test 690900-LTS2 that the MASH test vehicle interacted with at least ten (10) barrier units during the impact event, including one VLB unit. Those barrier units located within the impact zone were modeled with higher fidelity (e.g., deformable concrete). The barrier units located outside the impact zone were modeled with rigid concrete properties; however, all pin-hook connections were modeled as deformable throughout the system. Figure 1 shows the overall model of the CRTS. Additional model details are provided in the following sections of this chapter.

CRTS Model

Three different models of CRTS barrier segments were developed:

- **CRTS-Detailed**: This model includes the highest fidelity for both geometric and material properties and thus requires the highest demand on computational resources. The model includes detailed concrete properties and explicit modeling of steel reinforcing bars.

- **CRTS-Reduced**: This model uses rigid concrete properties for most of the barrier segment, with deformable concrete properties on the ends of the segments; no steel reinforcing is included. This model requires relatively low computational resources and from preliminary work (not shown here) was found to provide results similar to the detailed model. As such, this model was selected for use in the impact zone for assessment of barrier performance.
- **CRTS-Rigid**: This model uses rigid properties for all concrete in the segment as well as for the section of the pin-bar embedded within the concrete. This model requires the least computational resources and was used for barrier segments outside the impact zone.

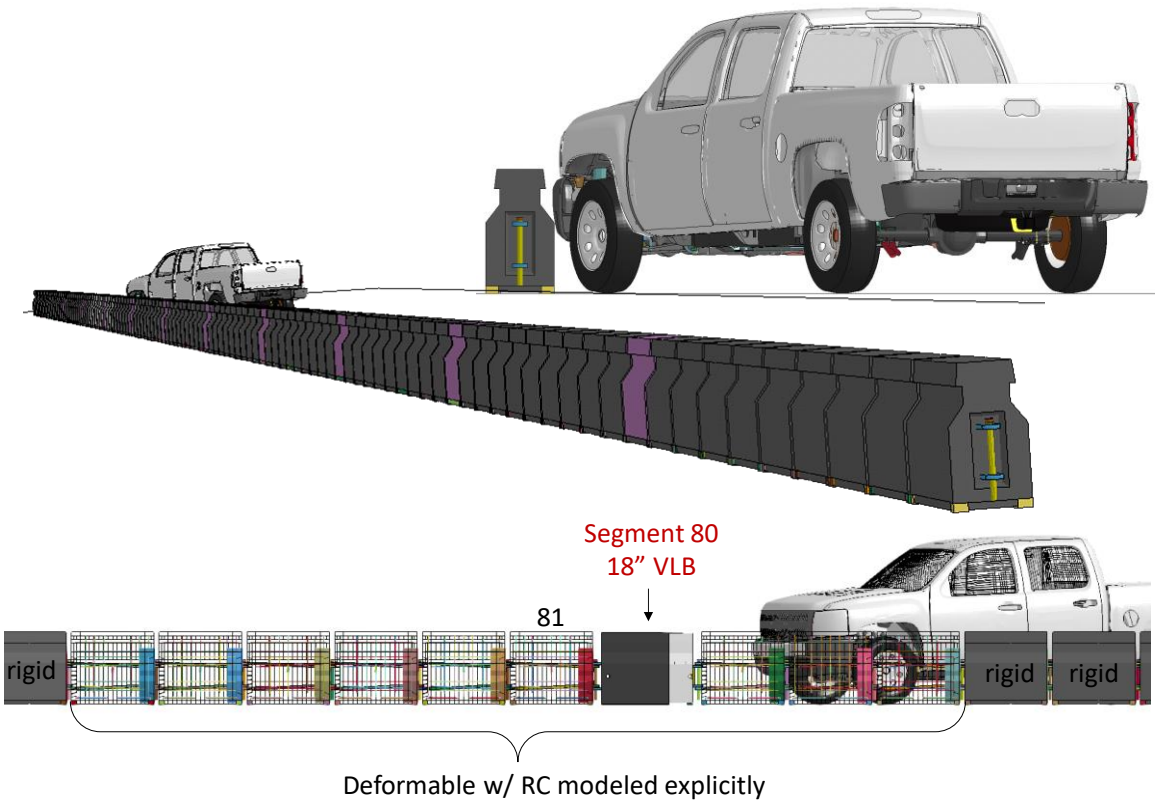

Figure 1. Finite element model of the 170-segment CRTS barrier system.

CRTS-Detailed Model

The finite element model of the CRTS-Detailed model is shown in Figure 2 including an image with the concrete viewed in transparency mode to facilitate showing the steel reinforcing and the through-bar pin hooks inside the barrier segment. The overall height of the CRTS model is 32 inches excluding the rubber feet; the rubber feet add an additional 3/8 inch to the height of the barrier. The following sections describe the FE mesh, element formulation and constitutive model used for each component of the CRTS-Detailed model. The geometric dimensions are consistent with the detailed drawings shown in Appendix A.

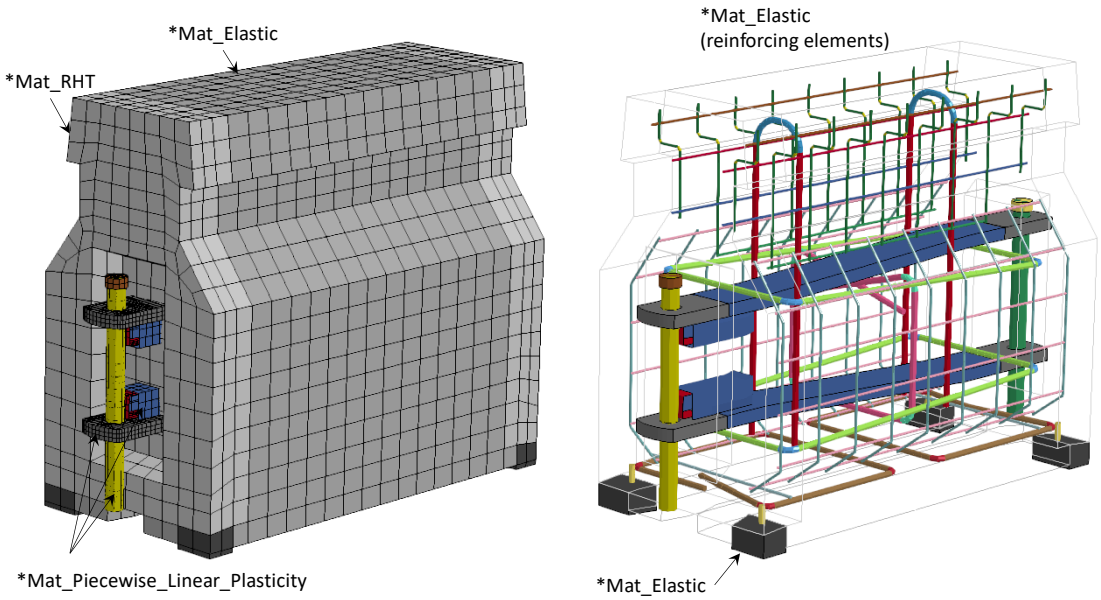

Figure 2. FE mesh of CRTS-Detailed model.

Concrete

The concrete was modeled with Type 1 brick elements in LS-DYNA. The nominal size of the elements was 1.5" x 1.5" x 2" with the smallest element side length equal to 1 inch. The ends of the barrier segment were expected to experience high forces as the barrier segments hinge and press against each other during impact. The constitutive properties of the concrete in this section of the barrier segment were modeled using *Mat_RHT in LS-DYNA, with default material properties based on an unconfined compressive strength of 4,000 psi. This model was selected based on the results of a recent study performed by the research team in which the material model was validated against pendulum impact tests on reinforced concrete columns where the columns were subjected to lateral impact forces.[*Ray16*]

Steel Reinforcing

All reinforcing bars were modeled with Type 1 beam elements with a nominal element length of 1 inch, except in the curved sections where a nominal element length of ½ inch was used. The material properties for the reinforcing steel was modeled using *Mat_Elastic in LS-DYNA with Young's modulus of 29,000 ksi and Poison's ratio of 0.3. The geometric dimensions of the steel reinforcing and its positioning within the concrete model was consistent with the detailed drawings shown in Appendix A. The welds for the steel reinforcing were simulated by merging nodes between the adjoining parts.

The *Constrained_Beam_in_Solid option in LS-DYNA was used to model the constraint of the steel reinforcement to the concrete. This method does not allow for slipping of the steel within the concrete; however, the damage to the concrete segments is expected to be negligible in these areas of the model (based on post-test photos of CRTS segments).

Hinge Bar

The model for the hinge bar is shown in Figure 3. The material was modeled with properties of A36 steel using the *Mat_Piecewise_Linear_Plasticity (*Mat_24) option in LS-

DYNA. The bar is 43-3/8 inches long and 1 inch thick. It was meshed using Type 1 solid elements in LS-DYNA with nominal size 1/3" x 1/3" x 1.0" for the section of the bar within the concrete, and nominal size 1/3" x 1/3" x 1/3" at the ends of the bar (e.g., hinge location). This resulted in three elements through the thickness of the bar. The resulting element time step was 1.039×10^{-6} seconds. The smallest element side-length was 0.25 inches (7.05 mm), located around the pin-hole surface, with a resulting minimum time-step of 6.77×10^{-7}. The analysis time-step will be set to 1 microsecond, which will result in 0.538 lbs added to each end of the bar at the pin hole and is considered acceptable for the analysis.

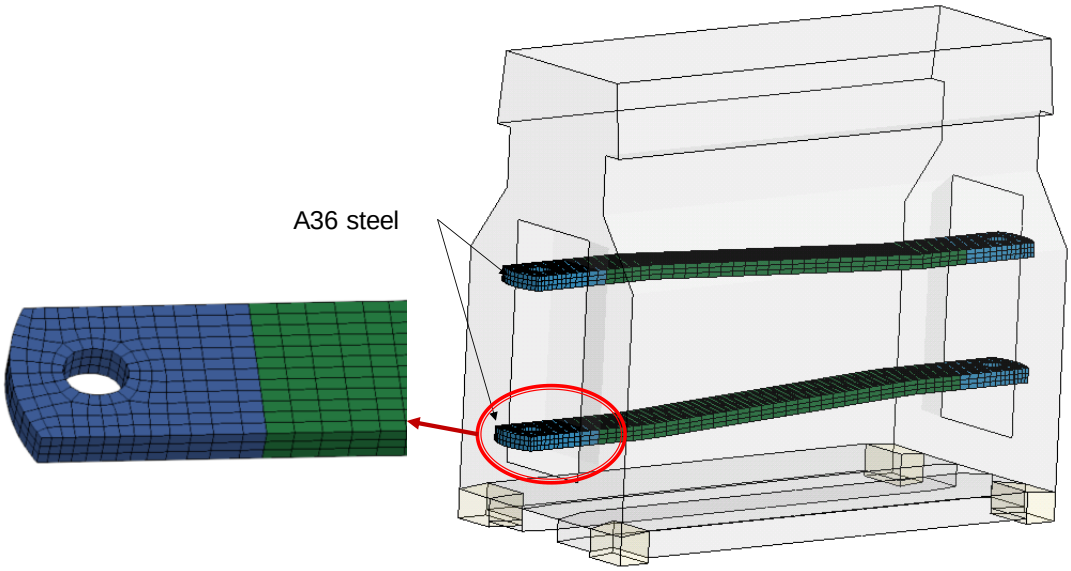

Figure 3. Model of the CRTS hinge bar.

RTS Spring, Push-Plate and Housing

The Reaction Tension Spring (RTS) housing was modeled using Type 2 thin shell elements in LS-DYNA with nominal element side length of 0.7 inches, and the push plate was modeled with nominal element size of 0.37" x 0.43" (Figure 4). The thickness for both parts was ¼ inch. The material was modeled with properties of A36 steel using the *Mat_24 option in LS-DYNA. The welded connection between the spring housing and the hinge bar was modeled using merged nodes. The RTS spring was modeled as a Linear_Elastic_Discrete_Beam in LS-DYNA with translational stiffness equal to 576 lb/in with a preload of 648 lb corresponding to a pre-compressed displacement of 1.125 inches. The ends of the spring element were connected to the back of the spring housing and the front of the push-plate using the *Constrained_Nodal_Rigid_Body (NRB) option in LS-DYNA. The sliding contact of the push-plate inside the spring housing was modeled using the *contact_automatic_single_surface option in LS-DYNA with *soft* = 2 and *depth* = 5.

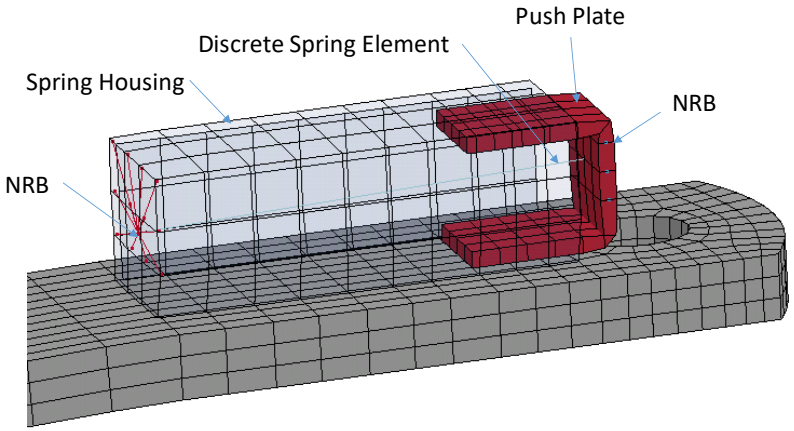

Figure 4. RTS model

Pin

The pin was modeled using Type 1 beam elements in LS-DYNA with nominal length of 0.5 inches and diameter equal to 1-3/8 inches (Figure 5). The overall length of the pin was 18-5/8 inches. The material was modeled with properties of 4140 QT steel using the *Mat_24 option in LS-DYNA. The yield strength of pin material is 138 ksi, corresponding to oil-quench and temper at 1390˚F. The true stress vs true strain curve used for the analysis is shown in Figure 6.

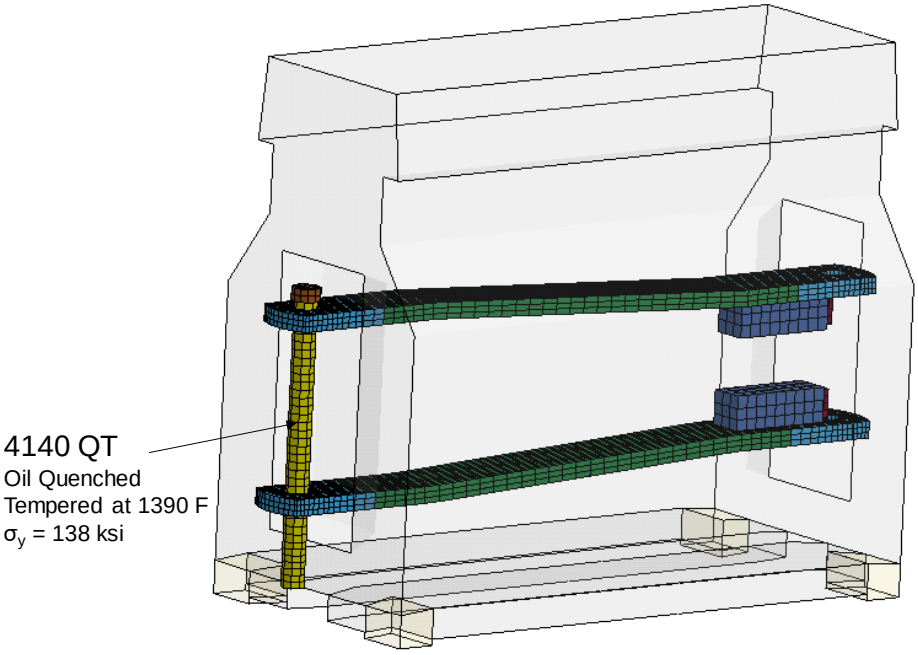

Figure 5. Model for Pin

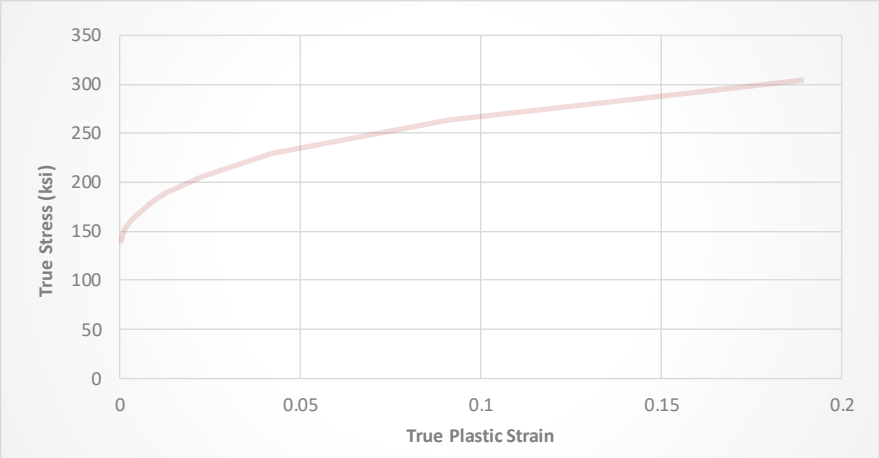

Figure 6. True-stress vs true-plastic-strain for 4140QT steel pin.

Feet

The model of the barrier feet is shown Figure 7. The feet are composed of compound NR-60A-2184 with Durometer = 60A (similar to car tire tread hardness). The exact properties of the feet material are uncertain; however, they are assumed to behave elastically with modulus equal to 145 psi (1000 MPa) and Poison's ratio equal to 0.4. The dynamic friction between the feet and ground pavement was measured by STI to be approximately 0.52 for "fast actuation rates" of the load apparatus[1]. The contact between the feet and the ground was modeled using the *Contact_Automatic_Nodes_to_Surface option in LS-DYNA with static friction set to 0.8, dynamic friction set to 0.52, and decay constant to 0.001 s/mm.

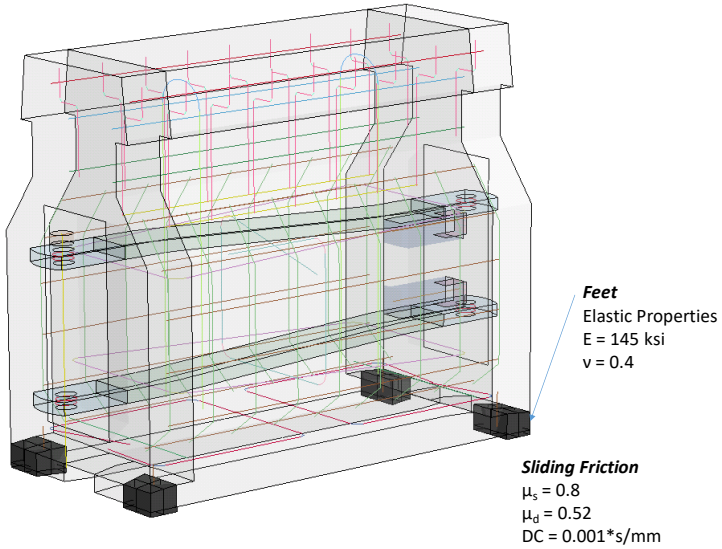

Figure 7. CRTS barrier feet.

[1] Test Number 1351 performed by STI on 7/17/2015.

Part Contact

Three separate contact definitions were included in the model for defining the interaction between adjacent CRTS segments:

1. *Contact_Automatic_Single_Surface: This contact definition includes all concrete and models the interaction between contacting barrier segments during impact. The contact definition also includes parameters: *soft* = 2 and *depth* = 5.
2. *Contact_Automatic_General: This contact definition includes the beam elements of the pin, the null beam element of the hinge bar holes and the null beam elements of the push plate of the RTS spring, as illustrated in Figure 8. The contact definition also includes *soft* = 1. Null beam elements were added to the edges of the solid elements forming the hole in the hinge bar, and also to the edges of the shell elements forming the front face of the RTS push plate in order to improve contact calculations and stability between these components.

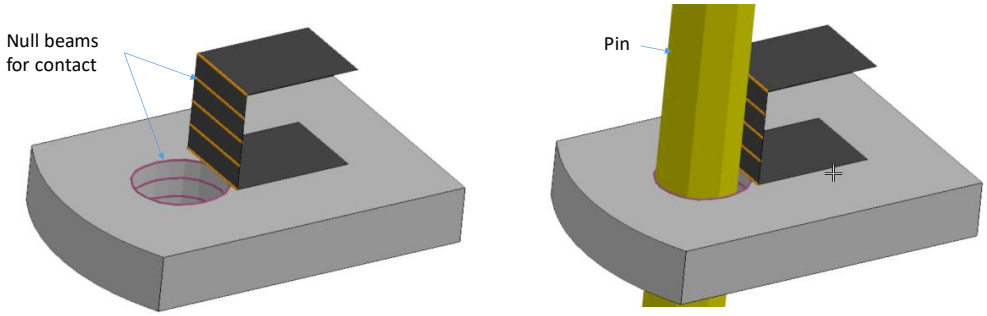

Figure 8. Contact between the pin and the null beams of the hinge bar and push plate.

3. *Contact_Automatic_Single_Surface: This contact definition includes the RTS spring housing and the push plate, as well as the pin head and the external portions of the hinge bar. The contact definition also includes parameters: *soft* = 2 and *depth* = 5 to better capture the shell edge to surface contact between the RTS housing and push plate.

CRTS-Reduced Model

The finite element model of the CRTS-Reduced model is shown in Figure 9 (concrete viewed in transparency mode). The middle portion of the concrete and the interior section of the hinge bar (i.e., green shaded region in Figure 9) are modeled as rigid. The concrete on the ends of the barrier segment is modeled as deformable using *Mat_RHT with the same properties as defined in the CRTS-Detailed model. The remaining components are also modeled as deformable, consistent with the detailed model; however, the steel reinforcing is excluded. This model requires considerably less computational resources than the detailed model and was shown to provide sufficiently accurate response of the barrier when compared to the full-scale test (see section Model Validation); thus, the CRTS-Reduced model was used in place of the detailed model in this study for computational efficiency.

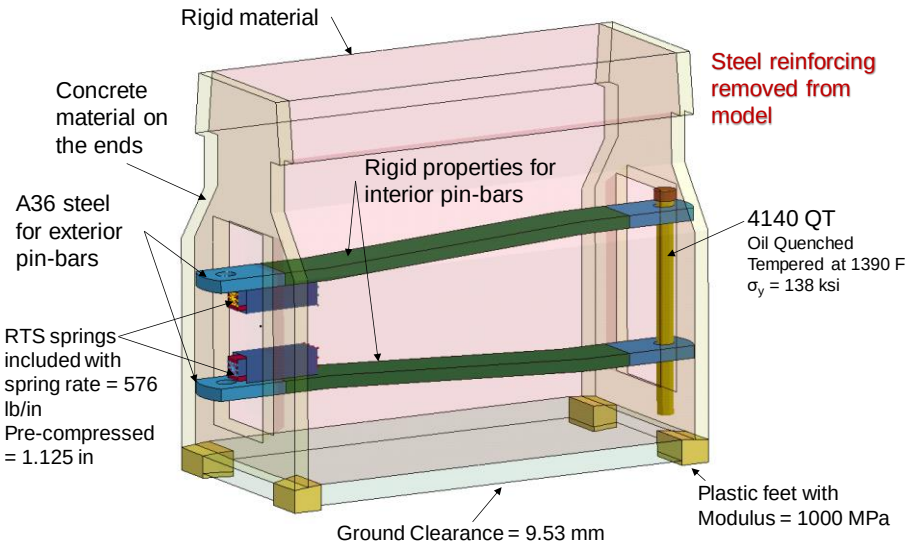

Figure 9. Image of the CRTS-Reduced model.

CRTS-Rigid Model

The finite element model of the CRTS-Rigid model is shown in Figure 10 (concrete again viewed in transparency mode). This model is identical to the CRTS-Reduced model except that all the concrete material is modeled as rigid. This model will be used exclusively in the non-impact regions of the model both upstream and downstream of the impact zone.

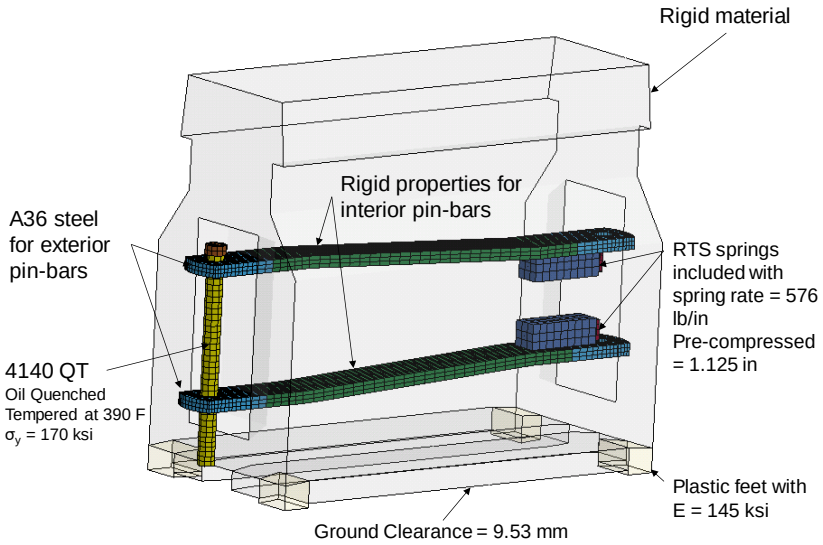

Figure 10. Image of the CRTS-Rigid model.

18-Inch VLB Model

The finite element model of the 18” VLB is shown in Figure 11. The detailed drawing for the VLB unit is provided in Appendix B. Since this unit is used in the impact region of the system, the external features of the barrier unit were modeled in relatively high geometric and

material detail. However, the internal components of the system, which include a hydraulic cylinder and fluid reservoir, were modeled as discrete elements (e.g., viscous damper and mass elements). The following sections provide information regarding FE mesh, element formulations and constitutive models used for each component of the 18" VLB model. Under-integrated elements were used for all deformable materials with zero-energy modes controlled using the stiffness hourglass options in LS-DYNA (e.g., type 4 for shell and type 5 for solids).

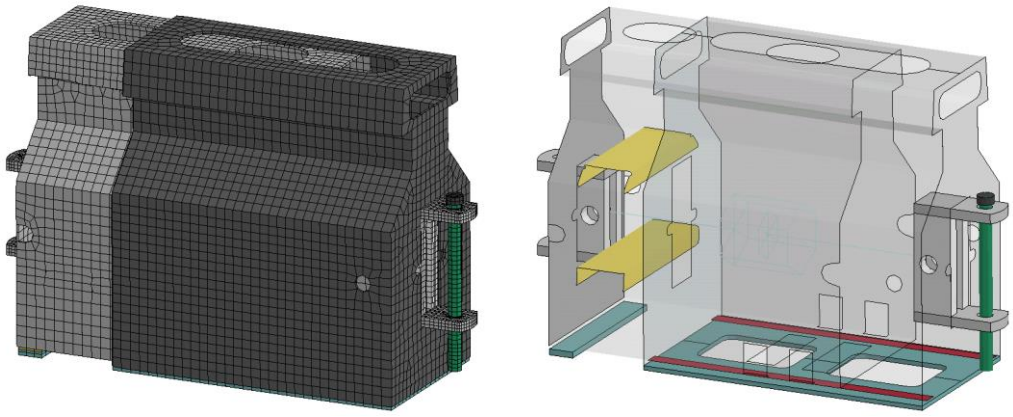

Figure 11. FE model of the 18" VLB.

Outer and Inner Shell

The geometry of the outer and inner shell weldments of the VLB unit was modeled based on the drawing details of drawings BSI-1010077-00 and BSI-1010076-00, respectively (refer to Appendix B). All welds were simulated via merged nodes, therefore the dimensions of the model varied slightly from the drawings at locations where the parts were overlapped and welded. The material properties were characterized based on AASHTO M183 (A36) steel using the properties provided by Wright and Ray.[*Wright97*] The minimum yield strength of AASHTO M183 is 36 ksi, however, the actual measured yield is approximately 45 ksi. [*Wright97*] The parts were modeled with thin-shell Belytschko-Tsay elements (Type 2 in LS-DYNA) with five integration points through the thickness. The part was meshed with a nominal element size of 1.0 x 1.0 inches. The mesh around the holes in the parts were modeled with nominal dimensions 0.5 x 0.5 inches; the smallest element side length was 0.43 inches.

Hinge Weldments

The model of the hinge weldments, shown in Figure 13 is consistent with drawings for Part Number BSI-1404017-00 in Appendix B. The hinge weldment was modeled with Type 1 brick elements in LS-DYNA. The model of the hinge component is the same as that used in the model of the CRTS model (refer to Figure 3) meshed with nominal element size 1/3" x 1/3" x 1/3" and with smallest element side-length of 0.25 inches around the pin-hole surface. The thickness of the hinge component is 1 inch. The model of the vertical weldment component was meshed with nominal element size of 1/3" x 0.55" x 0.55". All welds were modeled via merged nodes between the adjoining surfaces. The material for the weldment parts was A36 steel and was characterized based on AASHTO M183 (A36) steel using the properties provided by Wright and Ray.[*Wright97*]

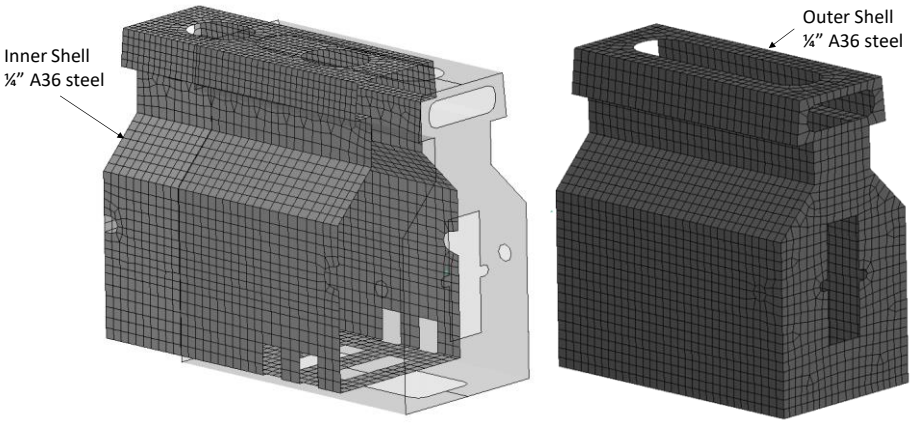

Figure 12. Model of outer and inner shell of the 18" VLB

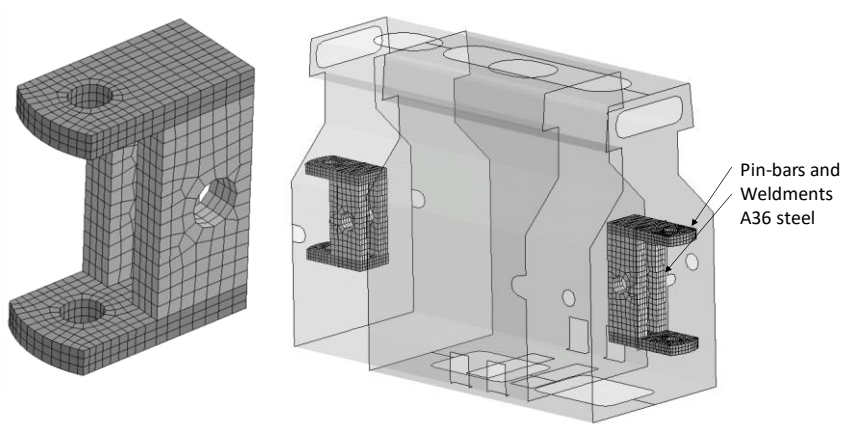

Figure 13. Model of hinge weldment for 18" VLB.

Cross Braces

The model of the upper and lower cross-braces, shown in Figure 14, is consistent with drawings for Part Numbers A050524 and A050532, respectively, in Appendix B. The parts were modeled with thin-shell Type 2 elements in LS-DYNA with five integration points through the thickness. The parts were meshed with a nominal element size of 0.5 x 0.5 inches. The material properties were characterized based on AASHTO M183 (A36) steel using the properties provided by Wright and Ray.[*Wright97*]

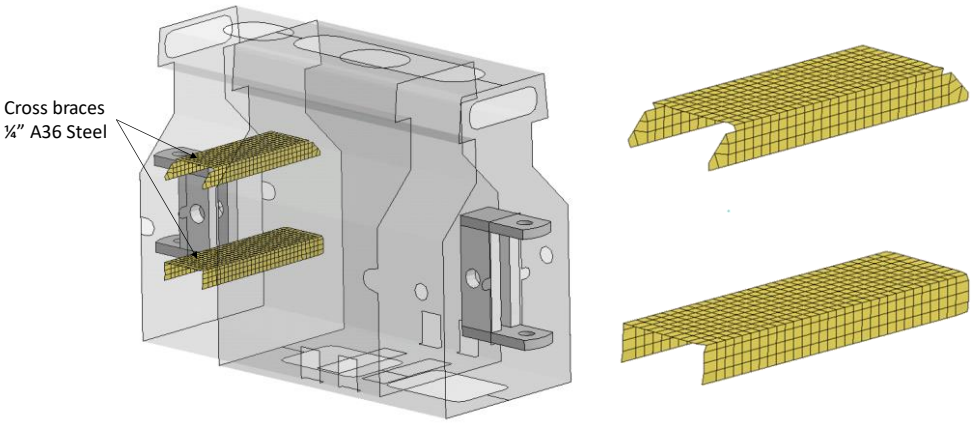

Figure 14. Model of cross brace for the 18" VLB.

Foot Bar and Inner Skid

The model of the foot bar and inner skid, shown in Figure 15, is consistent with drawings for Part Numbers BSI-1010071-00 and AA990822, respectively, in Appendix B. The parts were modeled with thin-shell Type 2 elements in LS-DYNA with five integration points through the thickness. The foot bar was meshed with a nominal element size of 1.0" x 1.0" with thickness of 0.5 inches. The inner skid was meshed with nominal element size of 0.5" x 1.0" with thickness of 0.25 inches. The material properties were characterized based on AASHTO M183 (A36) steel using the properties provided by Wright and Ray.[*Wright97*]

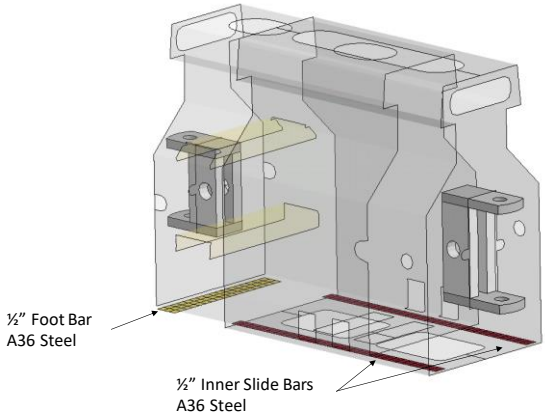

Figure 15. Model of foot bar and inner skid for the 18" VLB.

Model for Hydraulic Cylinder Response

The response of the hydraulic cylinder actuation inside the VLB unit was modeled using discrete mass and damper elements. The total mass of the cylinder and its associated components, including the oil reservoir, was modeled as lumped masses at the ends of the cylinder attachments on the hinge weldments. The actual mass of these components was not known at the time of this reporting but was set to 112 lb, based on the total mass of the model without the components and the actual overall mass of the VLB unit (i.e., 706 lb). The response

of the hydraulic cylinder was modeled as a linear viscous element; the damping coefficient was defined based on hydraulic dynamic bench testing performed by Barrier Systems, Inc.

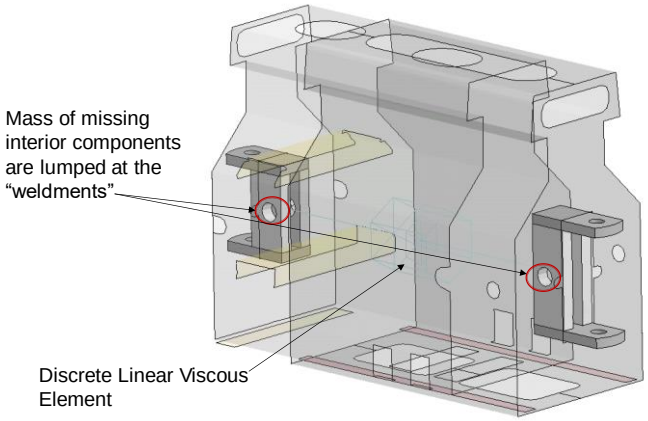

Figure 16. Model of hydraulic cylinder response for the 18" VLB.

Part Contact

The outer and inner shell components were included with the contact definitions for the CRTS model's concrete elements (refer to discussion on page 14). Likewise, the hinge components were included in the contact definitions for the pin-to-hinge parts in the CRTS model. For contact between the vehicle and barrier, an additional part was included in the model to better model the effects of the vehicle parts sliding on the outer surface of the inner shell and impacting against the edge of the outer shell part of the barrier. A thin contact sheet was modeled to cover the upstream end of the outer shell structure, as shown in Figure 17, to prevent vehicle nodes from passing behind the outer shell and resulting in "mesh tangle".

An additional part was also included in the model for correcting the contact between the bottom of the VLB and the ground. Since the outer shell and the foot of the VLB are modeled with thin shell elements, the contact surface between these components and the rigidwall for the ground does not include the thickness of the shell elements. Therefore, a solid element surface was created under the foot and outer shell parts to correct the contact gap. The friction between the VLB and ground was set to 0.6 - consistent with the ground friction coefficient defined for the CRTS units.

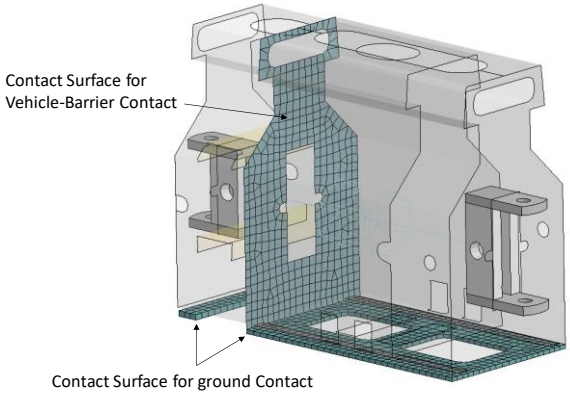

Figure 17. Added parts for improving contact.

MODEL VALIDATION

In order to gain confidence in the results of the finite element model, it was necessary to validate the model's predictions against full-scale crash tests. As part of the validation process, the validation procedures presented in NCHRP Web Document 179 (W179) were used to assess the fidelity of the model. [*Ray10*] The W179 validation procedure has three steps:

1. Solution verification: Indicates whether the analysis solution produced numerically stable results (ensures that basic physical laws are upheld in the model).
2. Time-history evaluation: Quantitative measure of the level of agreement of time-history data (e.g., x, y, z accelerations and roll, pitch, and yaw rates) between the analysis and test.
3. Phenomena Importance Ranking Table (PIRT): A table that documents the types of phenomena that a numerical model is intended to replicate and verifies that the model produces results consistent with its intended use.

The baseline model was used to simulate test 690900-LTS2 with impact conditions consistent with the full-scale test (i.e., MASH Test 3-11). Test 690900-LTS2 involved a 2009 Dodge Ram 1500 Quadcab pickup truck impacting the CRTS barrier. The gross static mass of the test vehicle was 4,928 lbs (2,235 kg). The test installation was 557.9 feet (170 m) with no end-anchorage for the test article. The test vehicle struck the barrier at 62.6 mph at an angle of 25.4 degrees. The initial point of contact was at 273.95 feet (83.5 m) from the upstream end of the system at the midpoint of barrier segment 84. The center-line of the vehicle was aligned with the center point of the system at barrier segment 86, as illustrated in Figure 18.

The test article installation included 168 CRTS elements and two VLB elements. One VLB element was positioned at barrier segment 86 (i.e., 2 barrier segments downstream of the impact point), which was determined to be the critical position for assessing snag of the vehicle on the VLB. The second VLB was positioned 17 barrier lengths downstream of the first VLB corresponding to barrier segment 103.

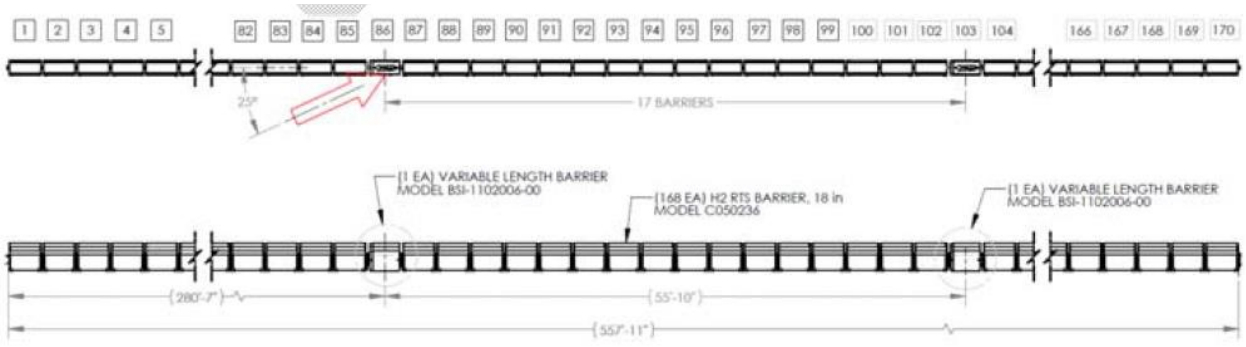

Figure 18. Target CIP for MASH Test 3-11 in full-scale crash test 690900-LTS2

The vehicle model used in the analysis was the CCSC Silverado model version 3a. This model has been used extensively in simulating MASH TL3 impact scenarios with much success. Validation PIRTs for the model were provided by George Mason University and are included with this report as Appendix H.

A comparison of the physical and inertial properties of the test and analysis vehicles is provided in Figure 19. Except for the bumper measurements, all other measurements were

within 5% difference. The most notable difference was the height measurements from the ground to the bottom of the front and back bumpers. The lower edge of the front and rear bumpers on the model was 2.9 inches (30.5 percent) higher and 2.81 inches (14.8 percent) higher, respectively, compared to that of the test vehicle. The center of gravity (c.g.) of the model was within 1.5 percent of the test vehicle c.g. The accelerometer at the c.g. for the model was in the same location as the accelerometer in the test vehicle, which was 0.17 inches behind the center of gravity.

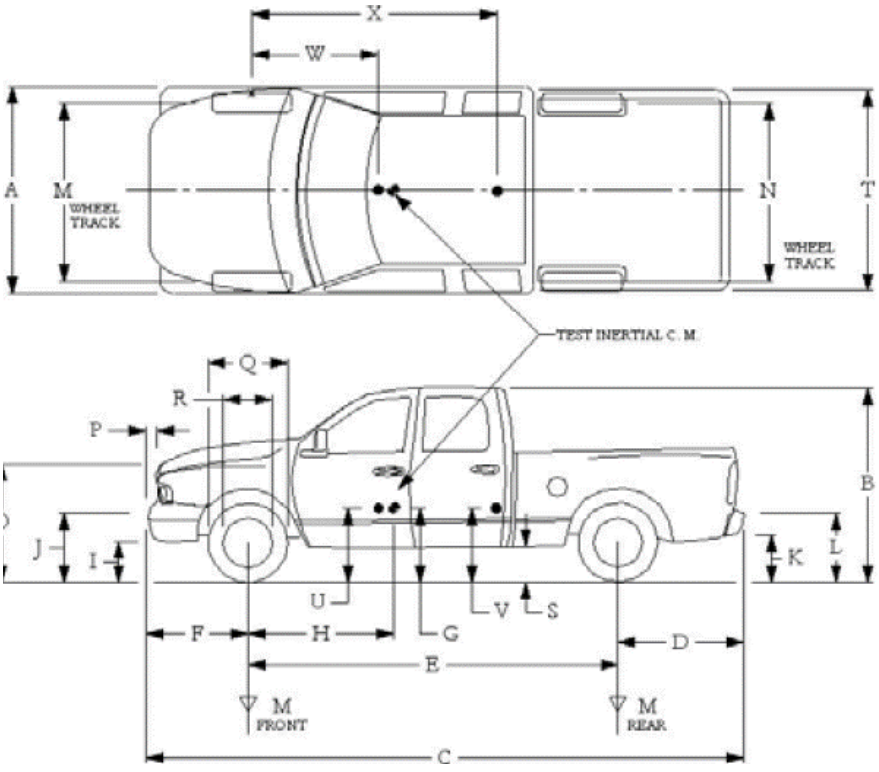

Vehicle Geomerty (inches)

	Test Vehicle	FE Model	Error %
A	78.5	78.9	0.5
B	73.5	75.3	2.5
C	227.5	229.7	1.0
D	47.0	46.7	-0.6
E	140.5	143.5	2.1
F	40.0	39.4	-1.6
G	28.4	28.8	1.5
H	60.3	60.1	-0.5
I	9.5	12.4	30.5
J	26.5	26.7	0.9
K	19.0	21.8	14.8
L	30.0	29.7	-0.9
M	68.5	69.5	1.4
N	68.0	67.3	-1.0
O	45.5	44.8	-1.6
P	3.0	3.2	6.3
Q	30.5	29.6	-2.8
R	18.0	18.8	4.3
S	12.3	12.5	2.2
T	77.0	78.0	1.3
U	28.5	27.5	-3.4
V	31.0	-	-
W	60.5	60.5	0.0
X	77.0	-	-

Mass -Properties

		Curb			Test Inertial			Gross Static		
		Test Vehicle	FE Model	Error %	Test Vehicle	FE Model	Error %	Test Vehicle	FE Model	Error %
M_1	(lb)	2,885			2,812			2,812	2,913	3.6
M_2	(lb)	2,136			2,116			2,116	2,093	-1.1
M_{Total}	(lb)	5,021			4,928			4,928	5,007	1.6
I_{11}	(lb - ft^2)								25,083	
I_{22}	(lb - ft^2)								141,834	
I_{33}	(lb - ft^2)								153,201	

Figure 19. Comparison of properties for the test and analysis vehicle.

The analysis was performed using LS-DYNA version mpp_s_R8.0.0 revision number 95309. The analysis was conducted with a time-step of 1.0 microsecond for a time period of 0.8 seconds. The exact timing of phenomenological events was not possible because plot states were only collected at 0.005 second intervals throughout the analysis. Therefore, a 0.005 second time window corresponding to range of time for which the event could have occurred in the analysis

was reported. The following is a commentary describing the timing and occurrence of various events during the simulated impact with comparison to the full-scale test. The commentary is based largely on the commentary provided in the full-scale crash test report.[*Alberson16*]

The vehicle was traveling at a speed of 62.6 mph and at an angle of 25.4 degrees at the point of contact with the barrier. At 0.02 seconds the left front tire began to climb the face of the barrier (0.025 seconds in test), and barrier segment 84 and 85 began to deflect toward the field side (0.029 seconds in test). The left front corner of the bumper contacted the upstream end of VBL 86, which began to deflect toward the field side, at 0.050 (0.050 seconds in test). At 0.075 seconds, barrier segment 87 began to deflect toward the field side (0.078 seconds in test). At 0.085 seconds, the left front tire contacted the sliding joint of VLB 86 (0.079 seconds in test); the tire model did not include the ability to deflate, but the tire on the test vehicle did blow out at this time in the full-scale test. Also at 0.85 seconds, barrier segment 88 began to slide toward the traffic side (0.091 seconds in test). Barrier segment 88 then began to deflect toward the field side at 0.105 seconds (0.112 seconds in test). The vehicle was parallel with the barrier at 0.236 seconds (0.238 seconds in test) traveling at 45.2 mph (43.8 mph in test). At 0.270 seconds (0.271 seconds in test), the left rear bumper contacted barrier segment 85. At 0.295 seconds (0.30 seconds in test) the rear bumper snagged on the sliding joint of VLB 86 and started to deform. At 0.31 seconds (0.32 seconds in test) the bumper released from the snag; the vehicle was traveling at a speed of 43.4 mph (40.6 mph in test). The analysis was terminated manually at 0.8 seconds, at which time the vehicle was still in contact with the barrier and:

- The roll angle of the vehicle was -12.4 degrees and stable (-1.14 degrees in test),
- The pitch angle was -6.4 degrees and stable (0 degrees in test),
- The yaw angle was -15.2 degrees relative to the barrier (-19.8 degrees in test), and
- The forward velocity of the vehicle was 43.4 mph (40.6 mph in test).

The vehicle lost contact with the barrier at 1.04 seconds in the full-scale test.

Sequential Views

A qualitative assessment was made by comparing sequential snapshots of the full-scale crash test with the results of the simulation to verify vehicle kinematic response as well as sequence and timing of key phenomenological events. The results from the FE analysis compare reasonably well with the results from full-scale crash test 690900-LTS2. Figure 20 and Figure 21 show sequential snapshots of the impact event from an overhead viewpoint and a downstream viewpoint, respectively. The model appears to simulate the basic kinematic behavior of the pickup and adequately captures the basic phenomenological events that occur during impact.

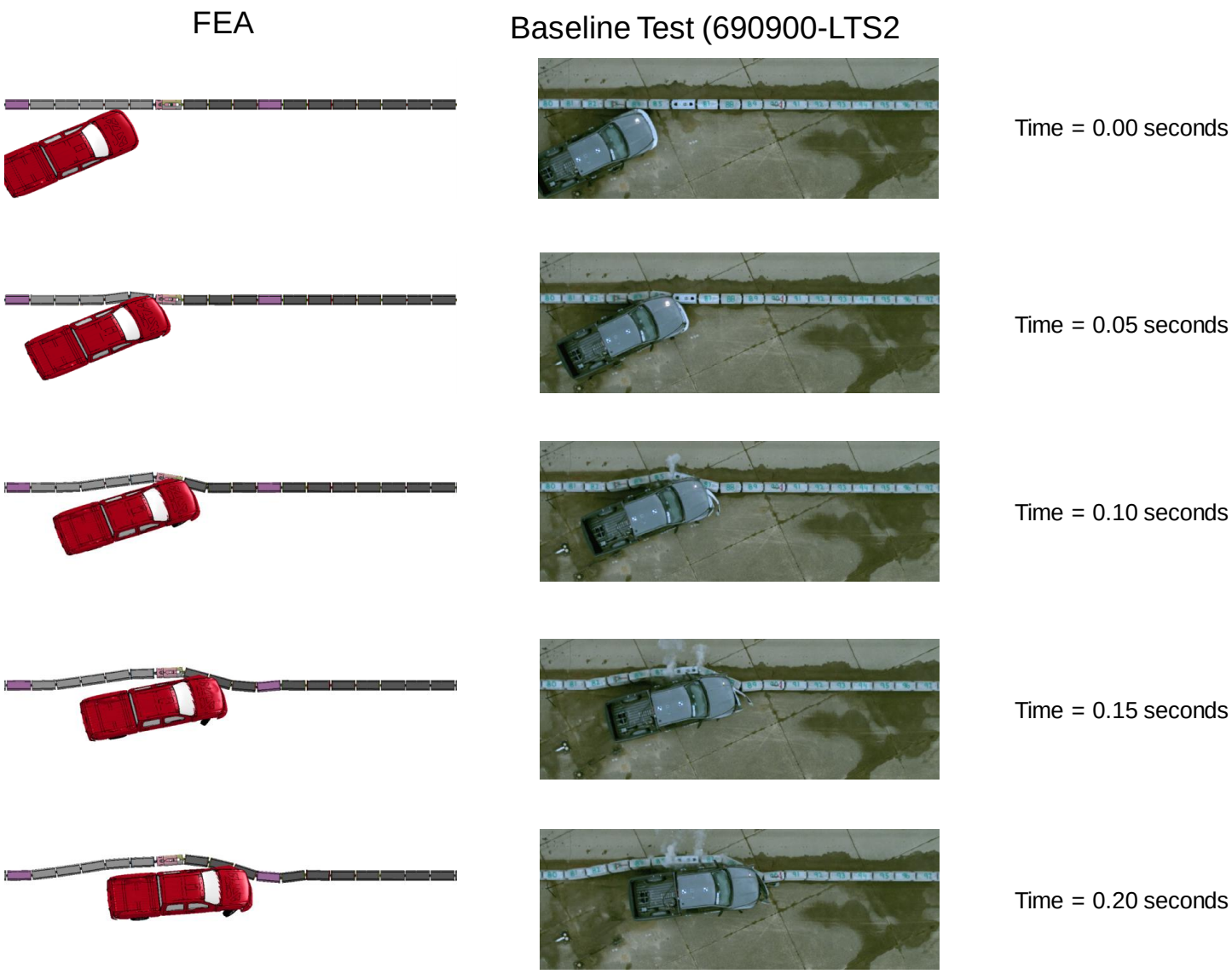

Figure 20. Sequential views of FEA and test 690900-LTS1 from an overhead viewpoint.

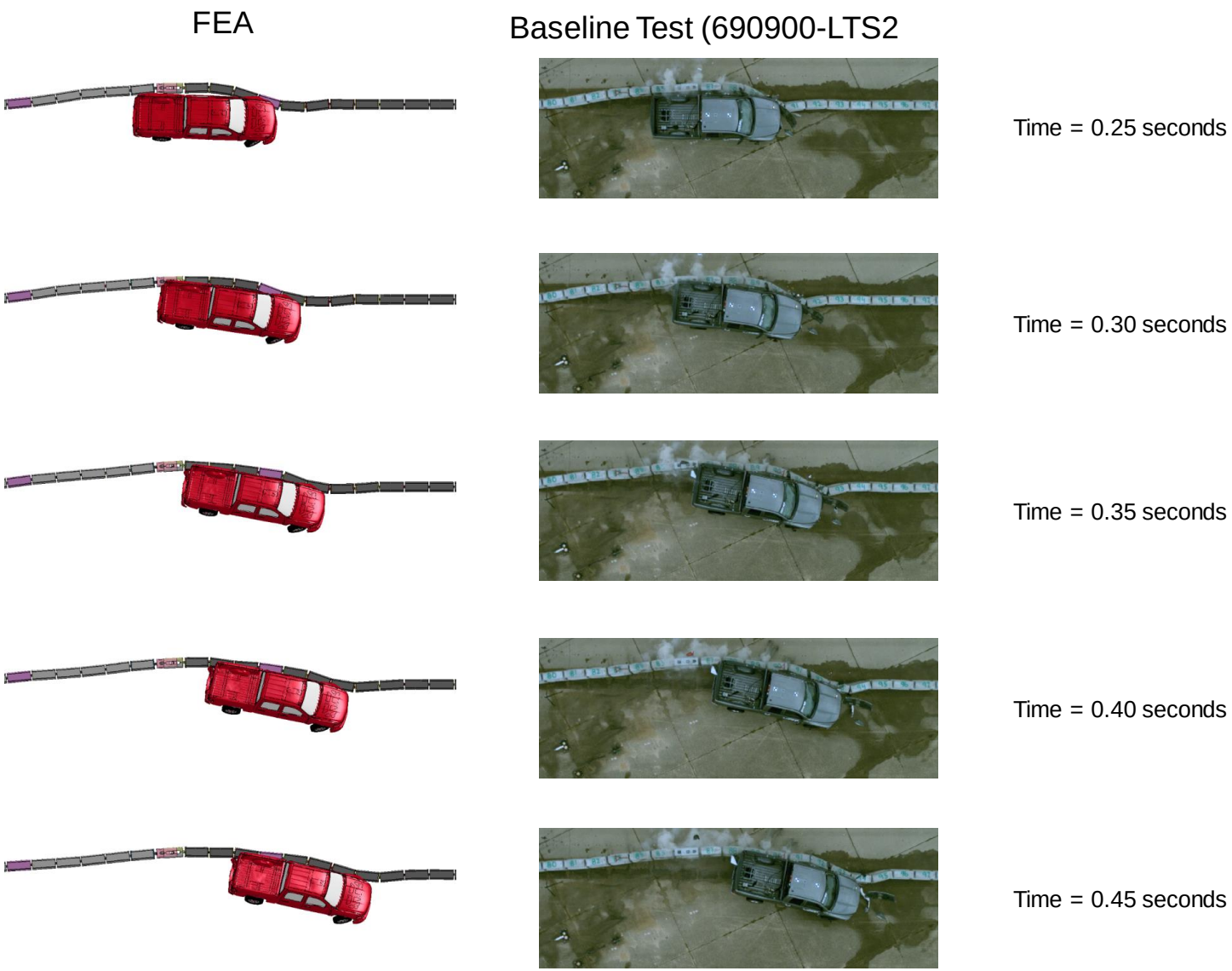

Figure 20. [Continued] Sequential views of FEA and test 690900-LTS1 from an overhead viewpoint.

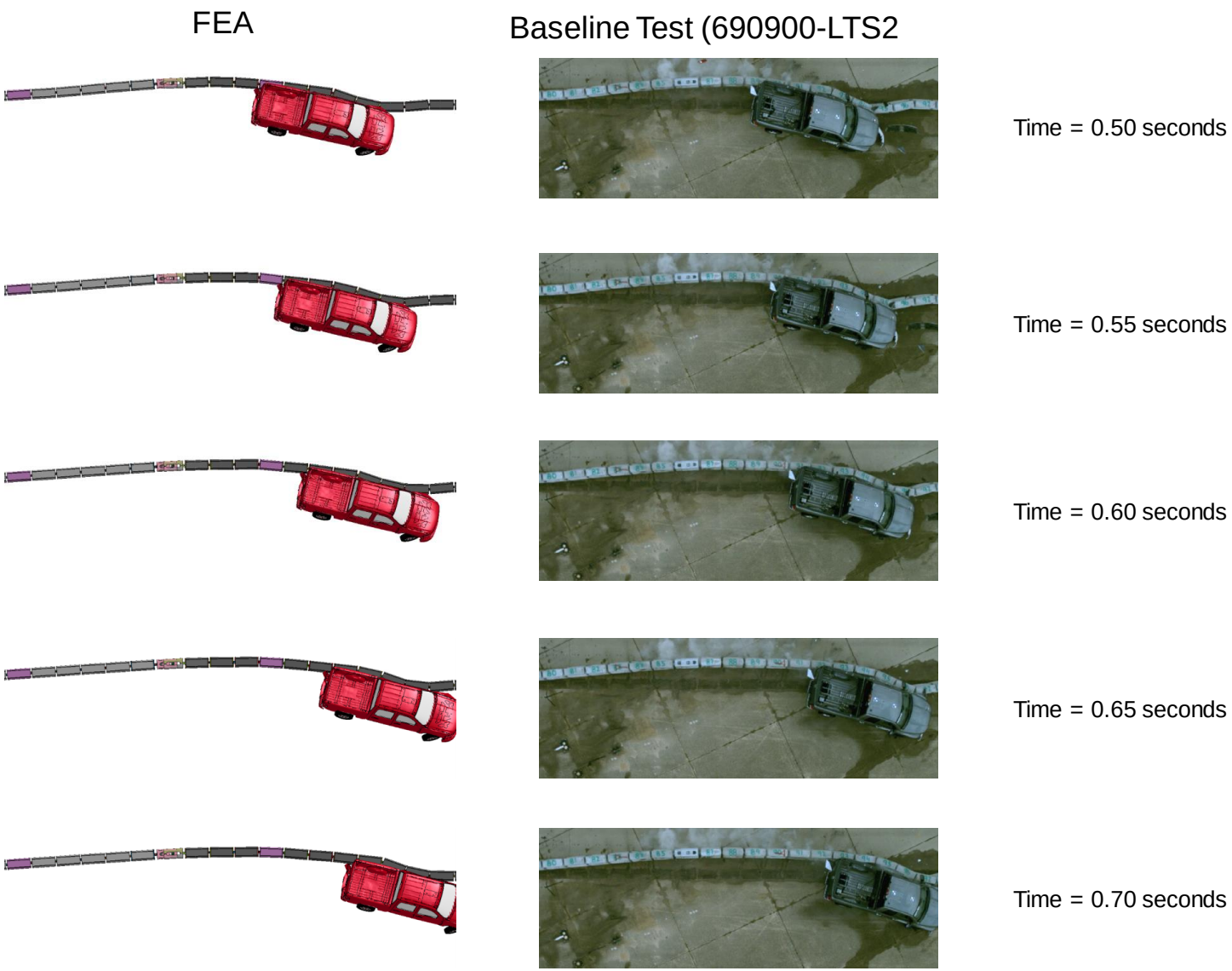

Figure 20. [Continued] Sequential views of FEA and test 690900-LTS1 from an overhead viewpoint.

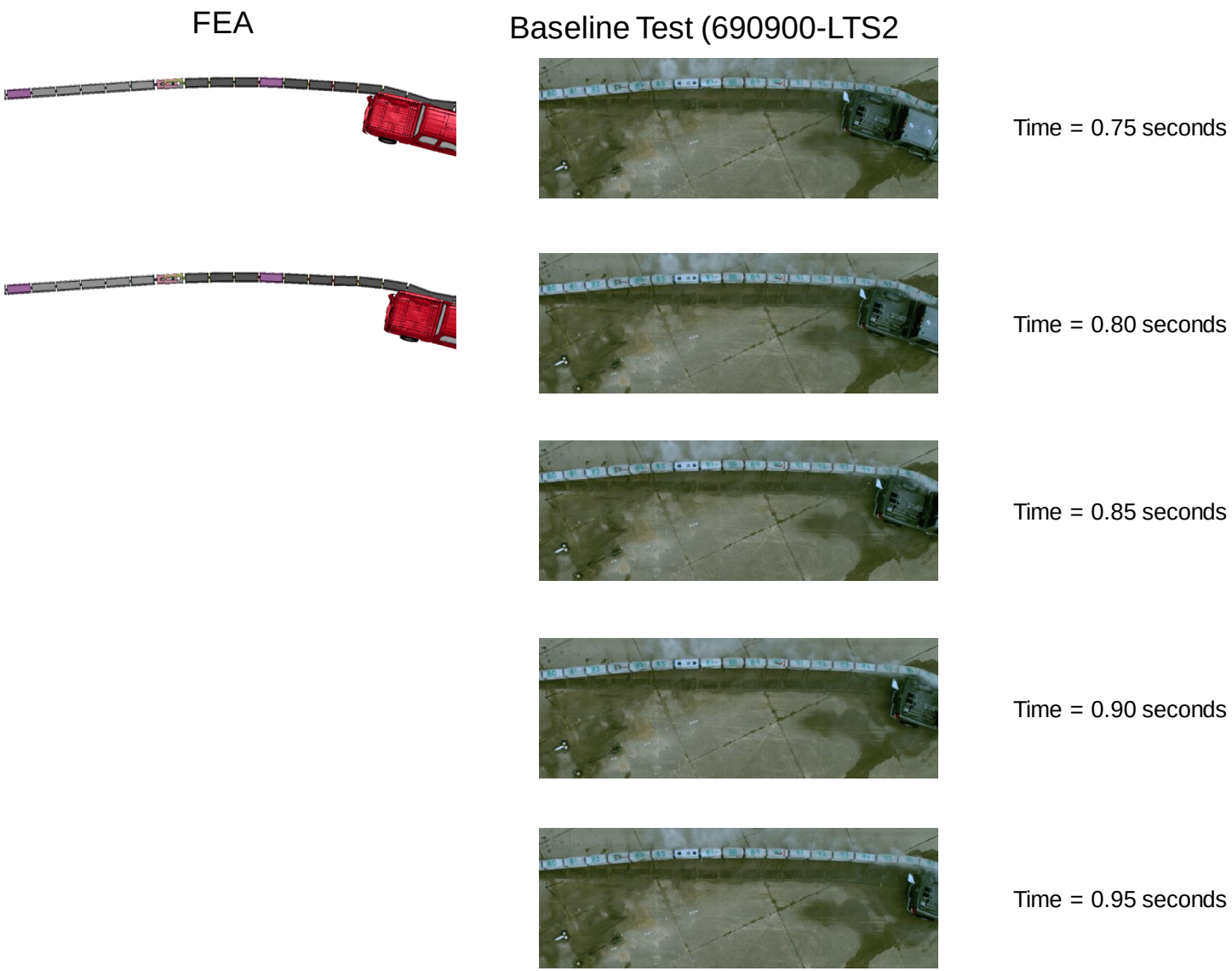

Figure 20. [Continued] Sequential views of FEA and test 690900-LTS1 from an overhead viewpoint.

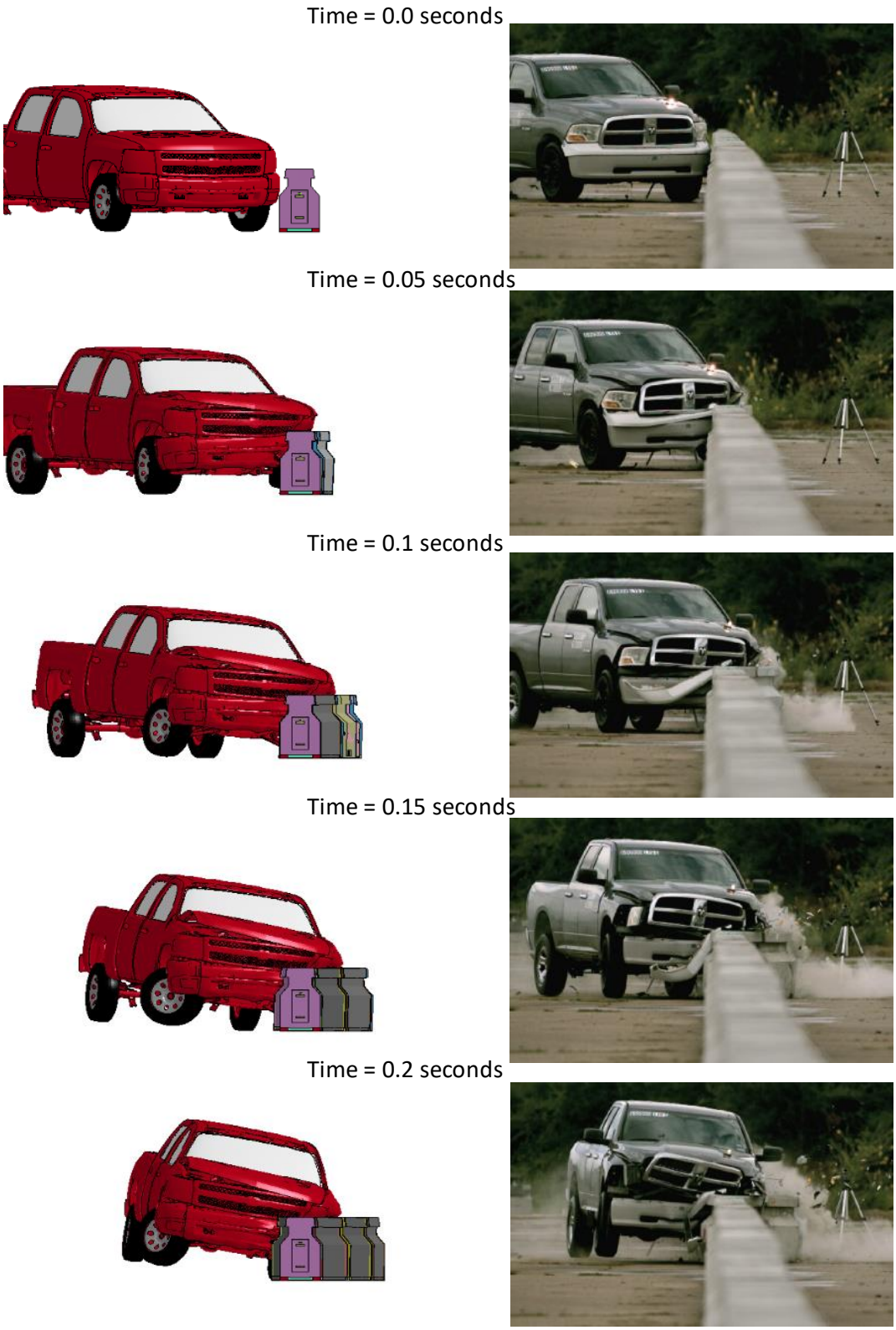

Figure 21. Sequential views of FEA and test 690900-LTS1 from a downstream viewpoint.

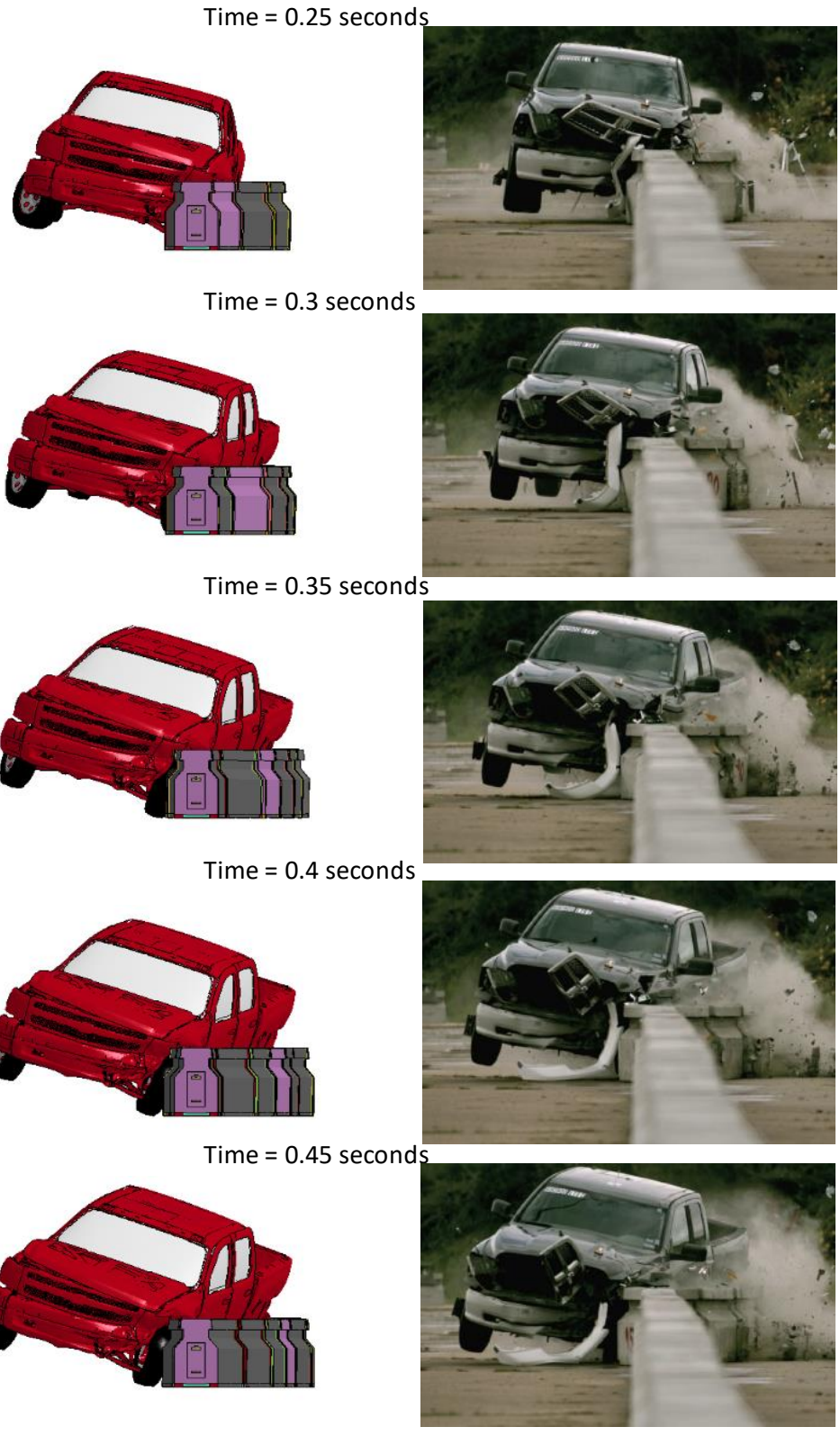

Figure 21. [Continued]Sequential views of FEA and test 690900-LTS1 from a downstream viewpoint.

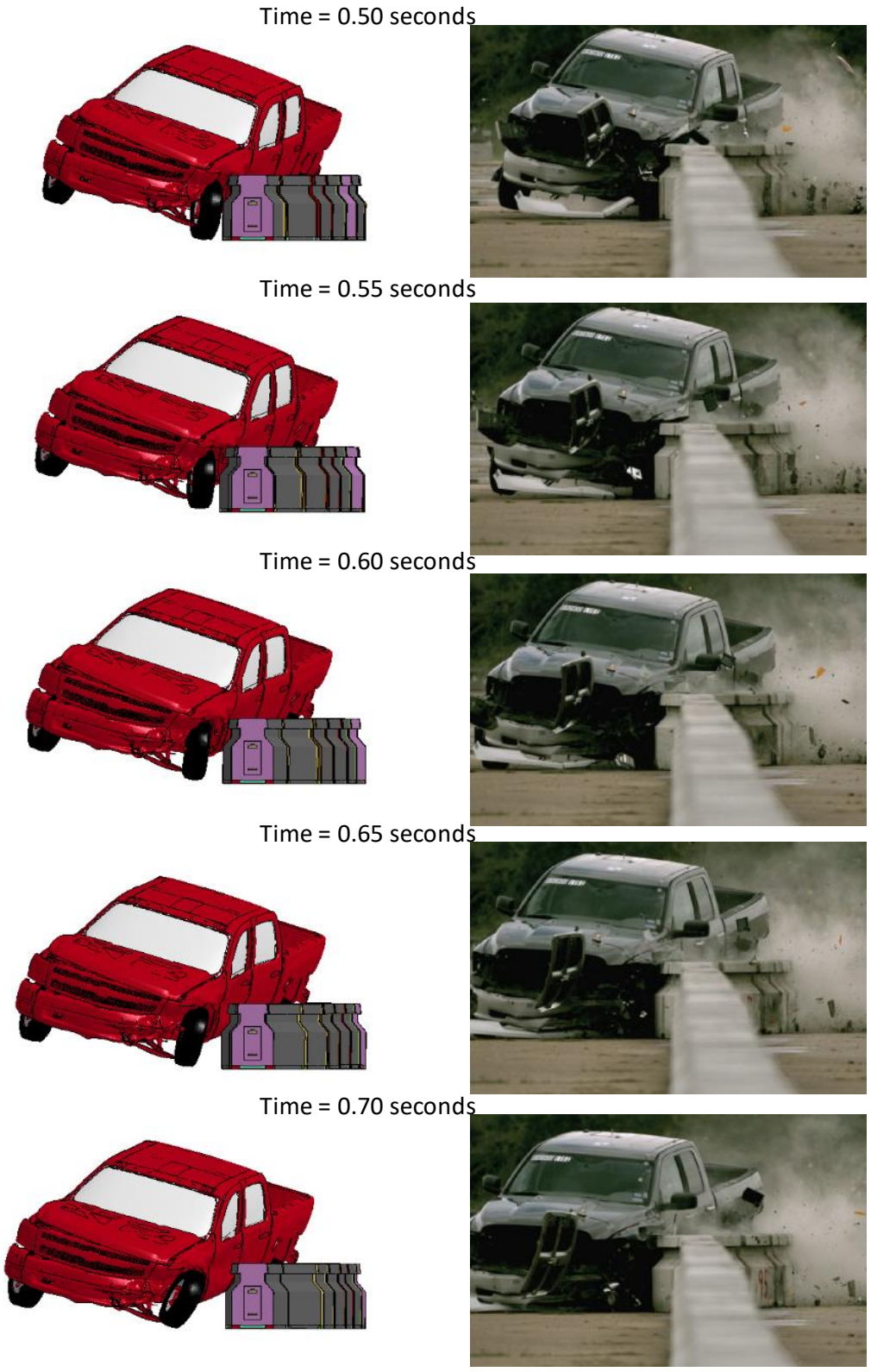

Figure 21. [Continued] Sequential views of FEA and test 690900-LTS1 from a downstream viewpoint.

Occupant Risk Measures

Acceleration-time histories and angular rate-time histories were collected at the center of gravity of the vehicle model using the *Element-Seatbelt-Accelerometer option in LS-DYNA, which is the preferred method suggested by LS-DYNA for collecting acceleration data.[*LSDYNA15*] The accelerometer was connected to the vehicle model using *Nodal-Rigid-Body-Constraint. The time-history data was collected from the accelerometer in a local reference coordinate system that was fixed to the vehicle with the x-direction coincident with the forward direction of the vehicle, the local y-direction is fixed toward the right side of the vehicle and the local z-direction is fixed downward; which was consistent with the way the test data was collected from physical accelerometers. The data was collected at a frequency of 50 kHz which was determined to be sufficient to avoid aliasing of the data. The model was instrumented with eight accelerometers with one positioned near the center of gravity of the vehicle on the cabin floor, as identified in Figure 22.

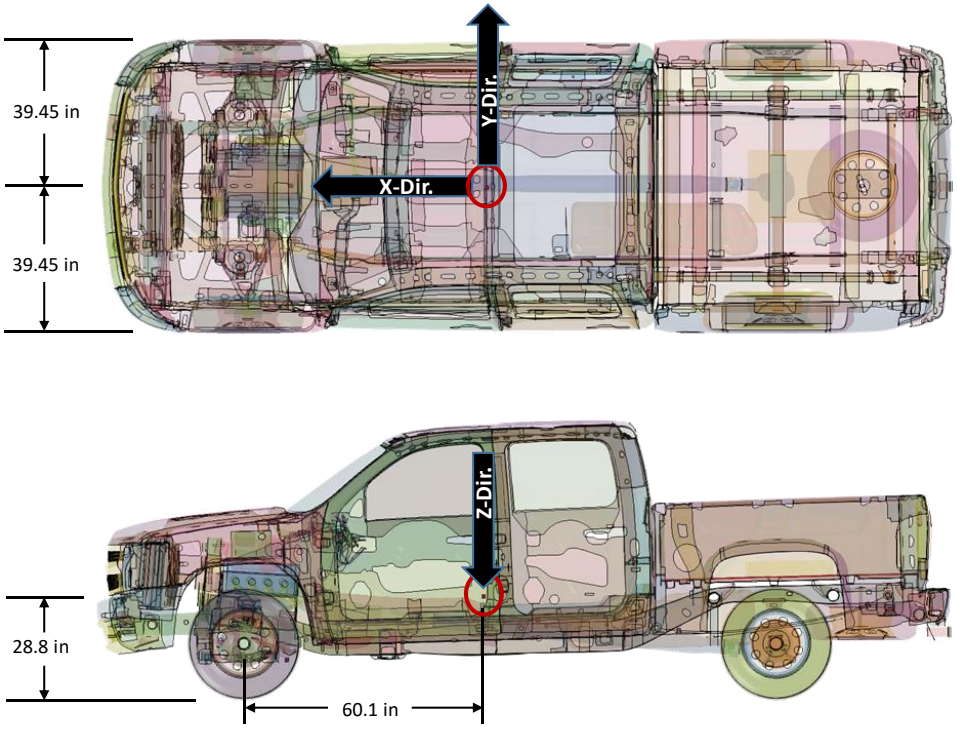

Figure 22. Location of c.g. accelerometer in the FEA model.

The occupant risk assessment measures were computed using the three acceleration-time histories and the three angular-rate time histories collected at the center of gravity of the vehicle. The Test Risk Assessment Program (TRAP version 2.3.2) calculates standardized occupant risk factors from vehicle crash data in accordance with MASH guidelines and the European Committee for Standardization (CEN).[*TTI98*]

The analysis results obtained from TRAP for the full-scale test and the FE analysis are shown in Table 1. The acceleration data used in the TRAP program was pre-filtered using the SAE Class 180 filter. The table shows the two occupant risk factors recommended by MASH: 1) the lateral and longitudinal components of Occupant Impact Velocity (OIV) and 2) the maximum

lateral and longitudinal Occupant Ridedown Acceleration (ORA) which corresponds to the local x- and y- accelerations, respectively, each averaged over a running 10-millisecond interval starting at the time of occupant impact. Also, provided in the table are the CEN risk factors including the Theoretical Head Impact Velocity (THIV), the Post Impact Head Deceleration (PHD) and the Acceleration Severity Index (ASI). The table also includes comparison of the 50-millisecond moving average of the accelerations.

Table 1. Occupant risk metrics computed using TRAP software for the FEA and test data for MASH Test 3-11.

Occupant Risk Factors		MASH Test 3-11			Error		W179 Criteria	
		FEA	Test 690900-LTS2					
		(0 - 0.8 seconds)	(0 - 0.8 seconds)	(0 - 2.0 seconds)	%	Absolute	Criteria	Pass
Occupant Impact Velocity (m/s)	x-direction	5.4	5.7	5.7	5.3%	0.3	<20% or < 2m/s	Y
	y-direction	-4.8	-5.3	-5.3	9.4%	0.5	<20% or < 2m/s	Y
	at time	at 0.1109 seconds on left side of interior	at 0.1152 seconds on left side of interior	at 0.1152 seconds on left side of interior				
THIV (m/s)		7 at 0.1056 seconds on left side of interior	7.9 at 0.1152 seconds on left side of interior	7.9 at 0.1152 seconds on left side of interior	11.4%	0.9	<20% or < 2m/s	Y
Ridedown Acceleration (g's)	x-direction	-7.8 (0.2509 - 0.2609 seconds)	-7.1 (0.1472 - 0.1572 seconds)	-7.1 (0.1472 - 0.1572 seconds)	9.9%	0.7	<20% or < 4G	Y
	y-direction	10.6 (0.2923 - 0.3023 seconds)	11.1 (0.2908 - 0.3008 seconds)	11.1 (0.2908 - 0.3008 seconds)	4.5%	0.5	<20% or < 4G	Y
PHD (g's)		11.9 (0.2923 - 0.3023 seconds)	11.1 (0.2909 - 0.3009 seconds)	11.1 (0.2909 - 0.3009 seconds)	7.2%	0.8	<20% or < 4G	Y
ASI		1.09 (0.0214 - 0.0714 seconds)	1.1 (0.0279 - 0.0779 seconds)	1.1 (0.0279 - 0.0779 seconds)	0.9%	0.01	<20% or < 0.2	Y
Max 50-ms moving avg. acc. (g's)	x-direction	-7.6 (0.0227 - 0.0727 seconds)	-8.8 (0.0278 - 0.0778 seconds)	-8.8 (0.0278 - 0.0778 seconds)	13.6%	1.2	<20% or < 4G	Y
	y-direction	8.2 (0.0199 - 0.0699 seconds)	7.2 (0.0313 - 0.0813 seconds)	7.2 (0.0313 - 0.0813 seconds)	13.9%	1	<20% or < 4G	Y
	z-direction	-2 (0.0233 - 0.0733 seconds)	-2.7 (0.0254 - 0.0754 seconds)	-2.7 (0.0254 - 0.0754 seconds)	25.9%	0.7	<20% or < 4G	Y
Maximum Angular Disp. (deg)	Roll	-21.9 (0.5216 seconds)	-10.9 (0.4692 seconds)	-10.9 (0.4692 seconds)	100.9%	11		
	Pitch	-6.7 (0.7664 seconds)	-3.6 (0.5877 seconds)	5.5 (1.9999 seconds)	86.1%	3.1		
	Yaw	41.2 (0.7350 seconds)	45.3 (0.7999 seconds)	46.2 (0.9078 seconds)	9.1%	4.1		

The results indicate that the occupant risk factors for both the full-scale test and the simulation are similar. The occupant impact velocity in the longitudinal direction was predicted from the simulation to be 5.4 m/s (0.3 m/s lower than the test OIV of 5.7 m/s) at 0.1109 seconds. In the transverse direction, the occupant impact velocity predicted in the simulation was 4.8 m/s (0.5 m/s lower than the test OIV of 5.3 m/s). The highest 0.010-second occupant ridedown acceleration in the longitudinal direction was 7.8 g (0.7 g higher than test ORA of 7.1 g) between 0.2509 and 0.2609 seconds. In the transverse direction, the highest 0.010-second occupant ridedown acceleration was 10.6 g (0.8 g lower than test ORA of 11.1) between 0.2923 and 0.3023 seconds. The THIV, PHD and ASI predicted from the simulation were 7.0 m/s (11.4 percent higher), 11.9 g's (4.5 percent higher), and 1.09 (0.9 percent higher), respectively. The maximum 50-millisecond moving average accelerations in the x-, y-, and z-directions were 7.6 g (13.6 percent lower), 8.2 g (13.9 percent higher), and 2.0 g (25.9 percent or 0.7 g lower), respectively.

The criteria from Report W179 recommends that the differences between the analysis and test for each of the occupant risk measures be less than 20 percent, unless the magnitude is relatively small; in which case the absolute difference between the FEA and test values should be

used. For example, the percent difference for the 50-ms moving average acceleration in the z-direction was 25.9 percent; but the absolute difference was only 0.7 g. The results of the FEA were well within the recommended limits of Report W179 for each of the comparison metrics except the roll angle, which will be discussed later.

Time-History Data Comparison

Figure 23 shows a comparison of the 10-millisecond moving average and the 50-millisecond moving average acceleration-time history at the c.g. of the pickup for the longitudinal, transverse and vertical channels. Figure 24 shows comparisons of the angular rates and angular displacements (i.e., yaw, roll, and pitch) at the c.g. of the pickup for the test and FEA. Values for the quantitative evaluation metrics are also shown on the time-history plots. For example, "S-G M" and "S-G P" are the Sprague-Geers magnitude and phase metrics, respectively, and "Mean" and "SD" correspond to the analysis of variance mean and standard deviation metrics, respectively. These quantities were computed from the acceleration- and angular rate-time history data collected at the c.g. of the vehicle and are reported with the plots only for reference. The values in red font indicate poor correlation between test and analysis results, while the values in black font indicate good correlation. The quantitative metrics are discussed in more detail later in the Quantitative Evaluation section of this report.

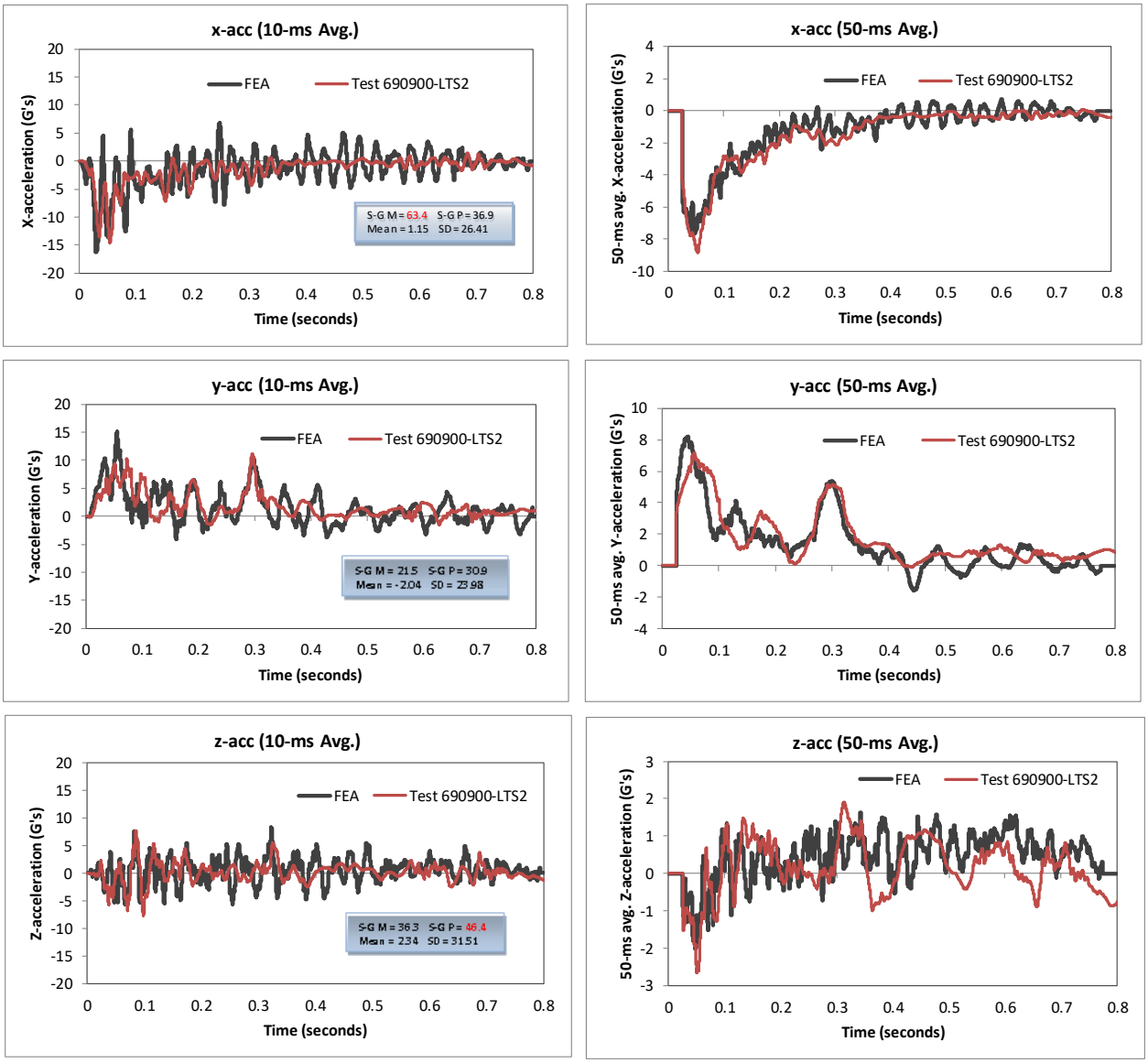

Figure 23. Acceleration-time history plots from the c.g. accelerometer for full-scale test 690900-LTS2 and FEA (10-ms and 50-ms moving averages).

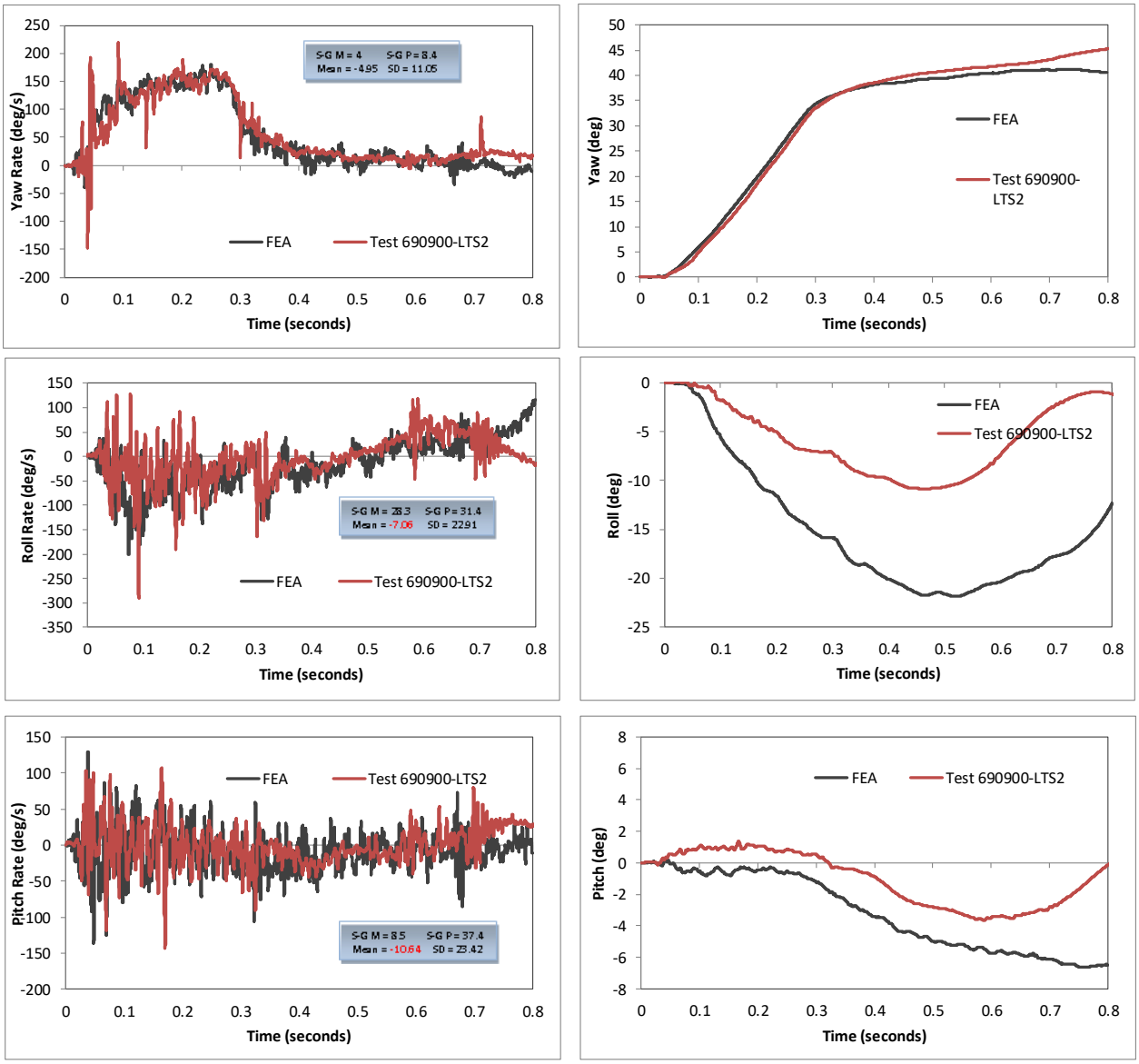

Figure 24. Angular rate- and displacement-time history plots measured at the c.g. of the vehicle in full-scale test 690900-LTS2 and FEA.

Quantitative Validation

The quantitative evaluation was based on comparison of acceleration-time histories and angular rate-time histories computed in the analysis to those measured in full-scale crash test 690900-LTS2. The impact conditions for the simulation matched exactly those from the full-scale test which correspond to MASH Test 3-11. A summary of the quantitative comparison results is provided herein. Additional comparison data can be found in Appendix C.

Solution Verification

The first step in the validation process is to perform global energy checks for the analysis to verify that the numerical solution is stable and is producing physical results (e.g., results conform to the basic laws of conservation). The analysis was modeled as a closed system, which means that energy is not being added or removed during the analysis. Thus, the total energy should remain constant throughout the analysis and should be equal to the initial kinetic energy of the impacting vehicle. The one exception in this case would be any kinetic energy generated due to the gravity load (which should be minimal during the short time period of the crash event relative to the initial kinetic energy of the vehicle). Table 2 shows a summary of the global verification assessment based on criteria recommended in Report W179. Figure 25 shows a plot of the global energy-time histories from the analysis.

As shown in Table 2, all the solution verification parameters were satisfied except for the comparison of total hourglass energy to total internal energy (18.7%), which was higher than the recommended allowable of 10 percent stated in W179. In this case, the barrier system experienced only moderate deformations during the impact with the exception of some spalling of the concrete at the edges of the barrier segments (see the section on "Barrier Damages" for more details). The total hourglass energy for the barrier components was less than 1 percent of the total internal energy for those components. The primary source for the hourglass energy in the analysis was associated with the inner and outer rim components on the rear, impact side of the vehicle, as shown in Figure 26. An image of these parts at the time of termination of the analysis (i.e., 0.8 seconds) is included on Figure 26 where it is visually evident that the hourglass energy resulted in no noticeable effect on deformations (i.e., the shape of the elements remained acceptable and experienced only elastic strains during the impact event). The wheel also behaved normally throughout the impact event regarding its response during contact with the ground and the barrier. Based on this assessment the effects of the hourglass energy were considered to be inconsequential to the analysis; the solution was therefore deemed stable and to provide valid physical results.

Table 2. Analysis solution verification table.

Verification Evaluation Criteria	Change	Pass?
Total energy of the analysis solution (i.e., kinetic, potential, contact, etc.) must not vary more than 10 percent from the beginning of the run to the end of the run.	0.3	Y
Hourglass Energy of the analysis solution at the end of the run is less than *five percent* of the total *initial energy* at the *beginning* of the run.	4.5	Y
Hourglass Energy of the analysis solution at the end of the run is less than *ten percent* of the total *internal energy* at the *end* of the run.	18.7	N
The part/material with the highest amount of hourglass energy at the end of the run is less than ten percent of the total internal energy of the part/material at the end of the run.	-	N
Mass added to the total model is less than five percent of the total model mass at the beginning of the run.	0	Y
The part/material with the most mass added had less than 10 percent of its initial mass added.	0	Y
The moving parts/materials in the model have less than five percent of mass added to the initial moving mass of the model.	0	Y

	There are no shooting nodes in the solution?	Y	Y
	There are no solid elements with negative volumes?	Y	Y

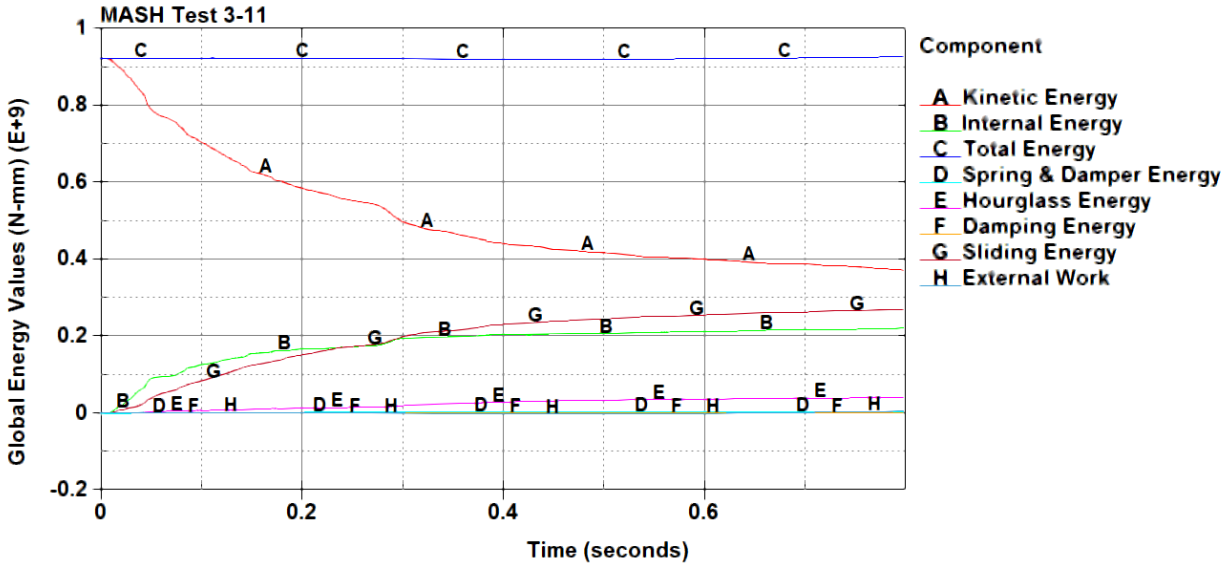

Figure 25. Plot of global energy-time histories from the analysis.

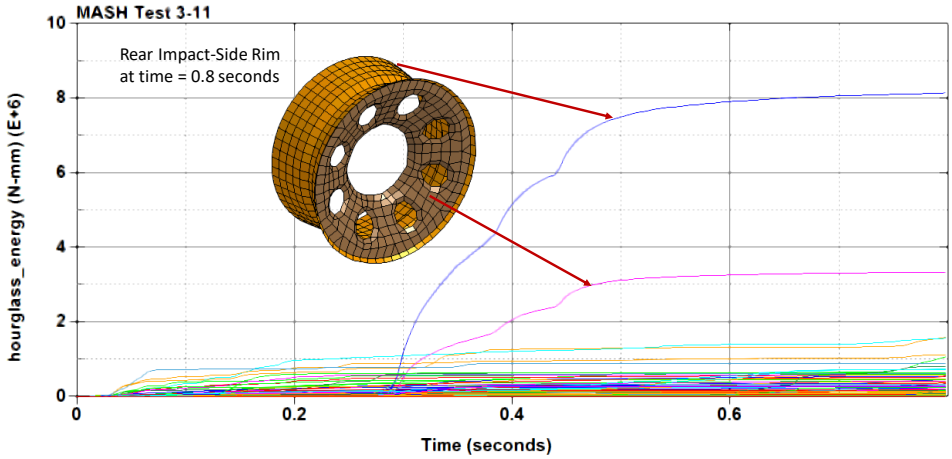

Figure 26. Hourglass energy from vehicle parts.

For those reasons, the analysis solution is considered to be valid.

Time-History Validation

Once a measure of comparison is obtained using a quantitative metric, it is necessary to establish an acceptance criterion for deciding if the comparison is acceptable. Because of the highly nonlinear nature of crash events, there are often considerable differences in the results of essentially identical full-scale crash tests – this was demonstrated in the W179 report. Likewise, a computational model may not match "exactly" the results of a physical test, but the difference

should be no greater than what is expected between physical tests. The approach taken in the W179 was to determine the realistic variation in the deterministic shape comparison metrics for a set of identical physical experiments and use that variation as an acceptance criterion. The current acceptance criteria is based on the results of a quantitative comparison of ten essentially identical full-scale crash tests that were performed as part of the ROBUST project involving small car impact into a vertical rigid wall at 100 km/hr and 25 degrees.[*ROBUST02; Ray08*] The resulting acceptance criteria recommended by W179 for assessing the similarity of two time-history curves are:

- Sprague-Geers
  - Magnitude should be less than 40 percent
  - Phase should be less than 40 percent
- ANOVA metrics
  - Mean residual error should be less than 5 percent
  - Standard deviation should be less than 35 percent.

The RSVVP computer program was used to compute the Sprague-Geer metrics and ANOVA metrics using time-history data from the full-scale test (i.e., true curve) and analysis data (i.e., test curve). The multi-channel option in RSVVP was used since this option computes metrics for each individual channel as well as for the weighted composite of the combined channels. The data from each of the six data channels, which were located at the center of gravity of the vehicle, were input into RSVVP. These data included the x-acceleration, y-acceleration, z-acceleration, roll-rate, pitch-rate and yaw-rate. Since the data from the test report was pre-filtered to 180 Hz, the data from the analysis was also filtered to 180 Hz using the SAE filter in LS-PREPOST. The data was then further filtered in RSVVP using a CFC Class 60 filter. The shift and drift options in RSVVP were not used for the physical test data. From visual inspection, the physical test data appeared to show no initial offset of acceleration magnitude or drift. Since both the test and analysis data started at the time of impact with the barrier the synchronization of curves was determined to be unnecessary.

The default metrics evaluation options in RSVVP were used, which included the Sprague & Geers and the ANOVA metrics. The curves were evaluated over 0.8 seconds of the impact event, corresponding to the termination time of the analysis.

The results of the quantitative evaluation for the individual channels are shown in Table 3. A comparison of the individual components of acceleration based on the validation metrics indicated that the simulation was in good agreement for the y-acceleration and the yaw rate; while the remaining channels were considered to be borderline in agreement (e.g., only one of the four evaluations metrics did not pass the W179 criteria in each of those cases).

Since the metrics computed for the individual data channels did not all satisfy the acceptance criteria, the multi-channel option in RSVVP was used to calculate the weighted Sprague-Geer and ANOVA metrics for the six channels of data. The Area II method is the default method used in RSVVP for weighting the importance of each data channel. The Area (II) method determines the *weight* for each channel based on a pseudo-momentum approach using the area under the curves.

Table 4 shows the results from RSVVP for the multi-channel option using the Area (II) method. The resulting weight factors computed for each channel are shown in both tabular form

and graphical form in the tables. The results indicate that the x-acceleration, y-acceleration, and the yaw rate channels dominate the kinematics of the impact event. This implies that the velocity change in the z-direction was insignificant compared to the change in velocity in the x- and y-directions. Similarly, the roll and pitch angle magnitude was negligible compared to that for the yaw (refer to Figure 24). The weighted metrics computed in RSVVP in the multi-channel mode all satisfy the acceptance criteria; therefore, the time history comparison can be considered acceptable.

Table 3. Roadside safety validation metrics rating table – time history comparison (single-channel option).

Evaluation Criteria								**Time interval [0.00 – 0.8 sec]**		
	Sprague-Geers Metrics List all the data channels being compared. Calculate the M and P metrics using RSVVP and enter the results. Values less than or equal to 40 are acceptable.									
		RSVVP Curve Preprocessing Options						**M**	**P**	**Pass?**
		Filter Option	**Sync. Option**	**Shift**		**Drift**				
				True Curve	**Test Curve**	**True Curve**	**Test Curve**			
	X acceleration	CFC 60	none	none	none	none	none	63.4	36.9	N
	Y acceleration	CFC 60	none	none	none	none	none	21.5	30.9	Y
	Z acceleration	CFC 60	none	none	none	none	none	36.3	46.4	N
	Yaw rate	CFC 60	none	none	none	none	none	4	8.4	Y
	Roll rate	CFC 60	none	none	none	none	none	28.3	31.4	Y
	Pitch rate	CFC 60	none	none	none	none	none	8.5	37.4	Y
P	***ANOVA Metrics*** List all the data channels being compared. Calculate the ANOVA metrics using RSVVP and enter the results. Both of the following criteria must be met: • The mean residual error must be less than five percent of the peak acceleration ($\bar{e} \le 0.05 \cdot a_{Peak}$) and • The standard deviation of the residuals must be less than 35 percent of the peak acceleration ($\sigma \le 0.35 \cdot a_{Peak}$)							**Mean Residual**	**Standard Deviation of Residuals**	**Pass?**
	X acceleration/Peak							1.15	26.41	Y
	Y acceleration/Peak							2.04	23.98	Y
	Z acceleration/Peak							2.34	31.51	Y
	Yaw rate							4.95	11.05	Y
	Roll rate							7.06	22.91	N
	Pitch rate							10.64	23.42	N

Table 4. Roadside safety validation metrics rating table – (multi-channel option).

Evaluation Criteria (time interval [0.8 seconds])				
Channels (Select which were used)				
☒ X Acceleration	☒ Y Acceleration	☒ Z Acceleration		
☒ Roll rate	☒ Pitch rate	☒ Yaw rate		
Multi-Channel Weights (Area II Method)	**X Channel: 0.219** **Y Channel: 0.263** **Z Channel: 0.018** **Yaw Channel: 0.444** **Roll Channel: 0.013** **Pitch Channel: 0.042**	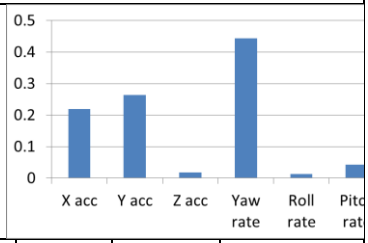		
Sprague-Geer Metrics Values less than or equal to 40 are acceptable.			**M** 2.7	**P** 22.8	**Pass?** **Y**
ANOVA Metrics Both of the following criteria must be met: • The mean residual error must be less than five percent of the peak acceleration ($\bar{e} \le 0.05 \cdot a_{Peak}$) • The standard deviation of the residuals must be less than 35 percent of the peak acceleration ($\sigma \le 0.35 \cdot a_{Peak}$)			**Mean Residual** 3	**Standard Deviation of Residuals** 8.9	**Pass?** **Y**
Exception Notes:					

Phenomena Importance Ranking Tables (PIRT)

The Phenomena Importance Ranking Tables (PIRT) includes evaluation criteria corresponding to *MASH* for TL-3 impacts and is patterned after the full-scale crash test evaluation criteria in MASH. [*AASHTO09*] The values for the individual metrics from the full-scale test and the computer analysis were reported and both the relative difference and absolute difference for each phenomenon were computed. If the relative difference was less than 20 percent, or if the absolute difference was less than 20 percent of the acceptance limit in MASH, then the phenomena are considered to be replicated.

Table 5 contains the MASH crash test criteria. Those that apply to Test 3-11 are marked in red. These include criteria A, D, F, H and I. Table 6 through Table 8 contain an expanded list of these same criteria including additional specific phenomena that were measured in the test and that could be directly compared to the numerical solution. Table 6 contains a comparison of phenomena related to structural adequacy, Table 7 contains a comparison of phenomena related to occupant risk, and Table 8 contains a comparison of phenomena related to vehicle trajectory. Some of this information has already been presented, but is repeated here for convenience.

Table 5. Report 350 crash test criteria with the applicable test numbers.

<table>
<tr><th>Evaluation Factors</th><th colspan="2">Evaluation Criteria</th><th>Applicable Tests</th></tr>
<tr><td rowspan="3">Structural Adequacy</td><td>A</td><td>Test article should contain and redirect the vehicle; the vehicle should not penetrate, under-ride, or override the installation although controlled lateral deflection of the test article is acceptable.</td><td>10, 11, 12, 20, 21, 22, 35, 36, 37, 38</td></tr>
<tr><td>B</td><td>The test article should readily activate in a predictable manner by breaking away, fracturing or yielding.</td><td>60, 61, 70, 71, 80, 81, 82</td></tr>
<tr><td>C</td><td>Acceptable test article performance may be by redirection, controlled penetration or controlled stopping of the vehicle.</td><td>30, 31, 32, 33, 34, 37, 38, 40, 41, 42, 43, 44, 50, 51, 52, 53, 90, 91</td></tr>
<tr><td rowspan="7">Occupant Risk</td><td>D</td><td>Detached elements, fragments or other debris from the test article should not penetrate or show potential for penetrating the occupant compartment, or present an undue hazard to other traffic, pedestrians or personnel in a work zone.
Deformations of, or intrusions into, the occupant compartment should not exceed limits set forth in Section 5.3 and Appendix E of MASH.</td><td>All</td></tr>
<tr><td>E</td><td>Detached elements, fragments or other debris from the test article, or vehicular damage should not block the driver’s vision or otherwise cause the driver to lose control of the vehicle. (Answer Yes or No)</td><td>70, 71, 72</td></tr>
<tr><td>F</td><td>The vehicle should remain upright during and after the collision. The maximum roll and pitch angles are not to exceed 75 degrees.</td><td>All except those listed in criterion G</td></tr>
<tr><td>G</td><td>It is preferable, although not essential, that the vehicle remain upright during and after collision.</td><td>12, 22</td></tr>
<tr><td rowspan="2">H</td><td>Occupant impact velocities should satisfy the following:
<table>
<tr><th colspan="3">Occupant Impact Velocity Limits (m/s)</th></tr>
<tr><th>Component</th><th>Preferred</th><th>Maximum</th></tr>
<tr><td>Longitudinal and Lateral</td><td>9.1</td><td>12.2</td></tr>
</table></td><td>10, 11, 20, 21, 30, 31, 32, 33, 34, 35, 36, 37, 38, 40, 41, 42, 43, 44, 50, 51, 52, 53, 80, 81, 90, 91</td></tr>
<tr><td>Longitudinal 3 4.9</td><td>60, 61, 70, 71, 72</td></tr>
<tr><td>I</td><td>Occupant ridedown accelerations should satisfy the following:
<table>
<tr><th colspan="3">Occupant Ridedown Acceleration Limits (g’s)</th></tr>
<tr><th>Component</th><th>Preferred</th><th>Maximum</th></tr>
<tr><td>Longitudinal and Lateral</td><td>15</td><td>20.49</td></tr>
</table></td><td>10, 11, 20, 21, 30, 31, 32, 33, 34, 35, 36, 37, 38, 40, 41, 42, 43, 44, 50, 51, 52, 53, 80, 81, 90, 91</td></tr>
<tr><td rowspan="3">Vehicle Trajectory</td><td>J</td><td>“Reserved”</td><td></td></tr>
<tr><td>M</td><td>“Reserved”</td><td></td></tr>
<tr><td>N</td><td>Vehicle trajectory behind the test article is acceptable.</td><td>30, 31, 32, 33, 34, 42, 43, 44, 60, 61, 70, 71, 80, 81</td></tr>
</table>

Table 6. Roadside safety phenomena importance ranking table (structural adequacy).

Evaluation Criteria				Known Result	Analysis Result	Difference Relative/ Absolute	Agree?
Structural Adequacy	A	A1	Test article should contain and redirect the vehicle; the vehicle should not penetrate, under-ride, or override the installation although controlled lateral deflection of the test article is acceptable. (Answer Yes or No)	Y	Y		Y
		A2	Maximum dynamic deflection: - Relative difference is less than 20 percent or - Absolute difference is less than 6 inches	41.4 in.	40.4 in.	2.4% 1 in.	Y
		A3	Maximum permanent deflection: - Relative difference is less than 20 percent or - Absolute difference is less than 6 inches	39 in.	40.21 in	3.1% 1.21 in.	Y
		A4	Number of broken or significantly bent posts is less than 20 percent.	0	0		Y
		A5	Did the rail element rupture or tear (Answer Yes or No)	No	No		Y
		A6	Concrete curb/deck failure	No	No		Y
		A7	Was there significant snagging between the vehicle wheels and barrier elements (Answer Yes or No).	No	No		Y
		A8	Was there significant snagging between vehicle body components and barrier elements (Answer Yes or No).	No	No		Y

Table 7. Roadside safety phenomena importance ranking table (occupant risk).

Evaluation Criteria				Known Result	Analysis Result	Difference Relative/ Absolute	Agree?
Occupant Risk	D		Detached elements, fragments or other debris from the test article should not penetrate or show potential for penetrating the occupant compartment, or present an undue hazard to other traffic, pedestrians or personnel in a work zone. (Answer Yes or No)	N	N		Y
	F	F1	The vehicle should remain upright during and after the collision although moderate roll, pitching and yawing are acceptable. (Answer Yes or No)	Y	Y		Y
		F2	Maximum roll of the vehicle through 0.8 seconds: - Relative difference is less than 20 percent or - Absolute difference is less than 5 degrees.	-10.9 deg	-24.9 deg	128.4% 14 deg	N
		F3	Maximum pitch of the vehicle through 0.8 seconds: - Relative difference is less than 20 percent or - Absolute difference is less than 5 degrees.	-3.6 deg	-6.7 deg	86.4% 3.1 deg	Y
		F4	Maximum yaw of the vehicle through 0.8 seconds: - Relative difference is less than 20 percent or - Absolute difference is less than 5 degrees.	45.3 deg	41.2 deg	9.1% 4.1 deg	Y
	H	L	Occupant impact velocities: - Relative difference is less than 20 percent or - Absolute difference is less than 2 m/s.				
		1	• Longitudinal OIV (m/s)	5.7	5.4	5.3% 0.3 m/s	Y
		2	• Lateral OIV (m/s)	-5.3	-4.8	9.4% 0.5 m/s	Y
		3	• THIV (m/s)	7.9	7	11.4% 0.9 m/s	Y
	I		Occupant accelerations: - Relative difference is less than 20 percent or - Absolute difference is less than 4 g's.				
		1	• Longitudinal ORA	-7.1	-7.8	9.9 % 0.7 g	Y
		2	• Lateral ORA	11.1	10.6	4.5 % 0.5 g	Y
		3	• PHD	11.1	11.9	7.2 % 0.8 g	Y
		4	• ASI	1.1	1.09	0.9% .01	Y

Table 8. Roadside safety phenomena importance ranking table (vehicle trajectory).

Evaluation Criteria				Known Result	Analysis Result	Difference Relative/ Absolute	Agree?
Vehicle Trajectory	M	M1	Exit angle at loss of contact: - Relative difference is less than 20 percent or - Absolute difference is less than 5 degrees.	19.9* deg	15.2** Deg	24% 4.7 deg	Y
		M2	Exit velocity at loss of contact: - Relative difference is less than 20 percent or - Absolute difference is less than 6.2 mph.	36.6 mph	40.5** mph	9.9% 3.9 mph	Y
		M3	One or more vehicle tires failed or de-beaded during the collision event (Answer Yes or No).	Y	N.A.		-
		M4	One or more vehicle tires failed or de-beaded during the collision event (Answer Yes or No).	Y	N.A.		-

* Result from test data at 0.8 seconds (for direct correlation with analysis)
** Result from FEA at 0.8 seconds (analysis termination time)

Comparisons for all the applicable crash specific phenomena between the FEA and test were within the allowable limits of Report W179, except for the item F2 (i.e., maximum roll angle). The roll angle in the FEA was notably higher than the roll angle that occurred in the full-scale test. It was not clear what the cause of this difference was related to. The test vehicle was a Dodge Ram and the model vehicle was based on a Chevrolet; however, the mass and c.g. of the two vehicles were very similar (refer to Figure 19). However, the model correlates well to the test in all other respects. The results from the model were therefore considered to be valid, although somewhat conservative for this impact scenario with the CRTS barrier.

Damage to the Barrier System

The initial and final deformed state of the barrier from the analysis is shown in Figure 27 illustrating the extent of the deflection as well as the post-impact trajectory of the vehicle. Figure 28 shows a plot of barrier deflections versus barrier segment location for both the test and FEA relative to the VLB barrier position (note that the centerline of the vehicle is aligned with the center of the VLB element). The blue bars in the plot represent the deflections reported from the test (deflections were only recorded for those shown); the yellow bars represent those from the FEA. The barrier deflections from the FEA were very similar to those of the full-scale test. In both the test and FEA the maximum deflection was 39 inches and 40 inches, respectively, and occurred at barrier segment "+3" which was the 5th barrier segment downstream of the impact point. This corresponded to a 3 percent error. The most notable difference was at barrier segment "+10" with 19 percent error; however, this barrier was still moving laterally at the termination of the analysis at 0.8 seconds. Figure 29 shows a comparison of the final longitudinal deflections of the upstream and downstream ends of the barrier. The maximum movement at the upstream end was 1.6 inches in the FEA, compared to 1.4 inches in the test. The maximum movement at the downstream end was 0.6 inches in the FEA, compared to 1.0 inch in the test.

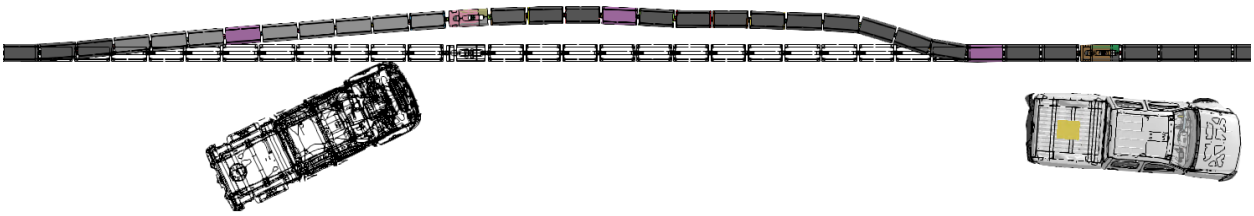

Figure 27. Overlay of initial and final state of analysis illustrating barrier deflection and vehicle trajectory.

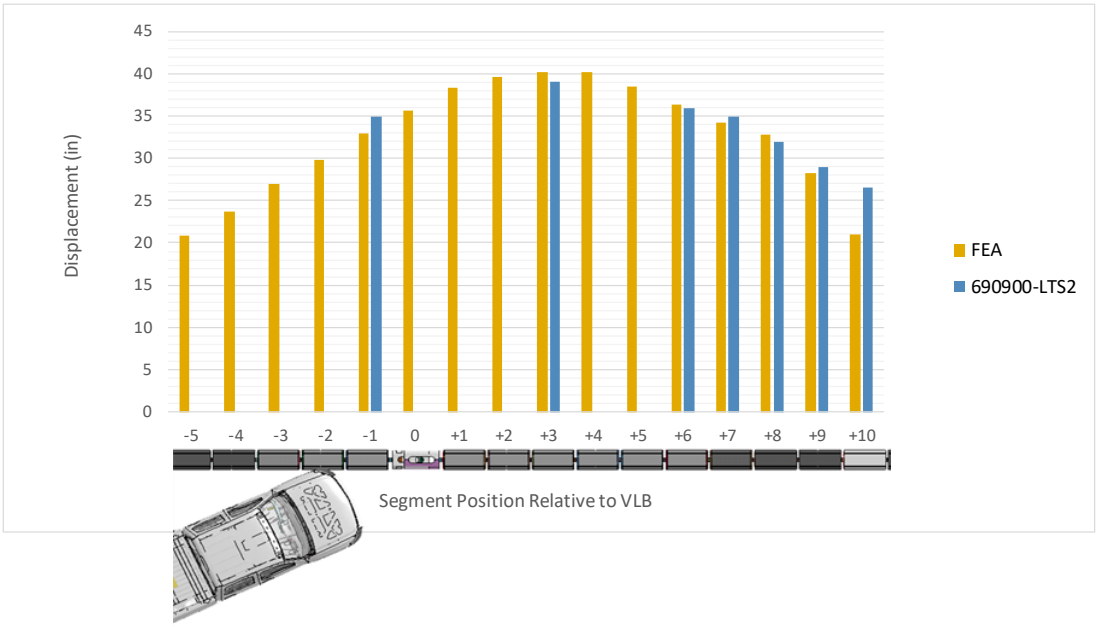

Figure 28. Final lateral deflection of the barrier segments in the impact region.

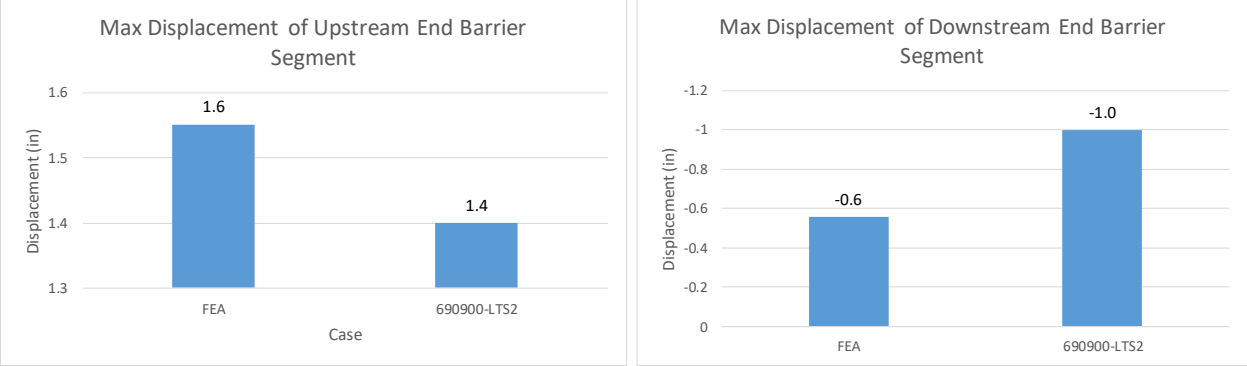

Figure 29. Comparison of the final longitudinal deflections of the upstream and downstream ends of the barrier from the test and FEA.

There was also minor spalling of the concrete at the edges of the barrier segments in the impact region as the barrier segments hinged and pressed against each other. This damage resulted in erosion of the elements in the FEA, as shown in Figure 30 (refer to the yellow shaded portion of CRTS segment in the image). The hinge-pin between barrier segments "+1" and "+2"

also experience permanent deformation in the FEA; no damage to the pins were reported in the full-scale test.

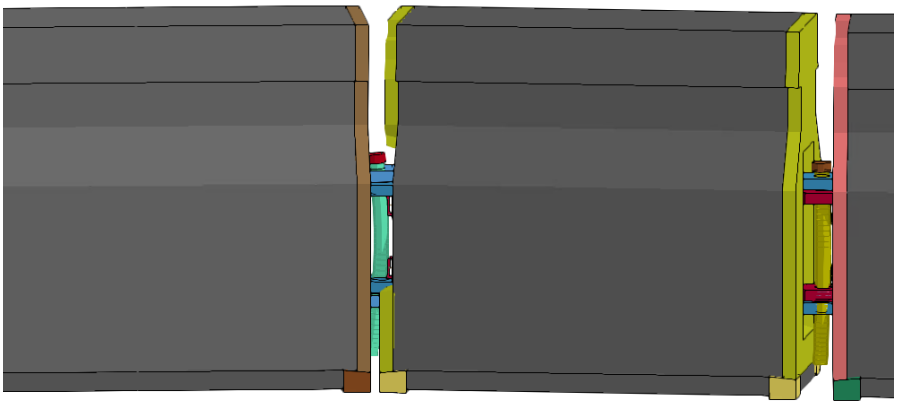

Figure 30. Permanent deformation of the pin at the hinge-joint between barrier segments "+1" and "+2" in the FEA.

Summary

The baseline finite element model of the CRTS was used to simulate full-scale crash test 690900-LTS2; which corresponded to MASH Test 3-11. The validation included both qualitative and quantitative elements. Qualitative assessments included comparing sequential snapshots of the test and simulation to verify vehicle kinematic response, as well as, the sequence and timing of key phenomenological events. The quantitative assessment was performed according to the procedures specified in NCHRP Web Report 179. These procedures included: (1) verifying that the analysis solution was stable and obeying basic laws of physics, (2) point-by-point comparison of the acceleration and angular-rate time-history data form the FEA and test (collected from accelerometers and rate gyros placed on-board the vehicle) using the RSVVP software, and (3) comparison of crash-specific phenomena from the event related to structural adequacy, occupant risk and vehicle trajectory.

In general, the results of the analyses demonstrated that the finite element model replicated the basic phenomenological behavior of the system under MASH Test 3-11 conditions. The response of the barrier, in particular, showed good agreement between the analysis and test; while the response of the vehicle differed only slightly. There was good agreement between the tests and the simulations with respect to event timing, overall kinematics of the vehicle, barrier damage, and deflections. Quantitative comparison of the time-history data indicated that the finite element model sufficiently replicated the results of the full-scale crash tests. The most notable discrepancy was related to the roll angle, which was higher in the FEA (i.e., 25 vs. 11 degrees). The results from the model were considered to be valid, although somewhat conservative regarding the roll angle for this impact scenario with the CRTS barrier. The model is further considered to be valid for assessing the effects of impact location on barrier performance. Table 9 provides a summary of key validation metrics for the evaluation of the model for Test 3-11.

Table 9. Summary of validation metrics for the FEA model compared to Test 690900-LTS2.

Summary of FEA vs. Test Validation Metrics

System Type:	PCB	Comparison:	Crash tested original design to FEA of original design
Device Name:/Variant:	CRTS	Submissions Type:	Non-Significant -- Effect is Uncertain
Testing Criterion:	MASH		Non-Significant -- Effect is Positive
Test Level:	TL3		Non-Significant -- Effect is Inconsequential
FHWA Letter:		X	Baseline Validation of Crash Test to FEA Analysis.

Crash Test


Time = 0.0 sec


0.2 sec


0.4 sec


0.6 sec


0.8 sec

FEA Analysis

Baseline Crash Test			W-179 Table E-5: Roadside PIRTS					
Test Number:	TTI 690900-LTS2		**Structural Adequacy**	**Test**	**FEA**	**Occupant Risk (cont.)**	**Test**	**FEA**
Vehicle:	2009 Dodge Ram 1500		A1 - Acceptable perf.?	yes	yes	H2 – Long. OIV	5.7 m/s	5.4 m/s
Vehicle Mass:	4,928 lb		A2 – Permanent Deflection:	39 in	40.2 in	H3 – Lat. OIV	5.3 m/s	4.8 m/s
Impact Speed:	62.6 mph		A3 – Contact Length			I2 – Long. ORA	7.1 g	7.8 g
Impact Location:	Midspan of Barrier Segment 84		A4 - Component Failure	no	no	I3 – Lat. ORA	11.2 g	10.6 g
Tested Hardware:	CRTS		A5 – Barrier Rupture?	no	no	**Vehicle Trajectory**		
FEA Hardware:	CRTS		A7 – Wheel Snagging?	no	no	K – Intruded into travel lanes?	no	no
W-179 Table E-1: Verification Evaluation Summary			A8 – Vehicle Snagging?	no	no	N – Travel behind barrier?	no	no
Total Energy:	0.3%	Pass	**Occupant Risk**	**Test**	**FEA**	**W-179 Table E-3 (Multi-Channel Method)**		
Hourglass Energy:	4.5%	Pass	D – Detached elements?	no	no	Sprague-Geer Magnitude < 40	22.7	Pass
Mass Added:	0%	Pass	F2 – Max. Vehicle Roll	11	25	Sprague-Geer Phase < 40	22.8	Pass
Shooting Nodes:	no	Pass	F3 – Max. Vehicle Pitch	3.6	6.7	ANOVA Mean	3	Pass
Negative Volumes:	no	Pass	F4 – Max. Vehicle Yaw	45.3	41.2	ANOVA Standard Deviation	18.9	Pass

BARRIER PERFORMANCE VS. IMPACT POINT LOCATION

The validated model was then used to evaluate the crash performance of the system for various impact locations approaching the leading and trailing ends of the barrier; including impact points at barrier segments 18, 28, 38, 58 and 85 relative to the upstream end of the barrier; and impact points at barrier segments 18, 28, 38, and 58 relative to the downstream end of the system. Note that the barrier model included 170 barrier segments (consistent with the tested system length), thus barrier segment 85 represents the midpoint of the system. Two barrier system cases were evaluated:

- Case 1 – 170 CRTS barrier segments with no VLB elements included in the barrier system.
- Case 2 – 168 CRTS barrier segments and two (2) VLB elements, consistent with the crash tested system. One VLB was positioned at 1.5 m downstream of the impact point and a second VLB was positioned at 17 m further downstream.

All analyses were conducted using the non-linear, explicit finite element code, LS-DYNA version MPP s R8.0.0 Revision 95309 on 32 cores. The results of the analyses are presented herein, in terms of maximum permanent lateral deflection of the system, maximum longitudinal movement of the barrier segments on the upstream and downstream ends, occupant risk metrics, occupant compartment intrusion, vehicle stability, and vehicle trajectory. The nomenclature used to identify each the analysis case in the figures and tables includes:

- "L" followed by "system length"
- "IP" followed by "impact point based on barrier position relative to the upstream end of the system"
- For cases on the trailing end of the system, "T" followed by "barrier position relative to the downstream end of the system"

For example, L170_IP28 corresponds to the analysis case involving impact on the upstream end of the system at Barrier Segment 28. Likewise, L170_IP159_T28 corresponds to the analysis case involving impact on the downstream end of the system at Barrier Segment 159 counting from the upstream end, which is the 28th barrier segment from the downstream trailing end. For the cases including the two VLB elements, the nomenclature will also include VLB at the end of the Case ID (e.g., L170_IP159_T28_VLB).

In all cases the impact occurs at the mid-length of the identified barrier segment. In all cases without VLB's, the 5006-lb Silverado model struck the barrier at a speed and angle of 63 mph and 25 degrees, respectively, which corresponds to an impact severity of 118,535 ft-lb. In all cases including the two VLB's, the impact speed and angle was 62.6 mph and 25.4 degrees (i.e., consistent with tested conditions), which corresponded to an impact severity of 120,559 ft-lb. The analysis matrices for the two study cases are shown in Table 10 and Table 11.

Table 10. Case 1 analysis matrix for the QMB study with all CRTS.

Impact Cases on the Leading End of the System

Case ID	Number of Barrier Segments from Upstream End	Impact Conditions			
		Vehicle	Weight (lbs)	Speed (mph)	Angle (deg)
L170_IP85	85	Silverado	5006	63	25
L170_IP58	58	Silverado	5006	63	25
L170_IP38	38	Silverado	5006	63	25
L170_IP28	28	Silverado	5006	63	25
L170_IP18	18	Silverado	5006	63	25

Impact Cases on the Trailing End of the System

Case ID	Number of Barrier Segments from Downstream End	Impact Conditions			
		Vehicle	Weight (lbs)	Speed (mph)	Angle (deg)
L170_IP113_T58	58	Silverado	5006	63	25
L170_IP133_T38	38	Silverado	5006	63	25
L170_IP143_T28	28	Silverado	5006	63	25
L170_IP159_T18	18	Silverado	5006	63	25
L170_IP159_T12	12	Silverado	5006	63	25

Table 11. Case 2 analysis matrix for the QMB study including VLB's.

Impact Cases on the Leading End of the System

Case ID	Number of Barrier Segments from Upstream End	Impact Conditions			
		Vehicle	Weight (lbs)	Speed (mph)	Angle (deg)
L170_IP85_VLB	85	Silverado	5006	62.6	25.4
L170_IP58_VLB	58	Silverado	5006	62.6	25.4
L170_IP38_VLB	38	Silverado	5006	62.6	25.4
L170_IP28_VLB	28	Silverado	5006	62.6	25.4
L170_IP18_VLB	18	Silverado	5006	62.6	25.4

Impact Cases on the Trailing End of the System

Case ID	Number of Barrier Segments from Downstream End	Impact Conditions			
		Vehicle	Weight (lbs)	Speed (mph)	Angle (deg)
L170_IP113_T58_VLB	58	Silverado	5006	62.6	25.4
L170_IP133_T38_VLB	38	Silverado	5006	62.6	25.4
L170_IP143_T28_VLB	28	Silverado	5006	62.6	25.4
L170_IP159_T18_VLB	18	Silverado	5006	62.6	25.4

Case 1 – QMB with Only CRTS Elements

Case 1 - Impacts on the Leading End of the System

Case 1 -Lateral Displacement

Sequential views showing a comparison of the impact cases on the leading end of the system are provided in Appendix D. Figures 31 through 35 show plots of final lateral displacement for several of the barrier segments located in the immediate impact region of the system for each analysis cases. A summary of maximum deflection versus impact location is shown in Figure 36. As the impact point gets nearer and nearer to the upstream end of the system the maximum lateral displacement of the barrier increases according the cubic polynomial defined by:

$$Max\ Lateral\ Deflection = -0.00018x^3 + 0.0416x^2 - 3.244x + 121.6$$

The inflection point for the barrier-deflection curve was obtained by taking the derivative of the curve and setting it equal to zero, which yielded a value of 73. This value represents the midpoint for the critical system length; thus, the critical system length for MASH Test 3-11 is 146 barrier segments or 479 feet with a maximum lateral deflection of approximately 36 inches.

Note that the impact conditions for these cases differ slightly from that of the validation case (i.e., 62.4 mph and 25.4 degrees and no VLB elements). The result is a slightly lower impact severity and a higher mass of the barrier in the impact region, which results in lower lateral deflections for this case compared to the validation case (e.g., 36 inches versus 39 inches).

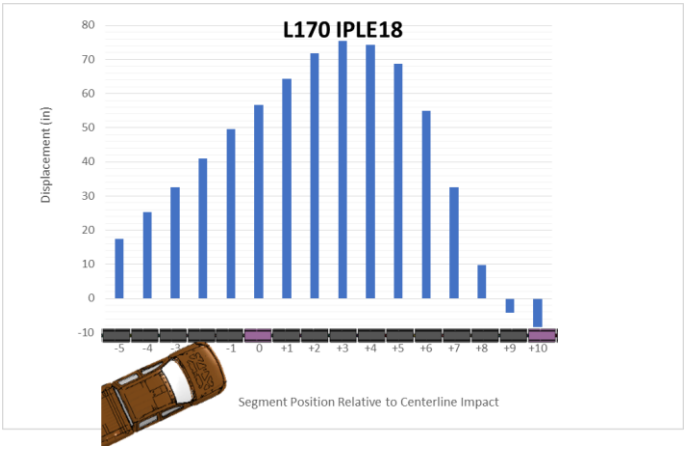

Figure 31. Case 1 – Leading End: Lateral deflection of individual barrier segments in the impact region of the CTRS system for impact at Barrier Segment 18.

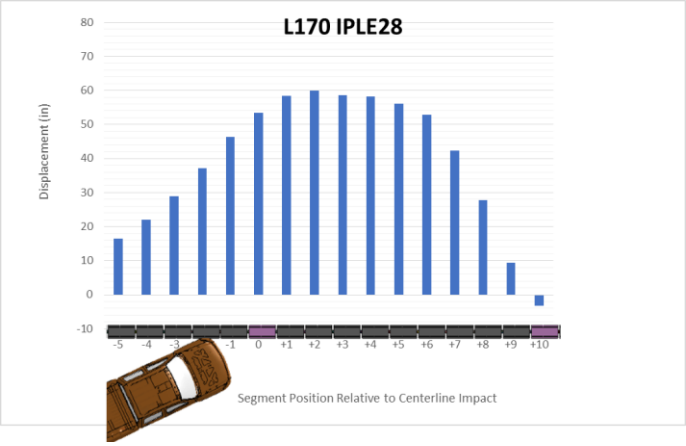

Figure 32. Case 1 – Leading End: Lateral deflection of individual barrier segments in the impact region of the CTRS system for impact at Barrier Segment 28.

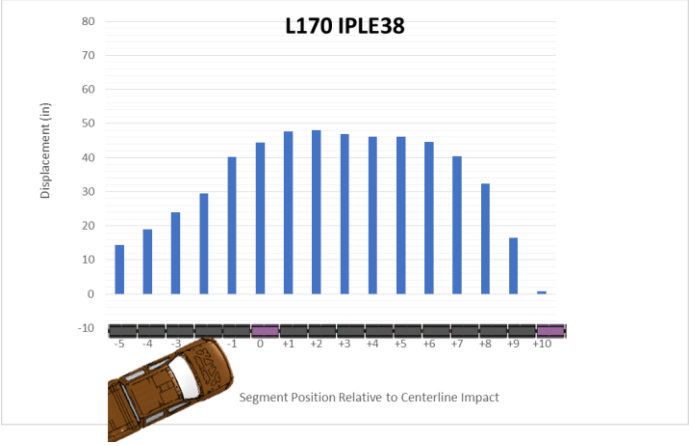

Figure 33. Case 1 – Leading End: Lateral deflection of individual barrier segments in the impact region of the CTRS system for impact at Barrier Segment 38.

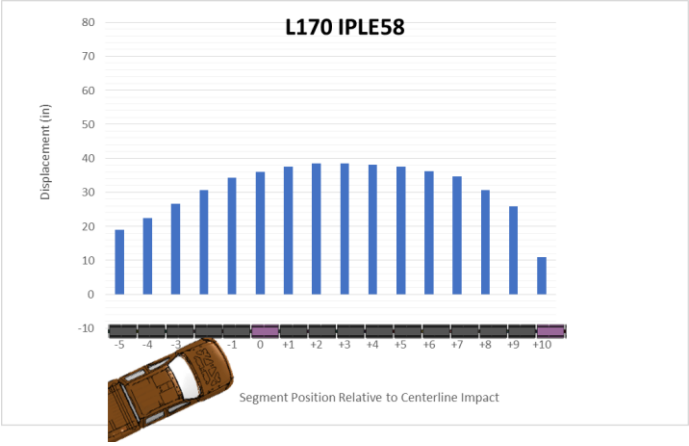

Figure 34. Case 1 – Leading End: Lateral deflection of individual barrier segments in the impact region of the CTRS system for impact at Barrier Segment 58.

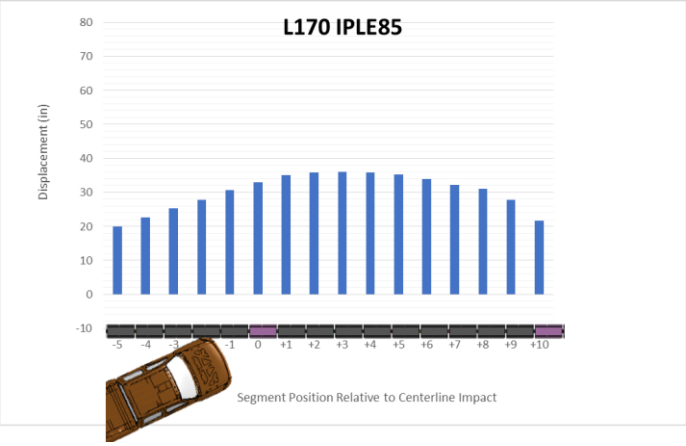

Figure 35. Case 1 – Leading End: Lateral deflection of individual barrier segments in the impact region of the CTRS system for impact at Barrier Segment 85 (LON case).

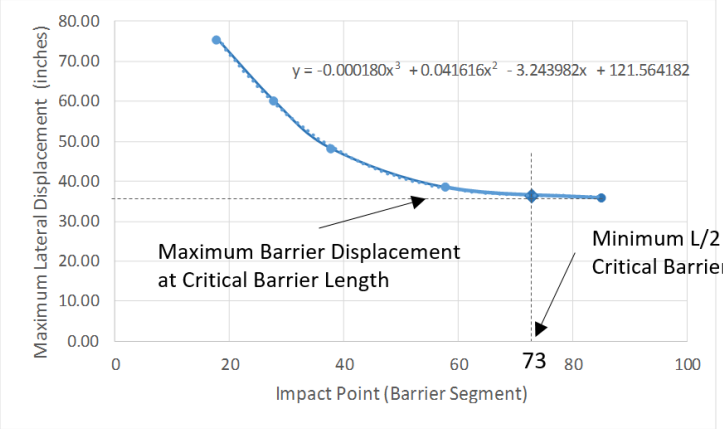

Figure 36. Case 1 – Leading End: Plot of maximum lateral displacement versus impact point.

Case 1 - Longitudinal Displacement

The maximum longitudinal displacement at the upstream and downstream ends of the system for each case is shown in Figure 37. As would be expected, the longitudinal displacement of the upstream barrier increased significantly as the impact point got nearer and nearer to the end of the barrier. At Impact Point 18 the maximum longitudinal displacement of the upstream end barrier was 26.7 inches; at Impact Point 85 the upstream displacement was 1.6 inches. On the downstream end, the movement of the barrier was negligible for all cases except for impact at Barrier Segment 85, which resulted in 0.28 inches of displacement.

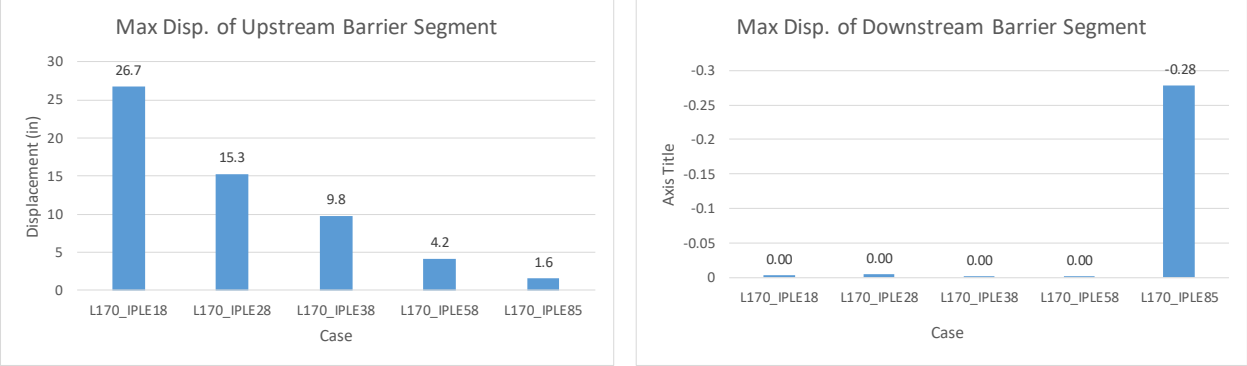

Figure 37. Case 1 – Leading End: Maximum longitudinal displacement at the upstream and downstream ends of the barrier.

Case 1 - Time-History Data

Figure 38 shows a comparison of the 10-millisecond moving average and the 50-millisecond moving average acceleration-time history at the c.g. of the vehicle for the longitudinal, transverse and vertical channels. Figure 39 shows comparisons of the angular rates and angular displacements (i.e., yaw, roll, and pitch) at the c.g. of the vehicle. For impact at Barrier Segment 28 and higher on the leading end of the system, the results showed that *impact location* had minimal effect on vehicle accelerations, attitude or trajectory. The vehicle response at the beginning of the crash event for impact at Barrier Segment 18 was also identical to the other impact cases, and began to diverge after about 0.25 seconds of the event. The difference was due to a much greater displacement of the barriers for that case, which resulted in the rear of the vehicle contacting the barrier much later in the event. The magnitude of the accelerations was similar, but vehicle instability was a concern as the roll angle was greater than 50 degrees and increasing at the termination of the analysis.

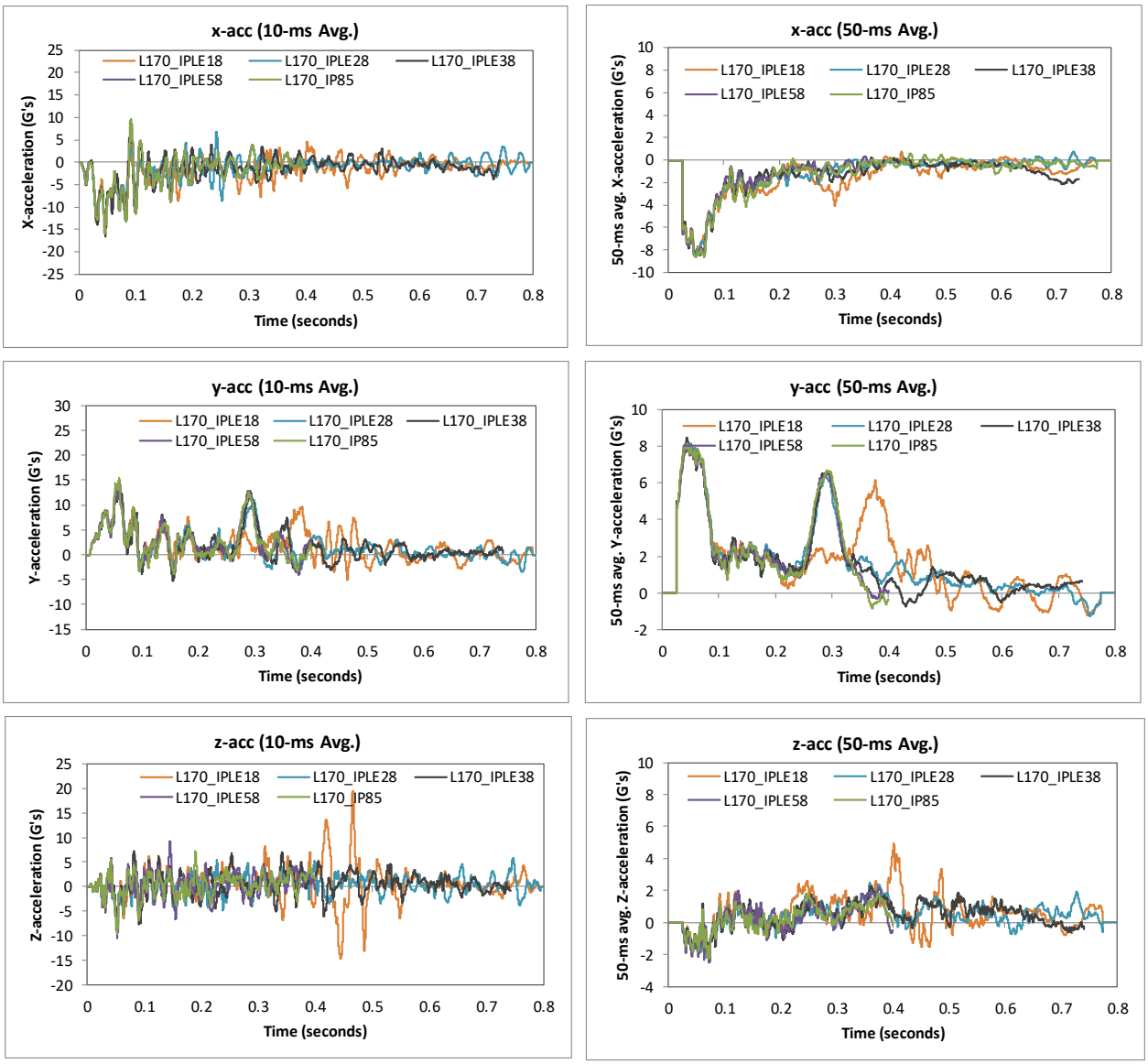

Figure 38. Case 1 – Leading End: Comparison of acceleration-time histories for MASH Test 3-11 impact conditions.

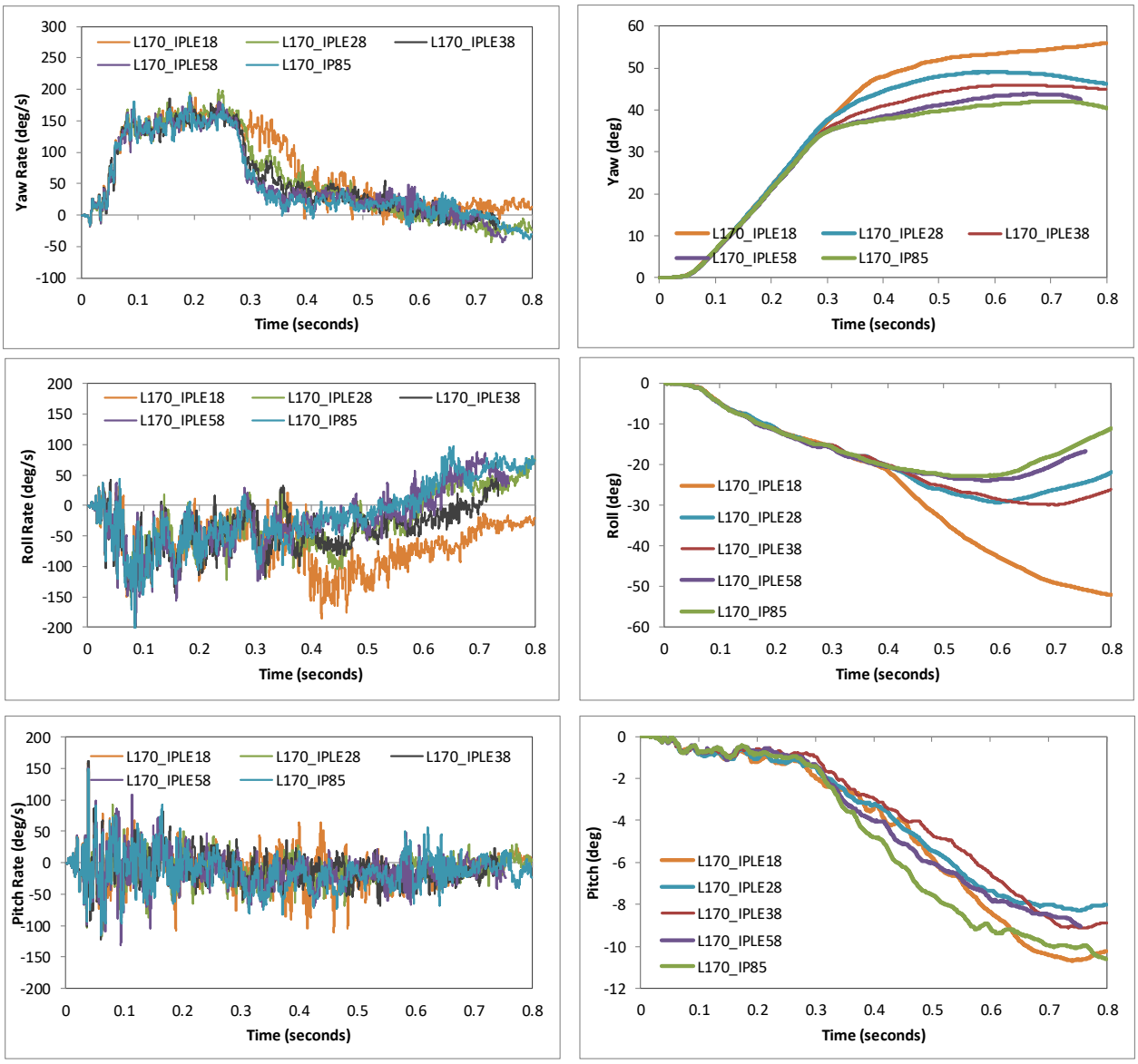

Figure 39. Case 1 – Leading End: Comparison of angular rate and displacement time histories for MASH Test 3-11 impact conditions.

Case 1 - Occupant Risk Measures

Table 12 and Figure 40 show summaries of the occupant risk measures for each of the leading-end analysis cases. The results indicated that the occupant impact velocities (OIV) were essentially identical for all analysis cases, with OIV in the longitudinal direction ranging from 17.7 ft/s (5.4 m/s) to 18.4 ft/s (5.6 m/s) and OIV in the lateral direction ranging from 16.7 ft/s (5.1 m/s) to 17.7 (5.4 m/s). The occupant ridedown acceleration (ORA) in the x-direction was also similar for all cases with values generally ranging from 8.2 g to 8.9 g, with the exception of the impact case at barrier 58, which resulted in ORA-x of 6.4 g. The ORA in the lateral direction tended to decrease as the impact point got closer to the upstream end of the system; likely due to the barriers moving away from the vehicle as the rear of the vehicle made contact during yaw

and redirection. In all cases, the OIV and ORA values were with recommended limits (i.e., ORA < 9 m/s and ORA < 15 g).

The values for the post-head deceleration (PHD) and the acceleration severity index, metrics computed as part of the European Committee for Standardization (CEN), are also shown in Table 12 and Figure 40. The PHD values followed closely with the ORA-y with values decreasing as the impact point moved closer to the upstream end. The ASI values were essentially equivalent for all cases with a value of 1.11 to 1.14.

Case 1 - Occupant Compartment Intrusion

According to MASH, acceptable limits of occupant compartment deformation varies by the region of the occupant compartment as follows:

- Roof ≤ 4.0 inches
- Windshield – no tear of plastic liner and maximum deformation of 3 inches
- Window – no shattering of a side window resulting from direct contact with a structural member of the test article
- Wheel/foot well and toe pan areas ≤ 9 inches
- Side front panel (forward of A-Pillar) ≤ 12 inches
- Front side door area (above seat) ≤ 9 inches
- Front side door area (below seat) ≤ 12 inches
- Floor pan and transmission tunnel areas ≤ 12 inches

The occupant compartment deformations were within critical values in all cases except for impact at Barrier Segment 18. In that case, there was a direct impact of the door on the corner of one of the barrier segment during yaw and redirection which resulted in 10.4 inches of intrusion to the door above the seat, as illustrated in Figure 41, which exceeds the limit of 9 inches specified in MASH.

Table 12. Case 1 – Leading End: Comparison of occupant risk measures for MASH Test 3-11 impact conditions.

Occupant Risk Factors		MASH 3-11				
		L170_IPLE18	L170_IPLE28	L170_IPLE38	L170_IPLE58	L170_IP85
Occupant Impact Velocity (m/s)	x-direction	5.4	5.5	5.5	5.5	5.6
	y-direction	-5.3	-5.4	-5.2	-5.1	-5.3
	at time	at 0.1041 seconds on left side of interior	at 0.1035 seconds on left side of interior	at 0.1039 seconds on left side of interior	at 0.1046 seconds on left side of interior	at 0.1036 seconds on left side of interior
THIV (m/s)		7.5 at 0.1041 seconds on left side of interior	7.6 at 0.1035 seconds on left side of interior	7.6 at 0.1039 seconds on left side of interior	7.6 at 0.1046 seconds on left side of interior	7.8 at 0.1036 seconds on left side of interior
Ridedown Acceleration (g's)	x-direction	-8.6 (0.1696 - 0.1796 seconds)	-8.6 (0.2469 - 0.2569 seconds)	-8.2 (0.1558 - 0.1658 seconds)	-6.4 (0.1268 - 0.1368 seconds)	-8.9 (0.1562 - 0.1662 seconds)
	y-direction	9.6 (0.3794 - 0.3894 seconds)	11 (0.2932 - 0.3032 seconds)	12.8 (0.2862 - 0.2962 seconds)	12.7 (0.2834 - 0.2934 seconds)	12.5 (0.2847 - 0.2947 seconds)
PHD (g's)		9.9 (0.3791 - 0.3891 seconds)	11.1 (0.2930 - 0.3030 seconds)	12.9 (0.2862 - 0.2962 seconds)	13.1 (0.2828 - 0.2928 seconds)	12.7 (0.2846 - 0.2946 seconds)
ASI		1.11 (0.0245 - 0.0745 seconds)	1.15 (0.0233 - 0.0733 seconds)	1.14 (0.0254 - 0.0754 seconds)	1.14 (0.0204 - 0.0704 seconds)	1.14 (0.0257 - 0.0757 seconds)
Max 50-ms moving avg. acc. (g's)	x-direction	-8.3 (0.0237 - 0.0737 seconds)	-8.4 (0.0225 - 0.0725 seconds)	-8.5 (0.0246 - 0.0746 seconds)	-8.5 (0.0216 - 0.0716 seconds)	-8.7 (0.0239 - 0.0739 seconds)
	y-direction	8.3 (0.0184 - 0.0684 seconds)	8.3 (0.0188 - 0.0688 seconds)	8.5 (0.0187 - 0.0687 seconds)	8.2 (0.0190 - 0.0690 seconds)	8.1 (0.0192 - 0.0692 seconds)
	z-direction	4.9 (0.3768 - 0.4268 seconds)	-2.5 (0.0473 - 0.0973 seconds)	-2.4 (0.0481 - 0.0981 seconds)	-2.4 (0.0481 - 0.0981 seconds)	-2.3 (0.0477 - 0.0977 seconds)
Maximum Angular Disp. (deg)	Roll	-52.1 (0.7996 seconds)	-29.3 (0.5938 seconds)	-29.9 (0.6997 seconds)	-24 (0.5781 seconds)	-22.9 (0.5467 seconds)
	Pitch	-10.7 (0.7405 seconds)	-8.3 (0.7515 seconds)	-9.1 (0.7547 seconds)	-9.1 (0.7543 seconds)	-10.6 (0.7996 seconds)
	Yaw	55.9 (0.7996 seconds)	49 (0.6136 seconds)	46 (0.6436 seconds)	43.8 (0.6598 seconds)	42.1 (0.7088 seconds)

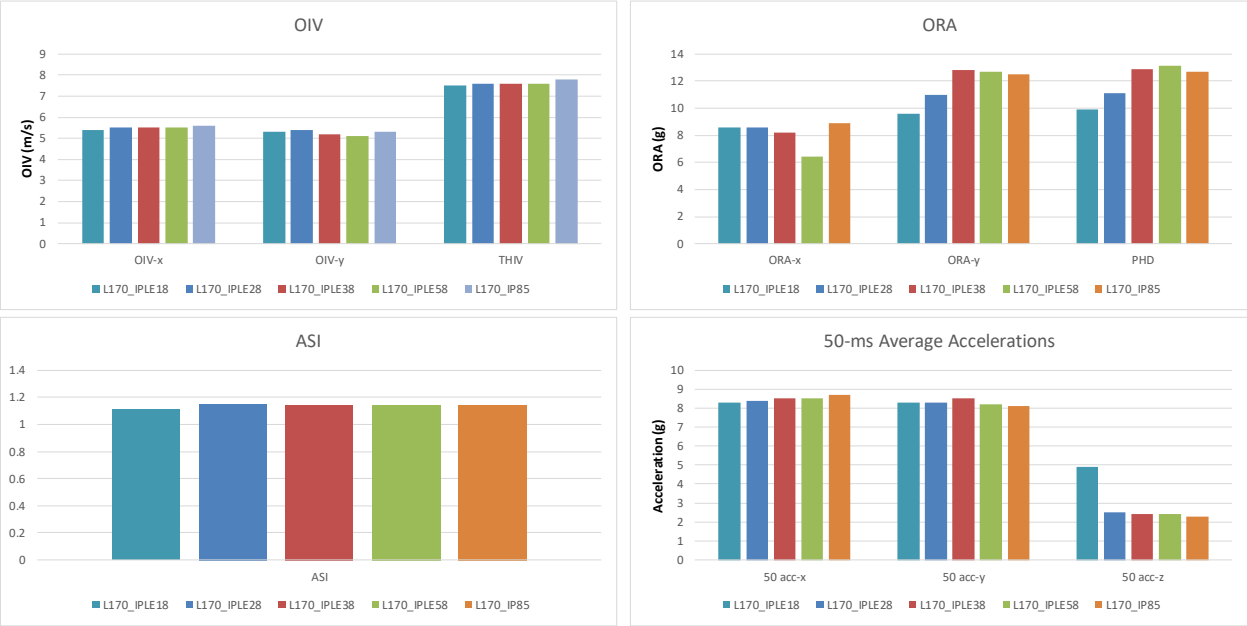

Figure 40. Case 1 – Leading End: Comparison of occupant risk measures for MASH Test 3-11 impact conditions.

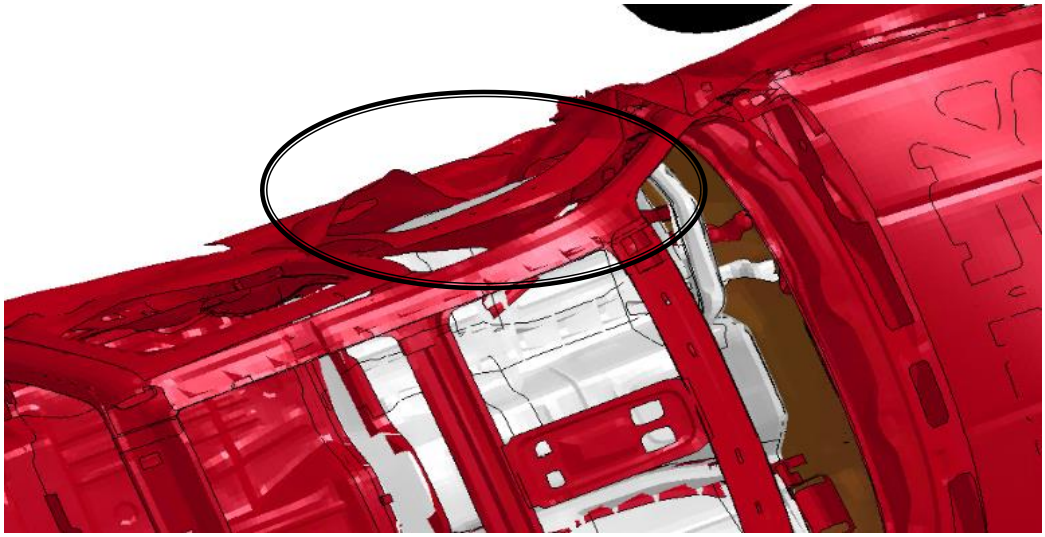

Figure 41. Case 1 – Leading End: Occupant compartment deformation for the analysis case with impact at Barrier Segment 18.

Case 1 - Impacts on the Trailing End of the System

Case 1 - Lateral Displacement

Sequential views showing a comparison of the impact cases on the trailing end of the system are provided in Appendix E. Figures 42 through 46 show plots of final lateral displacement for barrier segments located in the immediate impact region of the system for each

analysis cases. A summary of maximum deflection versus impact location is shown in Figure 47. The maximum deflection at impact points 85, 58, 38 and 28 fit well to the cubic polynomial:

$$Max\ Lateral\ Deflection = -0.000065x^3 - 0.00368x^2 - 0.564x + 70.8$$

When the impact point was nearer to the trailing end of the system (e.g., at Segment 18), the lateral deflection increased significantly and no longer fit the trend curve. The inflection point for the barrier-deflection curve was obtained by taking the derivative of the trend curve and setting it equal to zero, which yielded a value of 76 barrier segments. This value represents the minimum point from the trailing end for which the lateral deflections will be at a minimum. Thus, the system length used in these analyses (i.e., 170 barrier segments) is sufficient for achieving minimum lateral system deflection under MASH Test 3-11 impact conditions.

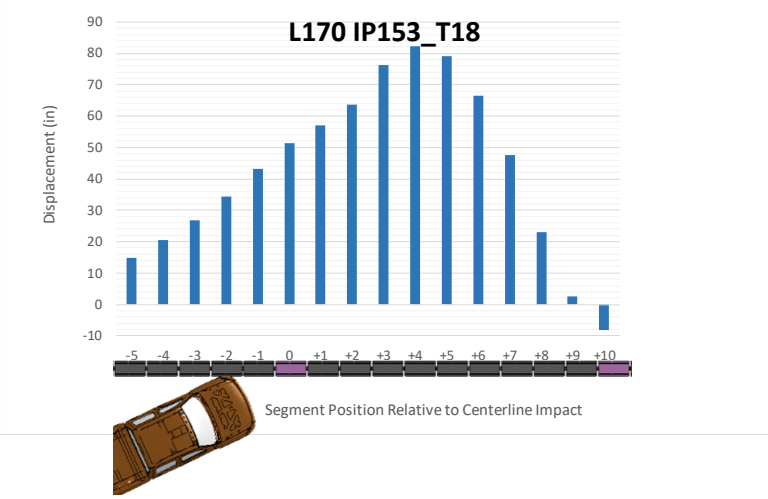

Figure 42. Case 1 – Trailing End: Lateral deflection of individual barrier segments in the impact region of the CTRS system for impact at Barrier Segment 18.

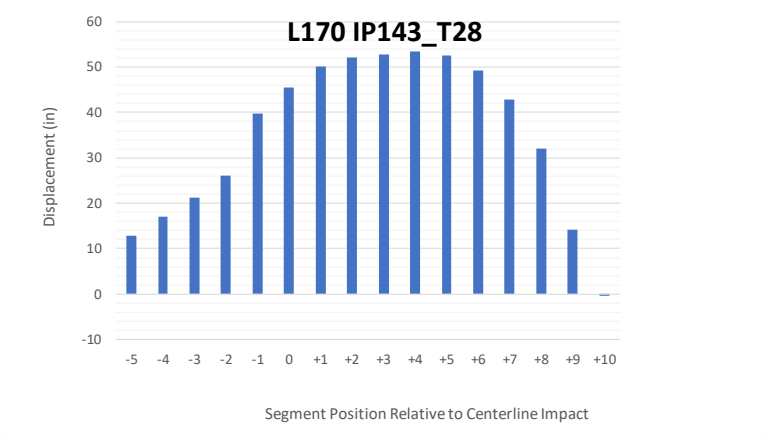

Figure 43. Case 1 – Trailing End: Lateral deflection of individual barrier segments in the impact region of the CTRS system for impact at Barrier Segment 28.

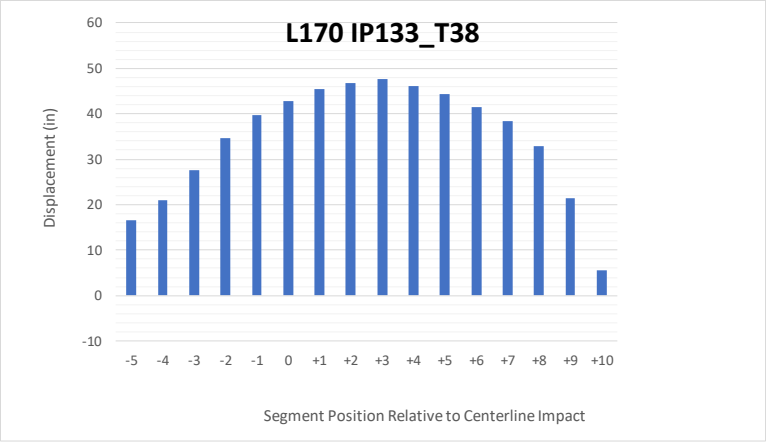

Figure 44. Case 1 – Trailing End: Lateral deflection of individual barrier segments in the impact region of the CTRS system for impact at Barrier Segment 38.

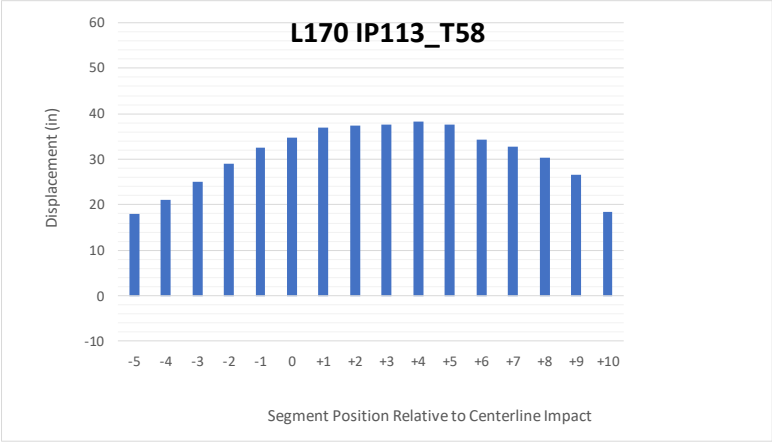

Figure 45. Case 1 – Trailing End: Lateral deflection of individual barrier segments in the impact region of the CTRS system for impact at Barrier Segment 58.

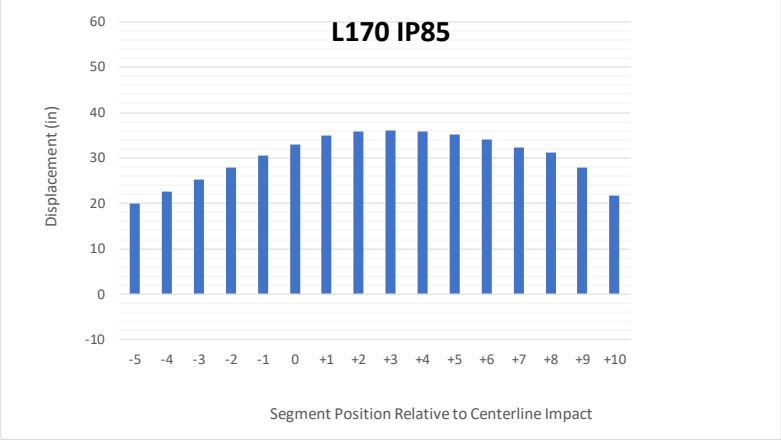

Figure 46. Case 1 – Trailing End: Lateral deflection of individual barrier segments in the impact region of the CTRS system for impact at Barrier Segment 85 (LON case).

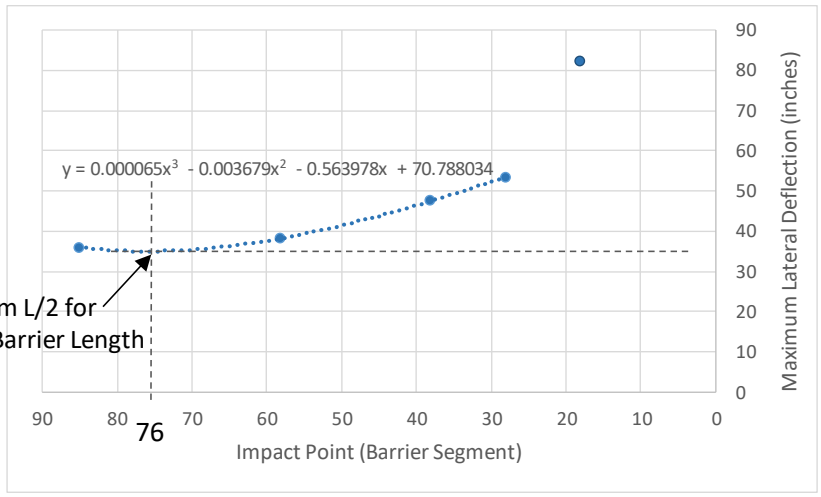

Figure 47. Case 1 – Trailing End: Plot of maximum lateral displacement versus impact point.

Case 1 -Longitudinal Displacement

The maximum longitudinal displacement at the upstream and downstream ends of the system for each case is shown in Figure 48. On the upstream end, the movement of the barrier was negligible for all cases except for impact at Barrier Segment 85, which resulted in 1.55 inches of displacement. The longitudinal displacement of the downstream barrier, however, increased significantly as the impact point got nearer and nearer to the downstream end of the barrier. At Impact Point 18 the maximum longitudinal displacement of the end barrier was 30.4 inches; at Impact Point 85 the downstream displacement was 0.28 inches.

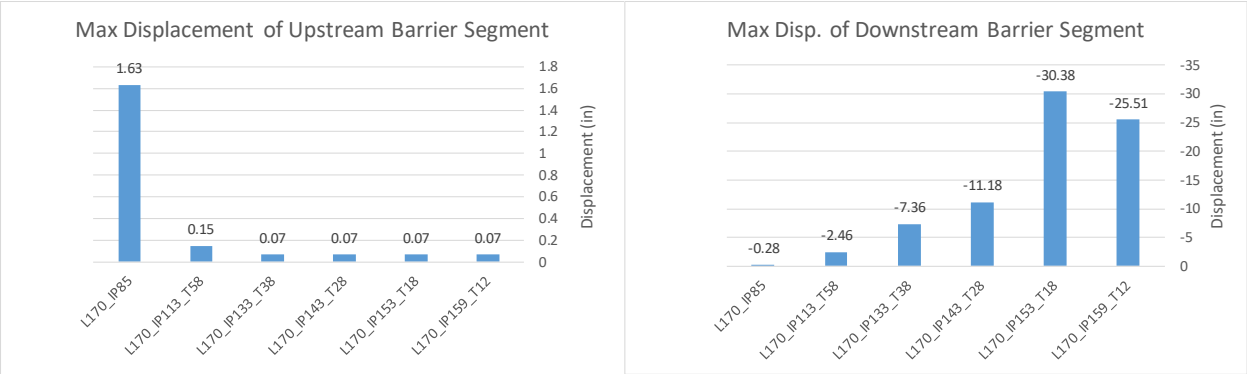

Figure 48. Case 1 – Trailing End: Maximum longitudinal displacement at the upstream and downstream ends of the barrier.

Case 1 - Time-History Data

Figure 49 shows a comparison of the 10-millisecond moving average and the 50-millisecond moving average acceleration-time history at the c.g. of the vehicle for the longitudinal, transverse and vertical channels. Figure 50 shows comparisons of the angular rates and angular displacements (i.e., yaw, roll, and pitch) at the c.g. of the vehicle. For impact at Barrier Segment 38 and higher on the trailing end of the system, the results showed that *impact location* had minimal effect on vehicle accelerations, attitude or trajectory. The vehicle response at the beginning of the crash event for impact at Barrier Segment 18 and at Barrier Segment 12

was also identical to the other impact cases, and then began to diverge after about 0.25 seconds. As with the leading end cases, the difference was due to a much greater displacement of the barriers which resulted in the rear of the vehicle contacting the barrier later in the event. For the case involving impact at Barrier Segment 12, there was a significantly higher acceleration in the x-direction which was caused by excessive damage and snagging on the door of the vehicle against the barrier (see Figure 51). The magnitude of the y-accelerations decreased as impact point got nearer to the downstream end; however, vehicle instability became more likely as the roll angle tended to increase for those cases. The roll angle for impact at Barrier Segments 18 and 12 was 52 degrees and 41 degrees, respectively, and was still increasing at the termination of the analysis at 0.8 seconds.

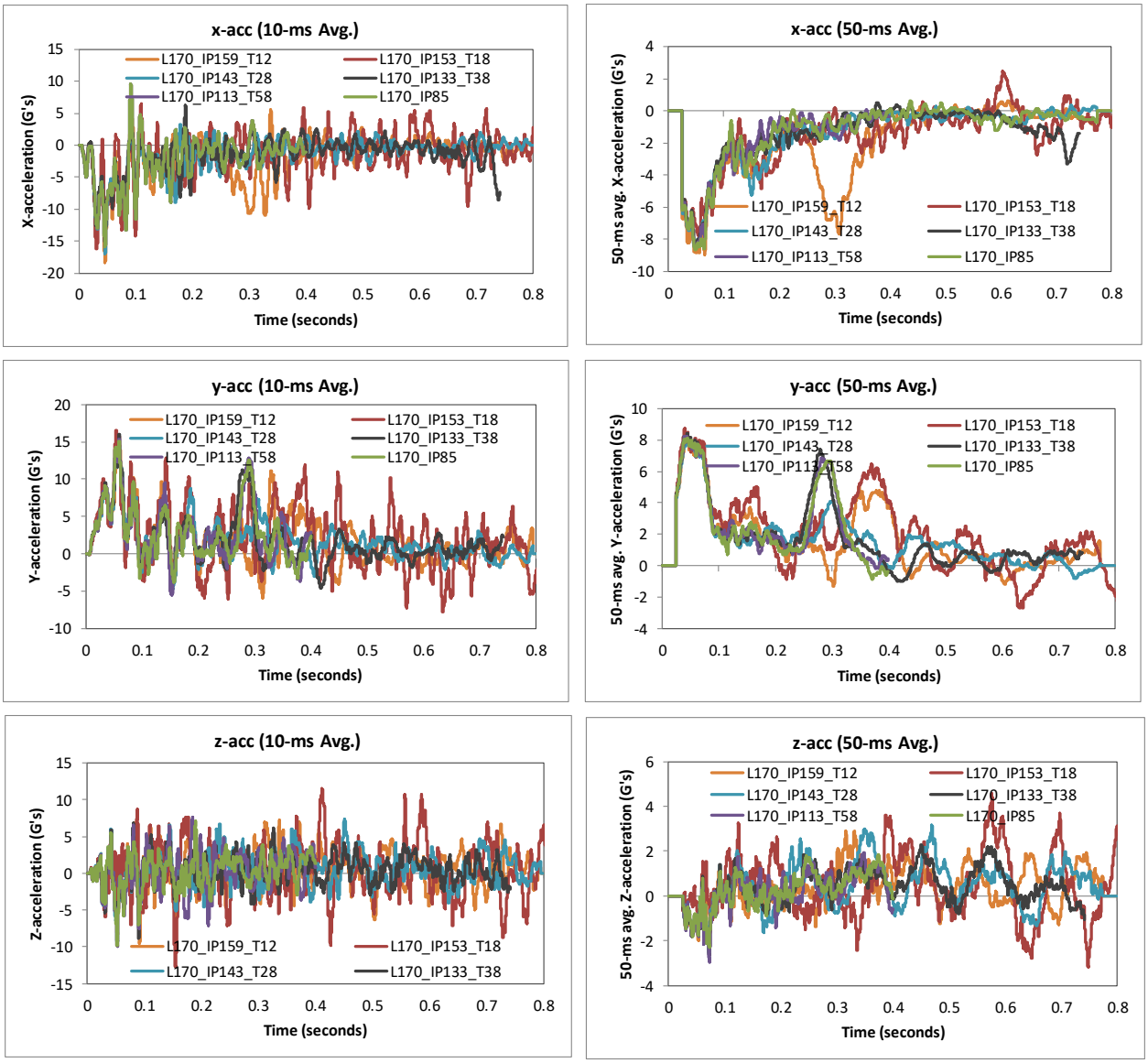

Figure 49. Case 1 – Trailing End: Comparison of acceleration-time histories for MASH Test 3-11 impact conditions.

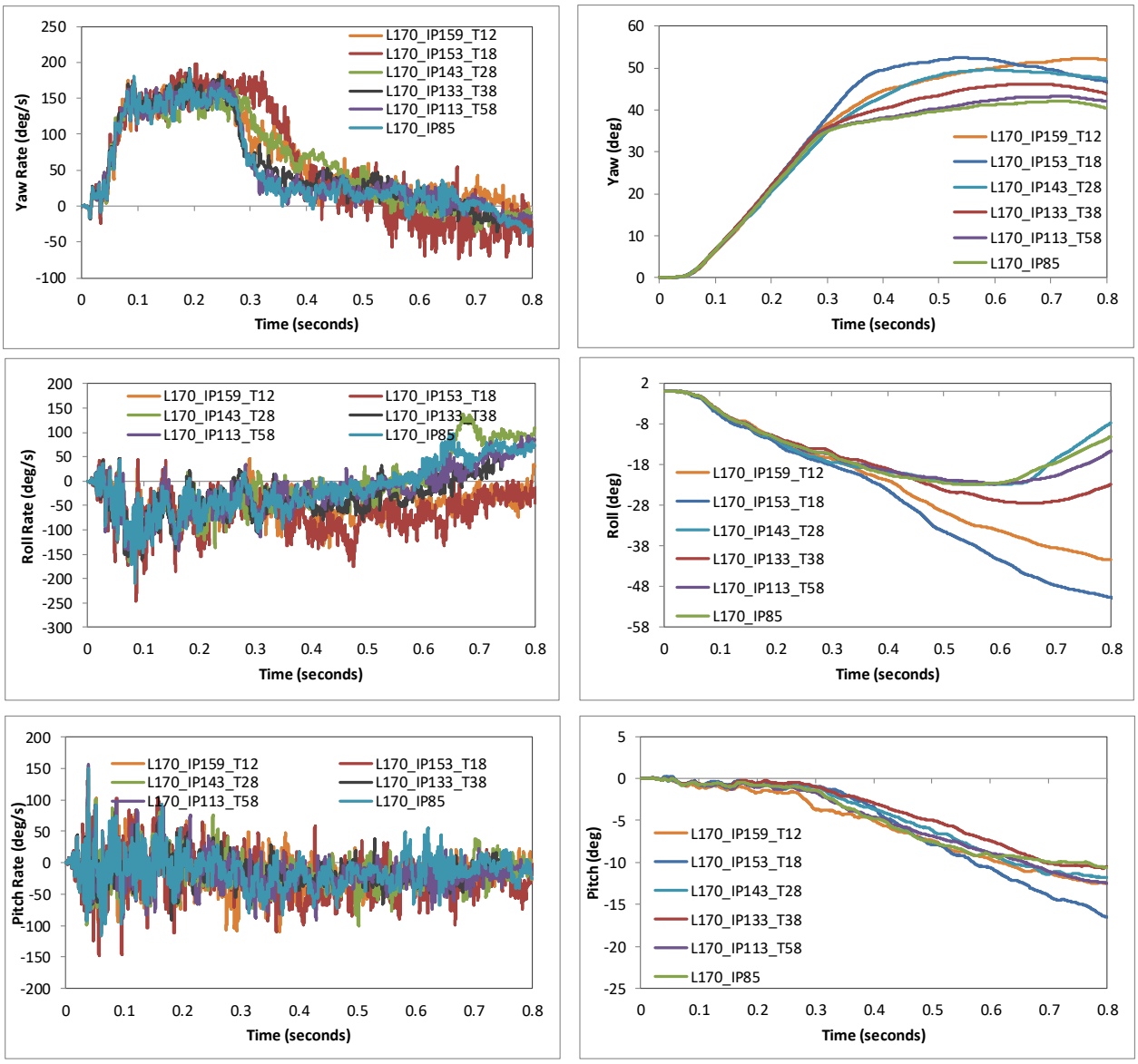

Figure 50. Case 1 – Trailing End: Comparison of angular rate and displacement time histories for MASH Test 3-11 impact conditions.

Case 1 - Occupant Risk Measures

Table 13 and Figure 52 show summaries of the occupant risk measures for each of the trailing-end analysis cases. The results indicated that the occupant impact velocities (OIV) were essentially identical for all analysis cases, with OIV in the longitudinal direction ranging from 17.4 ft/s (5.3 m/s) to 19.0 ft/s (5.8 m/s) and OIV in the lateral direction ranging from 17.1 ft/s (5.2 m/s) to 17.7 (5.4 m/s). The occupant ridedown acceleration (ORA) in the x-direction was also similar for cases involving impact at Barrier Segment 28 and greater from the downstream end with values generally ranging from 8.5 g to 9.0 g. For impact at Barrier Segment 12, the ORA-x increased to 11 g's. The ORA in the lateral direction tended to decrease as the impact point moved toward the downstream end (e.g., up to approximately 28 m from the downstream end); but then began to increase again as the impact point moved closer to the end of the system.

In all cases, the OIV and ORA values were with critical limits (i.e., ORA < 12.2 m/s and ORA < 20.49 g); and were within recommended limits (i.e., ORA < 9 m/s and ORA < 15 g) for impact at Barrier Segment 28 (91.9 ft) from the downstream end and greater.

The values for the post-head deceleration (PHD) and the acceleration severity index are also shown in Table 13 and Figure 52. The PHD values followed closely with the ORA-y with values decreasing as the impact point moved toward the downstream end, then increasing again as the impact moved closer to the end. The ASI values were essentially equivalent for all cases with a value of 1.13 to 1.16.

Case 1 - Occupant Compartment Intrusion

The occupant compartment deformations were within critical values in all cases except for impact at Barrier Segment 12. In that case, there was a direct impact of the door on the corner of one of the barrier segment during yaw and redirection which resulted in 10.4 inches of intrusion to the door above the seat, as illustrated in Figure 51, which exceeds the limit of 9 inches specified in MASH. This value was identical to the result during impact at Barrier Segment 18 on the leading end of the system.

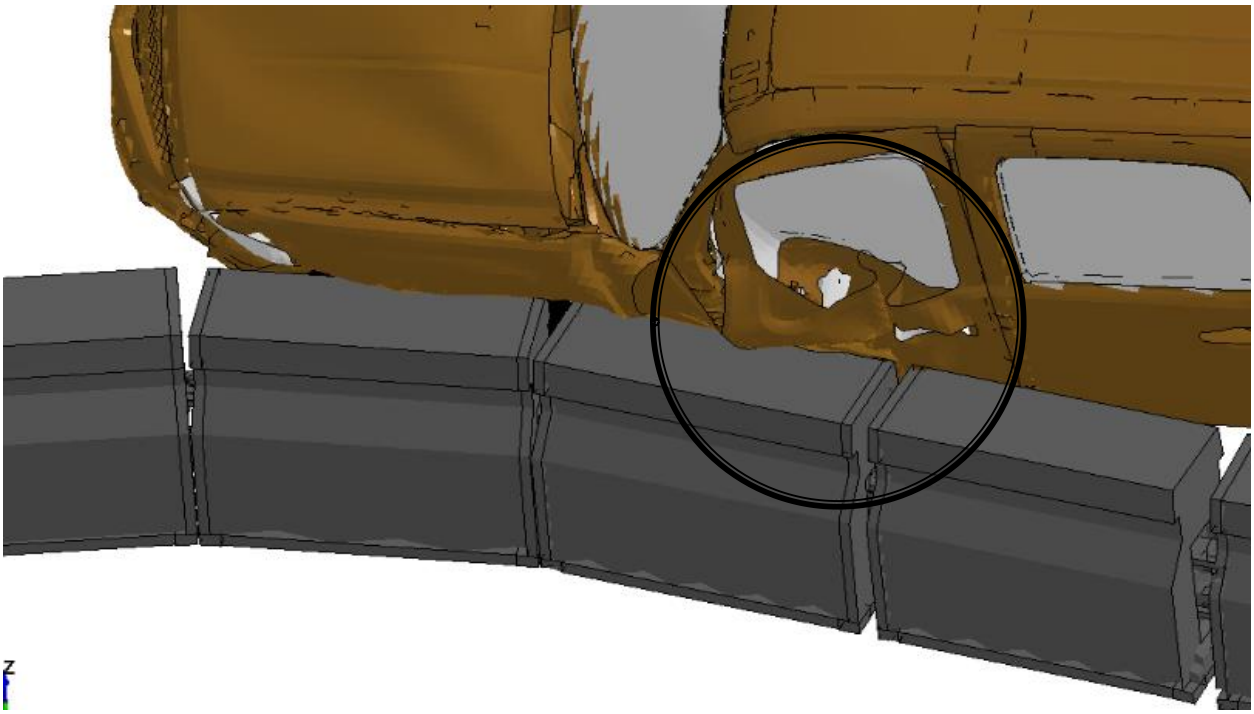

Figure 51. Case 1 -Trailing End: Occupant compartment deformation for the analysis case with impact at Barrier Segment 12 from the downstream end.

Table 13. Case 1 – Trialing End: Comparison of occupant risk measures for MASH Test 3-11 impact conditions.

Occupant Risk Factors		MASH 3-11					
		L170_IP159_T12	L170_IP153_T18	L170_IP143_T28	L170_IP133_T38	L170_IP113_T58	L170_IP85
Occupant Impact Velocity (m/s)	x-direction	5.8	5.8	5.4	5.3	5.7	5.6
	y-direction	-5.2	-5.5	-5.2	-5.4	-5.3	-5.3
	at time	at 0.1045 seconds on left side of interior	at 0.1011 seconds on left side of interior	at 0.1046 seconds on left side of interior	at 0.1032 seconds on left side of interior	at 0.1039 seconds on left side of interior	at 0.1036 seconds on left side of interior
THIV (m/s)		7.9 at 0.1045 seconds on left side of interior	7.9 at 0.1011 seconds on left side of interior	7.5 at 0.1046 seconds on left side of interior	7.5 at 0.1032 seconds on left side of interior	7.6 at 0.1039 seconds on left side of interior	7.8 at 0.1036 seconds on left side of interior
Ridedown Acceleration (g's)	x-direction	-11 (0.3236 - 0.3336 seconds)	-9.8 (0.4005 - 0.4105 seconds)	-9 (0.1646 - 0.1746 seconds)	-8.5 (0.7349 - 0.7449 seconds)	-9.6 (0.1514 - 0.1614 seconds)	-8.9 (0.1562 - 0.1662 seconds)
	y-direction	11.2 (0.3238 - 0.3338 seconds)	12.8 (0.1370 - 0.1470 seconds)	8.7 (0.1807 - 0.1907 seconds)	11.2 (0.2732 - 0.2832 seconds)	12.9 (0.2847 - 0.2947 seconds)	12.5 (0.2847 - 0.2947 seconds)
PHD (g's)		15.7 (0.3238 - 0.3338 seconds)	13 (0.1368 - 0.1468 seconds)	9.9 (0.1806 - 0.1906 seconds)	11.3 (0.2868 - 0.2968 seconds)	13.8 (0.2851 - 0.2951 seconds)	12.7 (0.2846 - 0.2946 seconds)
ASI		1.13 (0.0208 - 0.0708 seconds)	1.14 (0.0145 - 0.0645 seconds)	1.13 (0.0253 - 0.0753 seconds)	1.16 (0.0246 - 0.0746 seconds)	1.13 (0.0252 - 0.0752 seconds)	1.14 (0.0257 - 0.0757 seconds)
Max 50-ms moving avg. acc. (g's)	x-direction	-8.9 (0.0403 - 0.0903 seconds)	-7.9 (0.0301 - 0.0801 seconds)	-8.5 (0.0221 - 0.0721 seconds)	-8.5 (0.0242 - 0.0742 seconds)	-8.5 (0.0231 - 0.0731 seconds)	-8.7 (0.0239 - 0.0739 seconds)
	y-direction	8 (0.0192 - 0.0692 seconds)	8.7 (0.0147 - 0.0647 seconds)	8.1 (0.0188 - 0.0688 seconds)	8.4 (0.0190 - 0.0690 seconds)	8.2 (0.0184 - 0.0684 seconds)	8.1 (0.0192 - 0.0692 seconds)
	z-direction	2.9 (0.3063 - 0.3563 seconds)	4.6 (0.5517 - 0.6017 seconds)	3.1 (0.4447 - 0.4947 seconds)	-2.6 (0.0476 - 0.0976 seconds)	-3 (0.0479 - 0.0979 seconds)	-2.3 (0.0477 - 0.0977 seconds)
Maximum Angular Disp. (deg)	Roll	-41.4 (0.7945 seconds)	-51.6 (0.9305 seconds)	-22.9 (0.5443 seconds)	-27.6 (0.6535 seconds)	-22.8 (0.5857 seconds)	-22.9 (0.5467 seconds)
	Pitch	-12.5 (0.7763 seconds)	-20.8 (0.9844 seconds)	-11.8 (0.7996 seconds)	-10.7 (0.7937 seconds)	-12.5 (0.7996 seconds)	-10.6 (0.7996 seconds)
	Yaw	52.4 (0.7694 seconds)	52.6 (0.5371 seconds)	49.6 (0.5862 seconds)	46.2 (0.6678 seconds)	43.3 (0.7168 seconds)	42.1 (0.7088 seconds)

Figure 52. Case 1 – Trailing End: Comparison of occupant risk measures for MASH Test 3-11 impact conditions.

Case 2 – QMB CRTS with VLB Elements

Case 2 – Impacts on the Leading End of the System

Case 2 - Lateral Displacement

Sequential views showing a comparison of the impact cases on the leading end of the system are provided in Appendix F. Figure 53 through Figure 57 show plots of maximum lateral displacement for the barrier segments located in the impact region of the system for each analysis cases. A summary of maximum deflection versus impact location is shown in Figure 58.

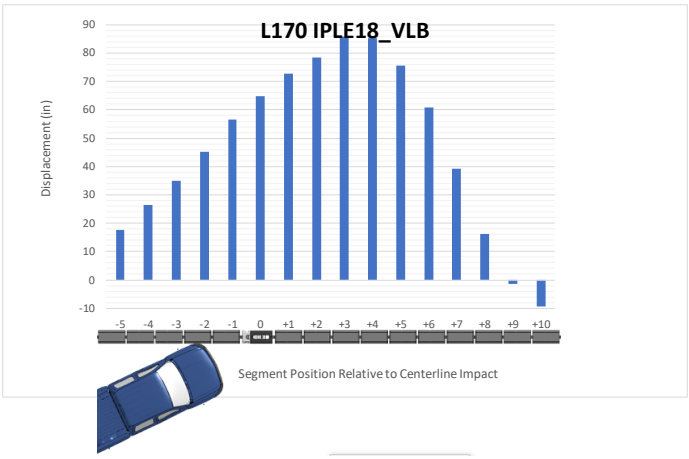

Figure 53. Case 2 – Leading End: Lateral deflection of individual barrier segments in the impact region of the CTRS system for impact at Barrier Segment 18 from.

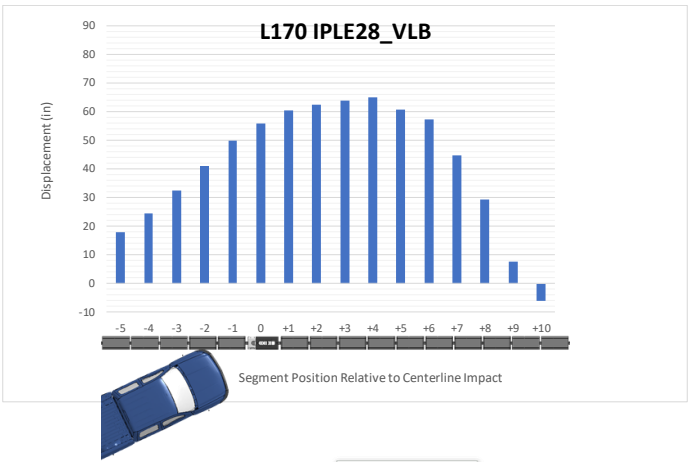

Figure 54. Case 2 – Leading End: Lateral deflection of individual barrier segments in the impact region of the CTRS system for impact at Barrier Segment 28.

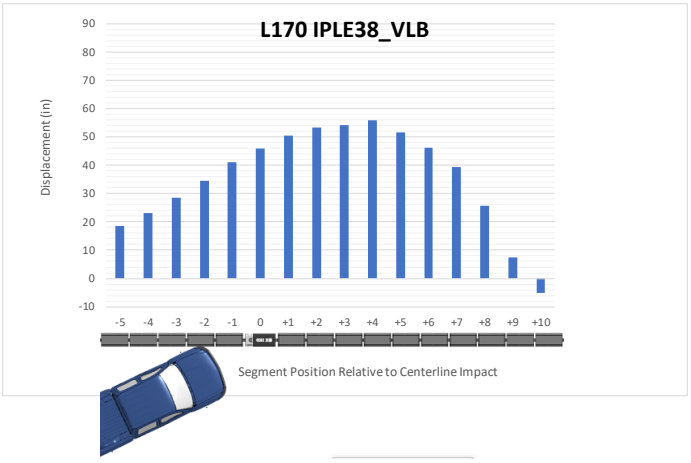

Figure 55. Case 2 – Leading End: Lateral deflection of individual barrier segments in the impact region of the CTRS system for impact at Barrier Segment 38.

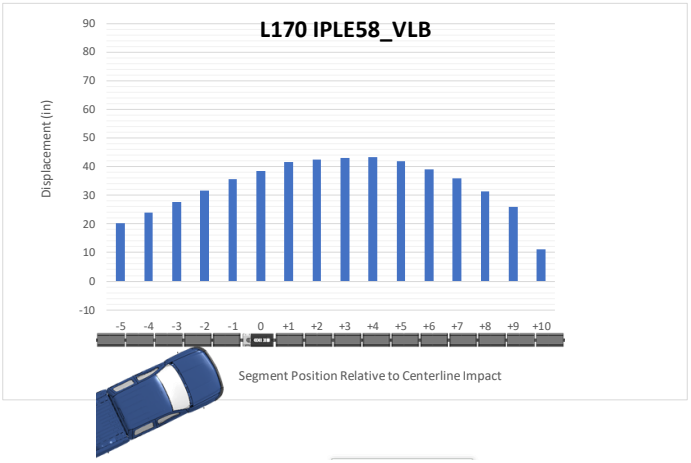

Figure 56. Case 2 – Leading End: Lateral deflection of individual barrier segments in the impact region of the CTRS system for impact at Barrier Segment 58.

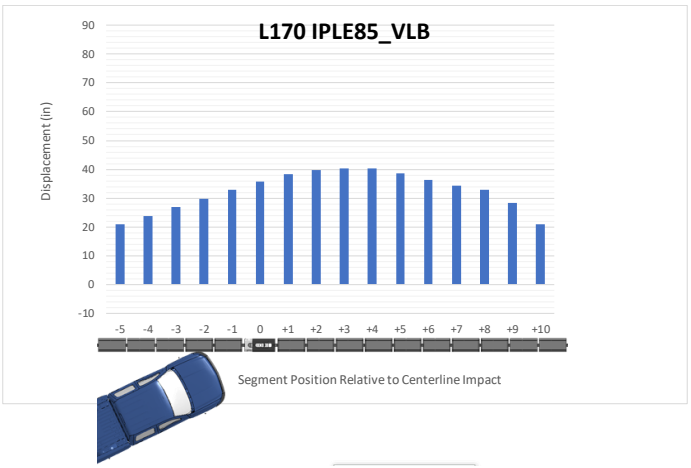

Figure 57. Case 2 – Leading End: Lateral deflection of individual barrier segments in the impact region of the CTRS system for impact at Barrier Segment 85.

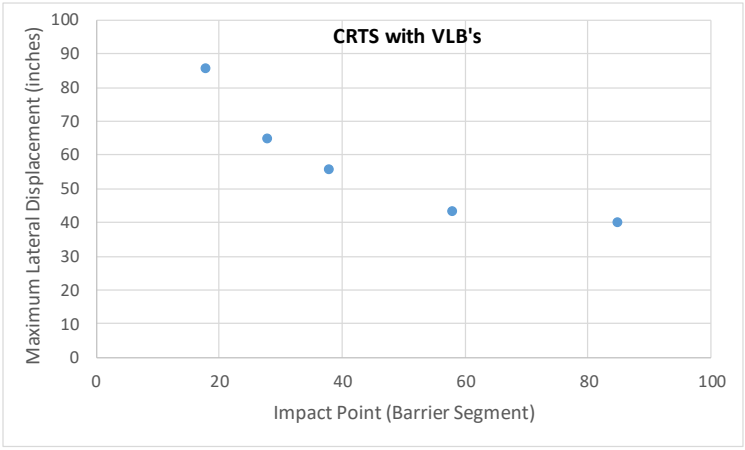

Figure 58. Case 2 – Leading End: Maximum lateral displacement versus impact point.

Case 2 - Longitudinal Displacement

The maximum longitudinal displacement at the upstream and downstream ends of the system for each case is shown in Figure 59. At Impact Point 18 the maximum longitudinal displacement of the upstream end barrier was 32 inches; at Impact Point 85 the upstream displacement was 1.6 inches. On the downstream end, the movement of the barrier was negligible for all cases except for impact at Barrier Segment 85, which resulted in 0.56 inches of displacement.

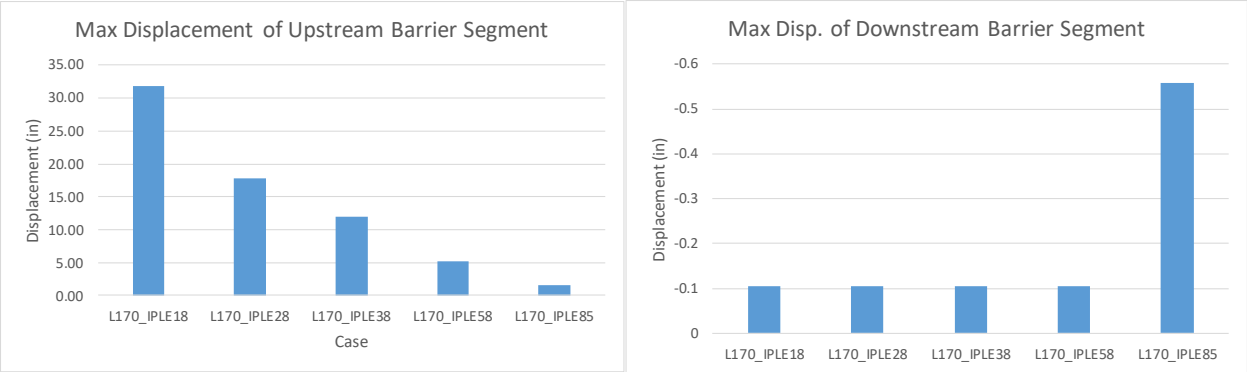

Figure 59. Case 2 – Leading End: Maximum longitudinal displacement at the upstream and downstream ends of the barrier.

Case 2 - Time-History Data

Figure 60 shows a comparison of the 10-millisecond moving average and the 50-millisecond moving average acceleration-time history at the c.g. of the vehicle for the longitudinal, transverse and vertical channels. Figure 61 shows comparisons of the angular rates and angular displacements (i.e., yaw, roll, and pitch) at the c.g. of the vehicle. The magnitude of the accelerations was similar for all cases; however, the roll angle for impact at Barrier Segment 18 was 45 degrees, which was much higher than the other cases.

Case 2 - Occupant Risk Measures

Table 14 and Figure 62 show summaries of the occupant risk measures for each of the leading-end analysis cases. The results indicated that the occupant impact velocities (OIV) were below 23 ft/s (7 m/s) for all analysis cases, which was well below the recommended limit of 30 ft/s (9 m/s). The occupant ridedown acceleration (ORA) were also below the recommended limit of 15 g's for all cases, with the exception of the impact case at Barrier 18, which resulted in ORA-y of 16 g. All cases were below the critical limit of 20.49.

The values for the post-head deceleration (PHD) and the acceleration severity index, metrics computed as part of the European Committee for Standardization (CEN), are also shown in Table 14 and Figure 62. The PHD values followed closely with the ORA-y, and the ASI values were essentially equivalent for all cases with a value of 1.03 to 1.09.

Case 2 - Occupant Compartment Intrusion

There was no occupant compartment deformation, except for the case with impact at Barrier 28, which resulted in 2.28 inches of occupant compartment deformation of the impact-side door. All cases were within critical values.

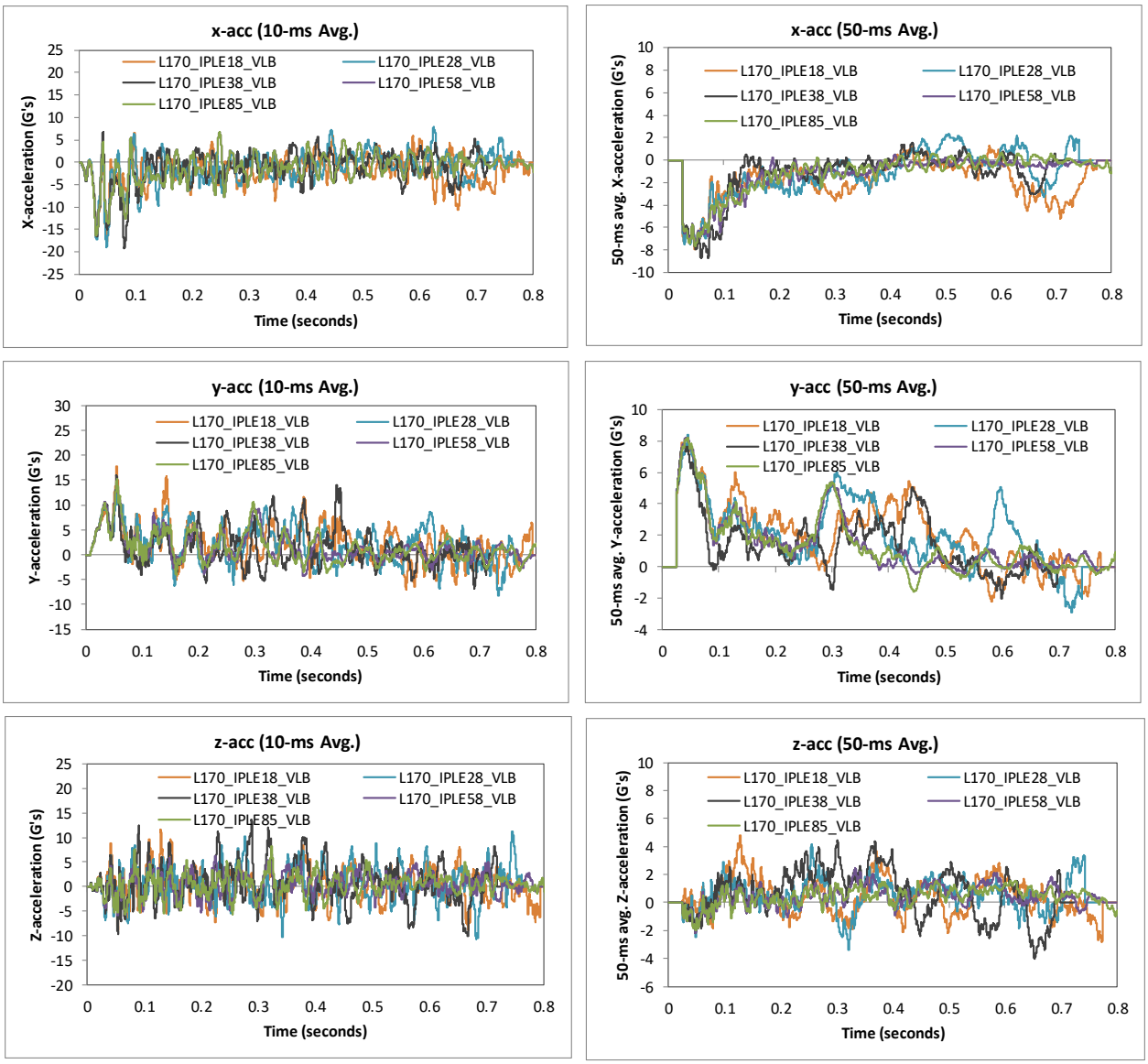

Figure 60. Case 2 – Leading End: Comparison of acceleration-time histories for MASH Test 3-11 impact conditions.

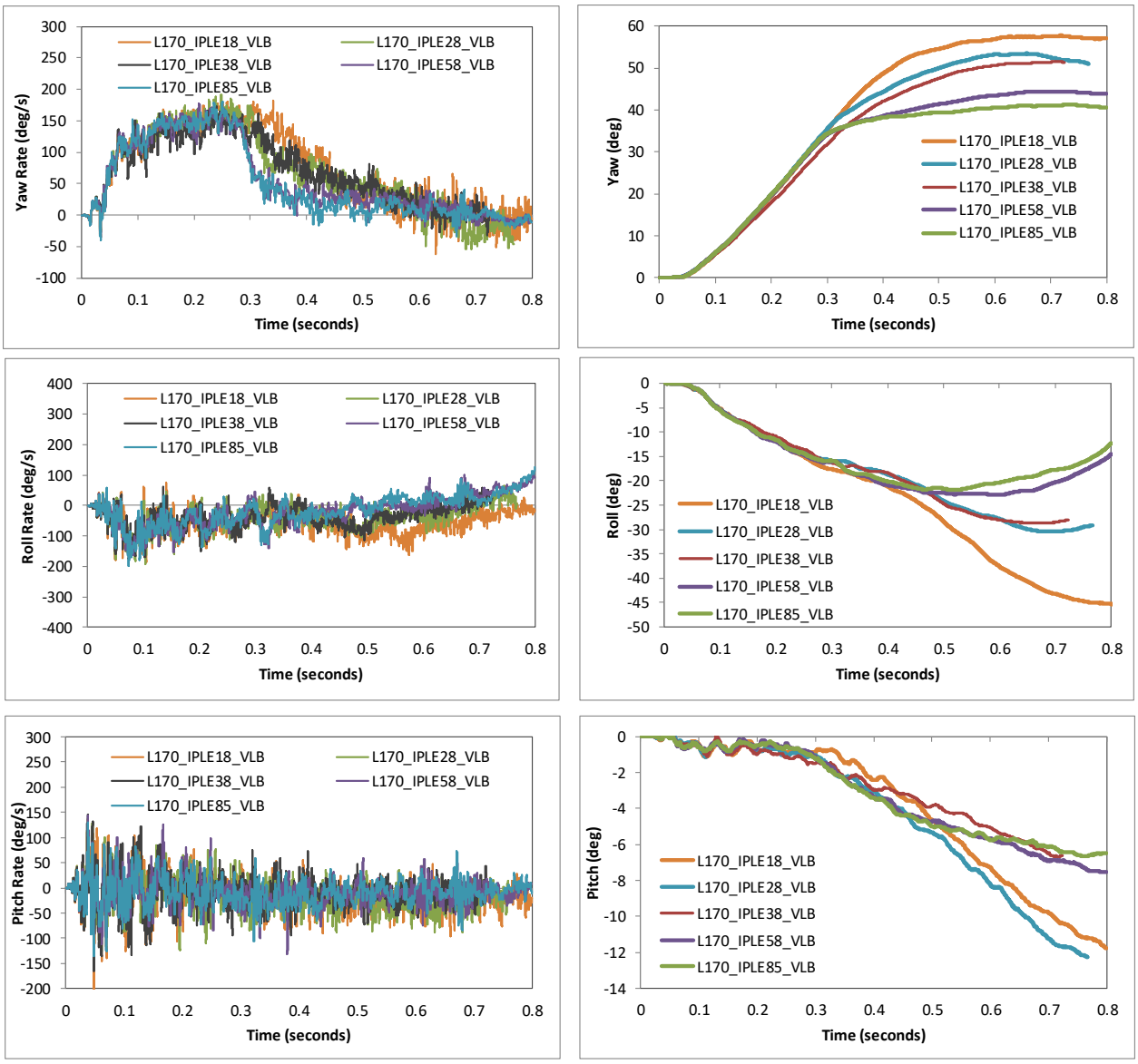

Figure 61. Case 2 – Leading End: Comparison of angular rate and displacement time histories for MASH Test 3-11 impact conditions.

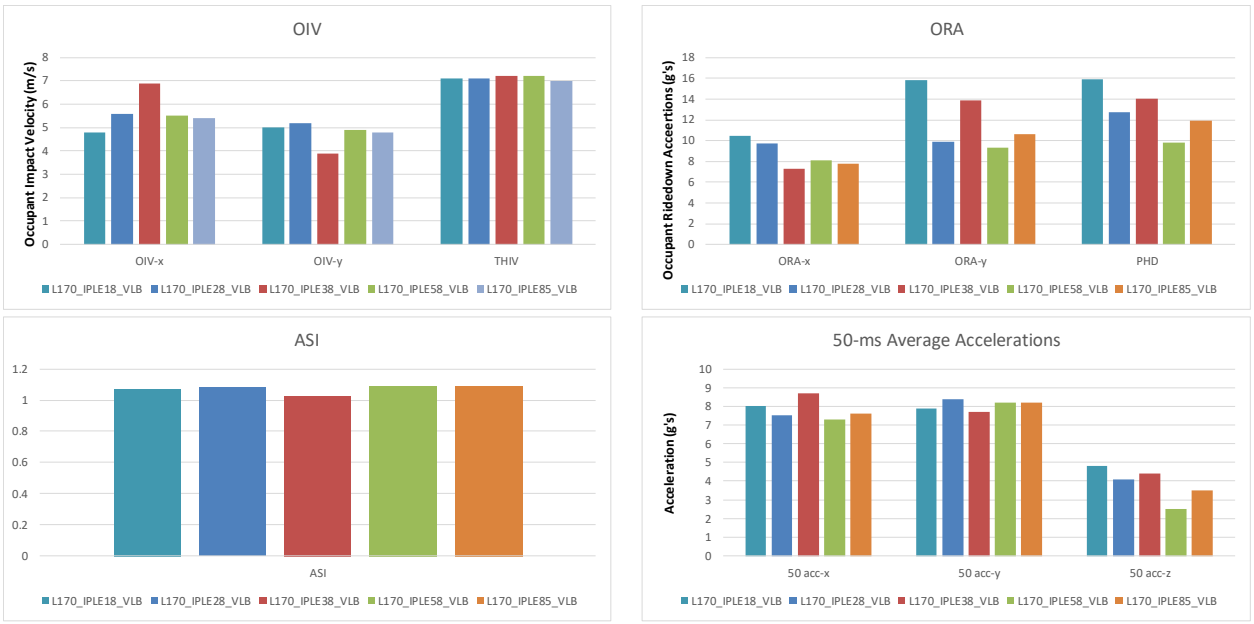

Figure 62. Case 2 – Leading End: Comparison of occupant risk measures for MASH Test 3-11 impact conditions.

Table 14. Case 2 – Leading End: Comparison of occupant risk measures for MASH Test 3-11 impact conditions.

Occupant Risk Factors		MASH 3-11				
		L170_IPLE18_VLB	L170_IPLE28_VLB	L170_IPLE38_VLB	L170_IPLE58_VLB	L170_IPLE85_VLB
Occupant Impact Velocity (m/s)	x-direction	4.8	5.6	6.9	5.5	5.4
	y-direction	-5	-5.2	-3.9	-4.9	-4.8
	at time	at 0.1064 seconds on left side of interior	at 0.1066 seconds on left side of interior	at 0.1100 seconds on left side of interior	at 0.1052 seconds on left side of interior	at 0.1056 seconds on left side of interior
THIV (m/s)		7.1 at 0.1064 seconds on left side of interior	7.1 at 0.1066 seconds on left side of interior	7.2 at 0.1100 seconds on left side of interior	7.2 at 0.1052 seconds on left side of interior	7 at 0.1056 seconds on left side of interior
Ridedown Acceleration (g's)	x-direction	-10.5 (0.6632 - 0.6732 seconds)	-9.7 (0.1343 - 0.1443 seconds)	-7.3 (0.6536 - 0.6636 seconds)	-8.1 (0.1538 - 0.1638 seconds)	-7.8 (0.2509 - 0.2609 seconds)
	y-direction	15.8 (0.1380 - 0.1480 seconds)	9.9 (0.1387 - 0.1487 seconds)	13.9 (0.4407 - 0.4507 seconds)	9.3 (0.3017 - 0.3117 seconds)	10.6 (0.2923 - 0.3023 seconds)
PHD (g's)		15.9 (0.1380 - 0.1480 seconds)	12.7 (0.1342 - 0.1442 seconds)	14 (0.4407 - 0.4507 seconds)	9.8 (0.2952 - 0.3052 seconds)	11.9 (0.2923 - 0.3023 seconds)
ASI		1.07 (0.0226 - 0.0726 seconds)	1.08 (0.0203 - 0.0703 seconds)	1.03 (0.0129 - 0.0629 seconds)	1.09 (0.0224 - 0.0724 seconds)	1.09 (0.0214 - 0.0714 seconds)
Max 50-ms moving avg. acc. (g's)	x-direction	-8 (0.0226 - 0.0726 seconds)	-7.5 (0.0142 - 0.0642 seconds)	-8.7 (0.0338 - 0.0838 seconds)	-7.3 (0.0231 - 0.0731 seconds)	-7.6 (0.0227 - 0.0727 seconds)
	y-direction	7.9 (0.0198 - 0.0698 seconds)	8.4 (0.0201 - 0.0701 seconds)	7.7 (0.0125 - 0.0625 seconds)	8.2 (0.0161 - 0.0661 seconds)	8.2 (0.0199 - 0.0699 seconds)
	z-direction	4.8 (0.1032 - 0.1532 seconds)	4.1 (0.2304 - 0.2804 seconds)	4.4 (0.2765 - 0.3265 seconds)	2.5 (0.3078 - 0.3578 seconds)	-3.5 (0.9099 - 0.9599 seconds)
Maximum Angular Disp. (deg)	Roll	-45.3 (0.7996 seconds)	-30.5 (0.7005 seconds)	-28.7 (0.6640 seconds)	-23 (0.6042 seconds)	-21.9 (0.5216 seconds)
	Pitch	-11.8 (0.7996 seconds)	-12.3 (0.7662 seconds)	-6.7 (0.7148 seconds)	-7.6 (0.7935 seconds)	-6.7 (0.7664 seconds)
	Yaw	57.7 (0.7191 seconds)	53.4 (0.6568 seconds)	51.5 (0.7151 seconds)	44.4 (0.6929 seconds)	41.2 (0.7350 seconds)

Case 2 - Impacts on the Trailing End of the System

Case 2 - Lateral Displacement

Sequential views showing a comparison of the impact cases on the trailing end of the system are provided in Appendix G. Figure 63 through Figure 66 show plots of maximum lateral displacement for barrier segments located in the impact region of the system for each analysis case. A summary plot of maximum deflection versus impact location is shown in Figure 67.

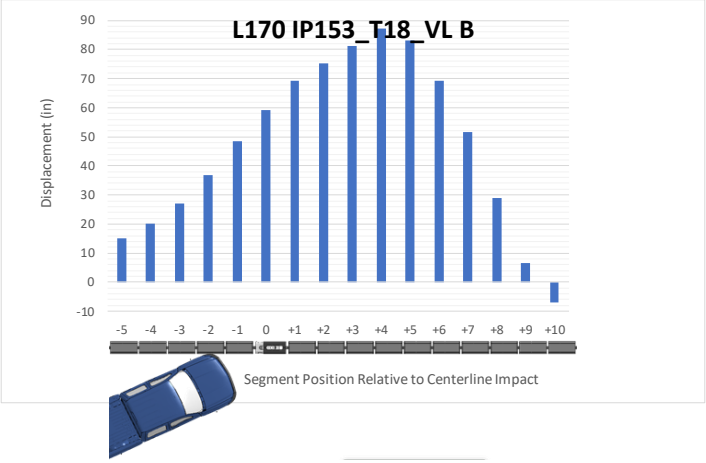

Figure 63. Case 2 – Trailing End: Lateral deflection of individual barrier segments in the impact region of the CTRS system for impact at Barrier Segment 18.

Figure 64. Case 2 – Trailing End: Lateral deflection of individual barrier segments in the impact region of the CTRS system for impact at Barrier Segment 28.

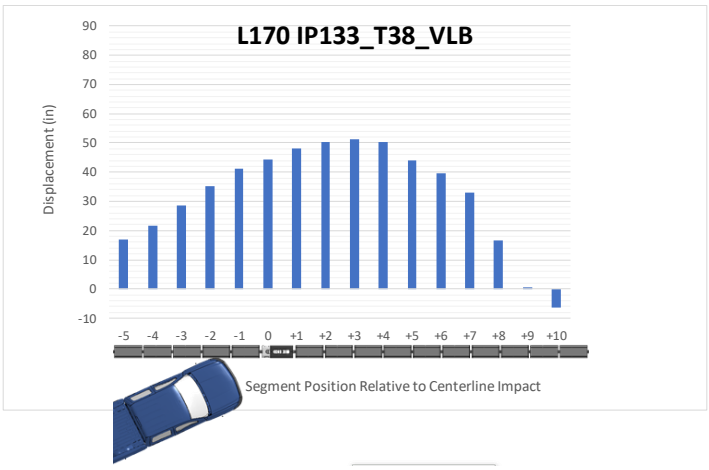

Figure 65. Case 2 – Trailing End: Lateral deflection of individual barrier segments in the impact region of the CTRS system for impact at Barrier Segment 38.

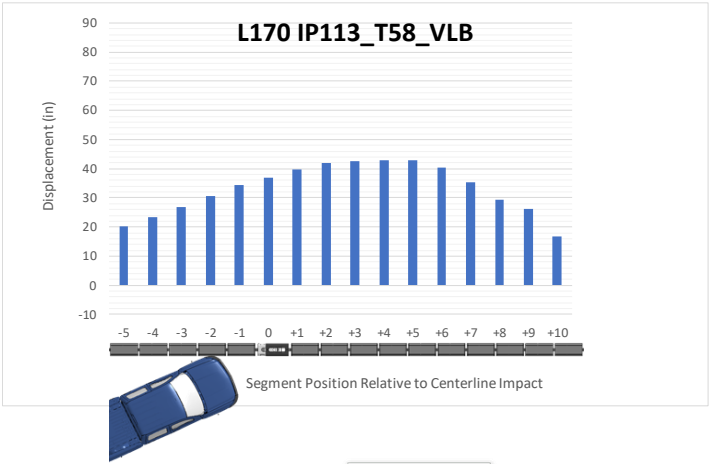

Figure 66. Case 2 – Trailing End: Lateral deflection of individual barrier segments in the impact region of the CTRS system for impact at Barrier Segment 58.

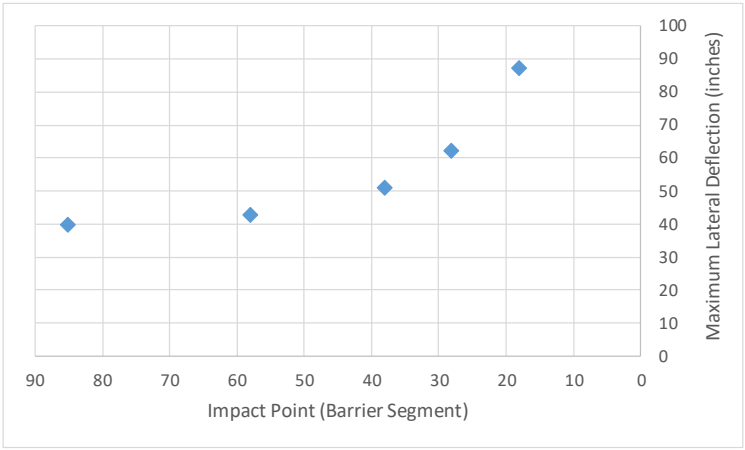

Figure 67. Case 2 – Trailing End: Maximum lateral displacement versus impact point.

Case 2 - Longitudinal Displacement

The maximum longitudinal displacement at the upstream and downstream ends of the system for each case is shown in Figure 68. On the upstream end, the movement of the barrier was negligible for all cases except for impact at Barrier Segment 85, which resulted in 1.55 inches of displacement. The longitudinal displacement of the downstream barrier increased significantly as the impact point got nearer to the downstream end of the system. At Impact Point 85 the downstream displacement was 0.56 inches; at Impact Point 18 the maximum longitudinal displacement of the end barrier was 31.9 inches.

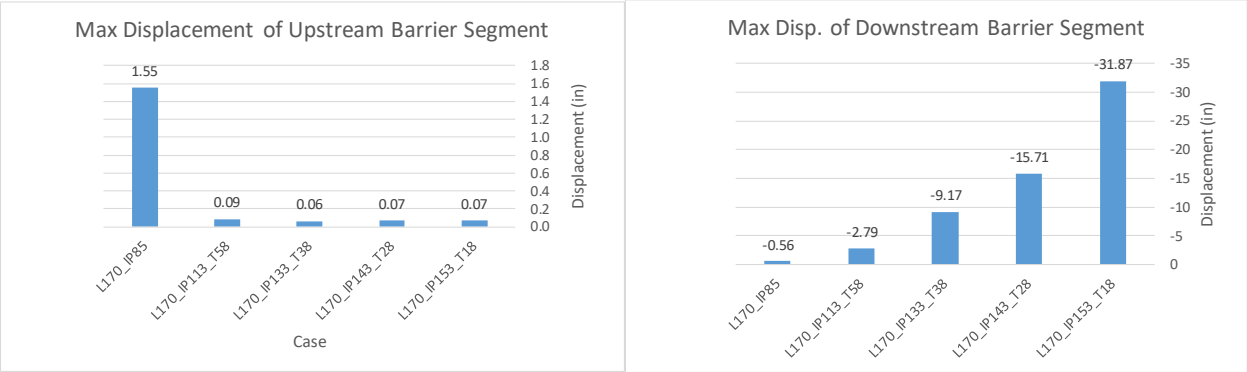

Figure 68. Case 2 – Trailing End: Maximum longitudinal displacement at the upstream and downstream ends of the barrier.

Case 2 - Time-History Data

Figure 69 shows a comparison of the 10-millisecond moving average and the 50-millisecond moving average acceleration-time history at the c.g. of the vehicle for the longitudinal, transverse and vertical channels. Figure 70 shows comparisons of the angular rates and angular displacements (i.e., yaw, roll, and pitch) at the c.g. of the vehicle. The magnitude of the accelerations was again similar for all cases and the roll angle for impact at Barrier Segment 18 was relatively high with a magnitude of 58.6 degrees and was still increasing at the termination of the analysis at 1.0 seconds.

Case 2 - Occupant Risk Measures

Table 15 and Figure 71 show summaries of the occupant risk measures for each of the trailing-end analysis cases. The results indicated that the occupant impact velocities (OIV) were below 24 ft/s (7.3 m/s) for all analysis cases, which was well below the recommended limit of 30 ft/s (9 m/s). The occupant ridedown acceleration (ORA) were also below the recommended limit of 15 g's for all cases.

The values for the post-head deceleration (PHD) and the acceleration severity index, metrics computed as part of the European Committee for Standardization (CEN), are also shown in Table 15 and Figure 71. The PHD was 12 g's for impact at Barrier Segment 85 (i.e., LON case) and was between 15 and 16.3 for all other cases. The ASI values ranged from 0.98 to 1.2 for all cases.

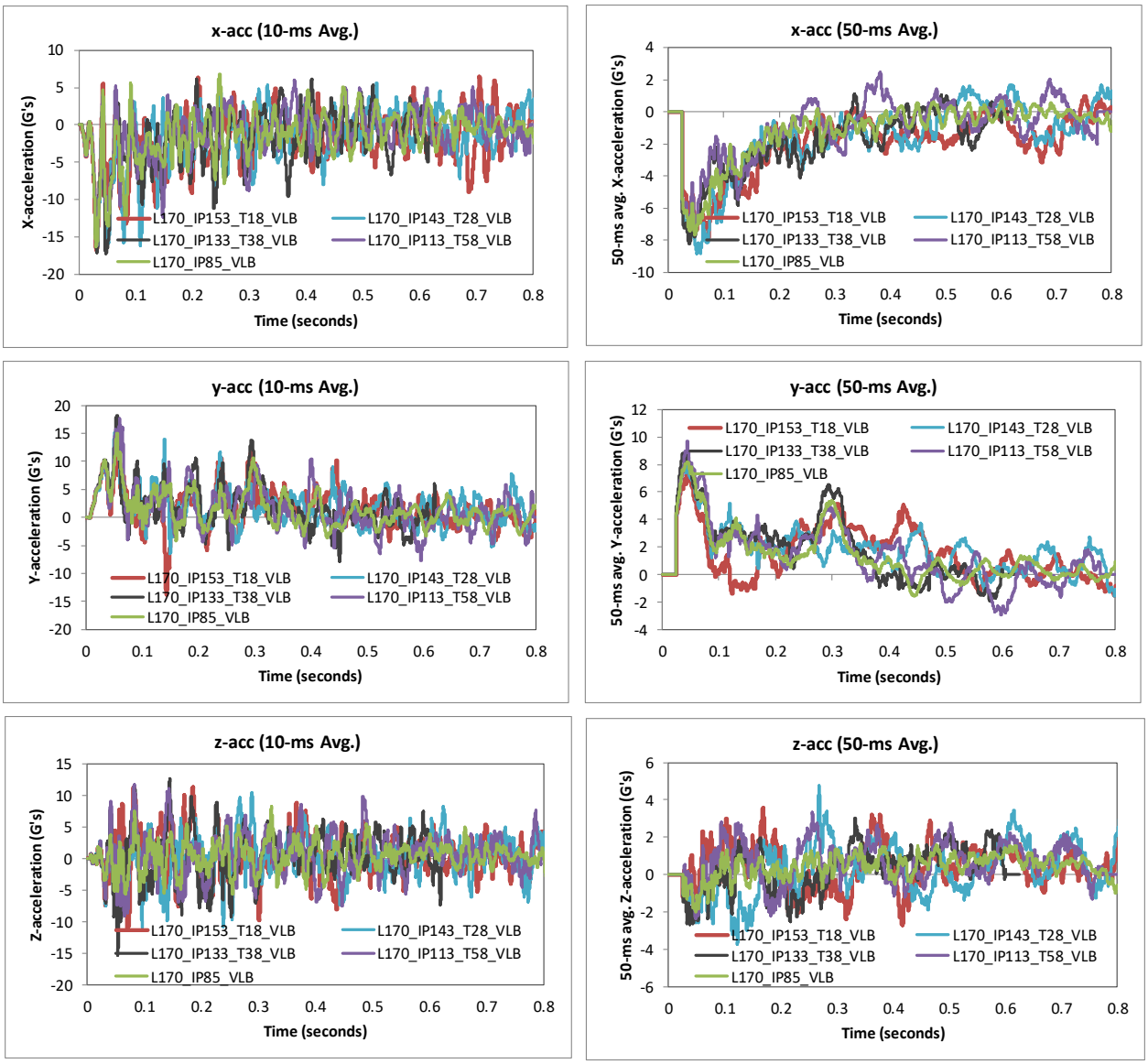

Figure 69. Case 2 – Trailing End: Comparison of acceleration-time histories for MASH Test 3-11 impact conditions.

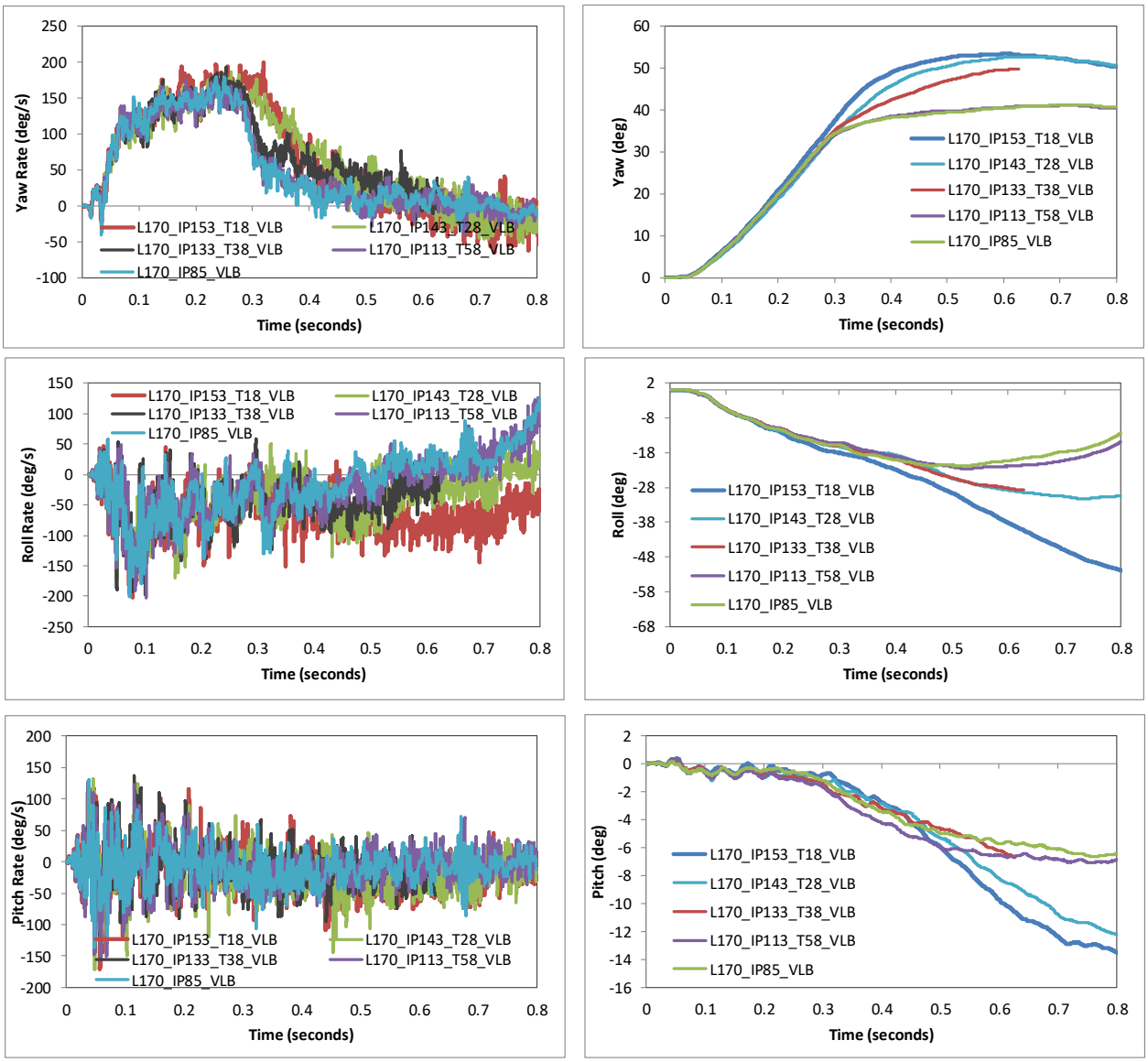

Figure 70. Case 2 – Trailing End: Comparison of angular rate and displacement time histories for MASH Test 3-11 impact conditions.

Table 15. Case 2 – Trailing End: Comparison of occupant risk measures for MASH Test 3-11 impact conditions.

Occupant Risk Factors		MASH 3-11				
		L170_IP153_T18_VLB	L170_IP143_T28_VLB	L170_IP133_T38_VLB	L170_IP113_T58_VLB	L170_IP85_VLB
Occupant Impact Velocity (m/s)	x-direction	5.9	7.3	5.1	4.3	5.4
	y-direction	-3.9	-4.6	-5.4	-5.4	-4.8
	at time	at 0.1139 seconds on left side of interior	at 0.1074 seconds on left side of interior	at 0.1031 seconds on left side of interior	at 0.1033 seconds on left side of interior	at 0.1056 seconds on left side of interior
THIV (m/s)		6.6 at 0.1139 seconds on left side of interior	7.6 at 0.1074 seconds on left side of interior	7.2 at 0.1031 seconds on left side of interior	6.8 at 0.1033 seconds on left side of interior	7 at 0.1056 seconds on left side of interior
Ridedown Acceleration (g's)	x-direction	-11 (0.1298 - 0.1398 seconds)	-11.2 (0.1330 - 0.1430 seconds)	-11.2 (0.2327 - 0.2427 seconds)	-12.4 (0.1424 - 0.1524 seconds)	-7.8 (0.2509 - 0.2609 seconds)
	y-direction	-13.8 (0.1381 - 0.1481 seconds)	14 (0.1348 - 0.1448 seconds)	13.9 (0.2898 - 0.2998 seconds)	10.4 (0.3948 - 0.4048 seconds)	10.6 (0.2923 - 0.3023 seconds)
PHD (g's)		15 (0.1380 - 0.1480 seconds)	16.3 (0.1339 - 0.1439 seconds)	15.5 (0.2898 - 0.2998 seconds)	15.8 (0.1424 - 0.1524 seconds)	11.9 (0.2923 - 0.3023 seconds)
ASI		0.98 (0.0253 - 0.0753 seconds)	1.1 (0.0203 - 0.0703 seconds)	1.22 (0.0128 - 0.0628 seconds)	1.18 (0.0199 - 0.0699 seconds)	1.09 (0.0214 - 0.0714 seconds)
Max 50-ms moving avg. acc. (g's)	x-direction	-7.9 (0.0470 - 0.0970 seconds)	-8.9 (0.0263 - 0.0763 seconds)	-8.2 (0.0127 - 0.0627 seconds)	-7.2 (0.0116 - 0.0616 seconds)	-7.6 (0.0227 - 0.0727 seconds)
	y-direction	7.4 (0.0193 - 0.0693 seconds)	8.1 (0.0200 - 0.0700 seconds)	8.9 (0.0115 - 0.0615 seconds)	9.7 (0.0196 - 0.0696 seconds)	8.2 (0.0199 - 0.0699 seconds)
	z-direction	3.6 (0.1437 - 0.1937 seconds)	4.8 (0.2435 - 0.2935 seconds)	3 (0.3077 - 0.3577 seconds)	3.3 (0.2317 - 0.2817 seconds)	-3.5 (0.9099 - 0.9599 seconds)
Maximum Angular Disp. (deg)	Roll	-58.6 (0.9993 seconds)	-31.3 (0.7341 seconds)	-28.8 (0.6227 seconds)	-22.7 (0.5226 seconds)	-21.9 (0.5216 seconds)
	Pitch	-14.7 (0.9947 seconds)	-12.7 (0.8567 seconds)	-6.8 (0.6266 seconds)	-7.1 (0.7613 seconds)	-6.7 (0.7664 seconds)
	Yaw	53.4 (0.6039 seconds)	52.7 (0.6734 seconds)	49.8 (0.6266 seconds)	41.1 (0.7167 seconds)	41.2 (0.7350 seconds)

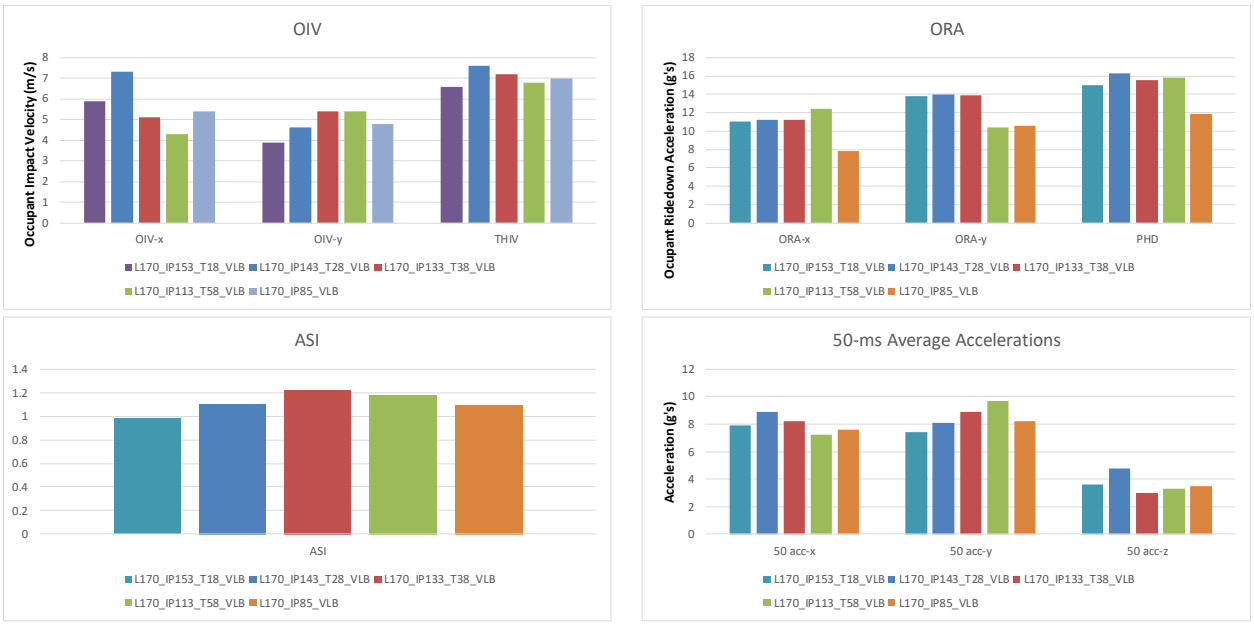

Figure 71. Case 2 – Trailing End: Comparison of occupant risk measures for MASH Test 3-11 impact conditions.

Case 2 – Trailing End: Occupant Compartment Intrusion

The occupant compartment intrusion (OCI) were within critical values for all cases. For impact at Barrier Segment 58 from the trailing end, there was no intrusion. At impact points 38, 28 and 18 barrier segments from the trailing end, the OCI values were 3.74 inches, 1.46 inches and 2.64 inches, respectively, and all occurred on the impact-side door.

SUMMARY AND CONCLUSIONS

The purpose of this study was to use FEA to (1) identify the critical length for the CRTS QMB system required to achieve minimum barrier deflection when the system is impacted at its midpoint under MASH Test 3-11 conditions and (2) to evaluate the crash performance of a critical-length system as a function of impact location relative to the leading and trailing ends of the system, under on MASH Test 3-11 impact conditions and criteria. Two system cases were evaluated: Case 1 involved a system composed of only CRTS elements while Case 2 included two VLB elements in the impact zone. For Case 2 there was one VLB element positioned at 4.92 ft (1.5 m) downstream of the impact point in each case and a second VLB positioned at (55.8 ft) 17 m further downstream.

The analysis model was developed and validated based on comparison to a full-scale impact test (Test 690900-LTS2) performed under MASH Test 3-11 impact conditions. The QMB system tested corresponded to Case 2 as described above and included 170 barrier segments with impact at Barrier Segment 85. The total length of the system was 557.8 ft. The validated model was then used to simulate MASH Test 3-11 impact conditions at various points relative to both the leading-end and trailing-ends of the barrier system.

The results indicated that the critical length of the system for achieving minimum deflection was 146 barrier segments (i.e., 479 ft) based on impact cases on the leading end of the

system for Case 1; and was 152 barrier segments (i.e., 499 feet) based on impact cases on the trailing end of the system for Case 1. The larger value governs, thus the critical system length for minimum deflection is 152 barrier segments with impact occurring at points ≥ 76 barrier segments (249 ft) from either end.

For the Case 1 system (with only CRTS elements), the results of the study indicated that the barrier successfully contained and redirected the 5000-lb pickup impacting at 63 mph and 25 degrees for all impact points at least 90 ft (i.e., at least 28 barrier segments) from either end. The occupant risk metrics for each of these cases were very similar to those resulting from the baseline test case (i.e., impact at the midpoint of the 557.8-ft long system) which were all within the recommended limits specified in MASH. The vehicle was also shown to be very stable throughout the impact event in each case. However, when the vehicle struck the barrier within 90 feet from either end of the system, the performance of the barrier did not meet MASH criteria. In these cases, there was excessive movement of the barrier segments in the impact region which ultimately led to vehicle instability (e.g., high roll angle) and excessive crushing of the vehicle door during contact with one of the barrier segments. The deformation of the door in those cases resulted in 10.4 inches of intrusion into the occupant compartment, which exceeds the MASH criteria of 9 inches. The maximum roll angle in those analysis cases ranged from were 40 – 50 degrees, which is less than the critical angle of 70 degrees in MASH; however, the roll angle was still increasing at 0.8 seconds when the analysis was terminated. A summary of the performance characteristics for MASH Test 3-11 impacts at baseline (i.e., full length-of-need) and reduced length-of-need impact points for Case 1 is shown in Table 16.

Table 16. Case 1 FEA performance characteristics for MASH T3-11 at baseline and reduced LON cases.

Case 1 - CRTS Only: Baseline and Reduced Upstream LON

LON Upstream	Maximum Dynamic Deflection	Occupant Risk				Vehicle Stability	
		OIV	ORA	Exit Box	OCI	Max Roll Angle	Max Pitch Angle
279 ft [85 m] (Baseline)	36.0 in [0.91m]	18.0 ft/s [5.6 m/s]	12.5 g	Pass	Pass	22.9 deg	10.6 deg
190 ft [58 m]	38.3 in [0.97m]	18.0 ft/s [5.5 m/s]	12.7 g	Pass	Pass	24.0 deg	9.1 deg
125 ft [38 m]	48.5 in [1.23m]	18.0 ft/s [5.5 m/s]	12.8 g	Pass	Pass	29.9 deg	9.1 deg
92 ft 28 m]	59.4 in [1.51m]	18.0 ft/s [5.5 m/s]	11.0 g	Pass	Pass	29.3 deg	8.3 deg
59 ft [18 m]	75.6 in [1.92m]	17.7 ft/s [5.4 m/s]	9.6 g	Marginal	Fail	52.1 deg	10.7 deg

Case 1 - CRTS Only: Reduced Downstream LON

LON Upstream	Maximum Dynamic Deflection	Occupant Risk				Vehicle Stability	
		OIV	ORA	Exit Box	OCI	Max Roll Angle	Max Pitch Angle
190 ft [58 m]	38.3 in [0.97m]	18.7 ft/s [5.7 m/s]	12.9 g	Pass	Pass	22.8 deg	12.5 deg
125 ft 38 m]	47.6 in [1.20m]	17.7 ft/s [5.4 m/s]	11.3 g	Pass	Pass	27.6 deg	10.7 deg
92 ft [28 m]	53.5 in [1.36m]	17.7 ft/s [5.4 m/s]	9.0 g	Pass	Pass	22.9 deg	11.8 deg
59 ft [18 m]	82.4 in [2.09m]	19.0 ft/s [5.8 m/s]	12.8 g	Pass	Pass	51.6 deg	20.8 deg

For the Case 2 system (with VLB elements in the impact region), the results indicated that the barrier successfully contained and redirected the 5000-lb pickup impacting at 63 mph and 25 degrees for all impact cases evaluated (i.e., impacts points at least 59 ft from either end). The occupant risk metrics for each of these cases were similar to those resulting from the baseline test case (i.e., impact at the midpoint of the 557.8-ft long system) which were all within the recommended limits specified in MASH. Although the analysis results indicated successful performance for all cases, the stability of the vehicle was considered questionable for those cases where the impact occurred nearer to the ends of the system. In particular, for impact point at 59 ft from either end (i.e., Barrier Segment 18 from either end), the roll angle reached magnitudes of 45.3 degrees and 58.6 degrees for the leading end and trailing end cases, respectively, and was increasing at termination of the analysis. A summary of the performance characteristics for MASH Test 3-11 impacts for both the full-scale test and the FEA for the baseline case (i.e., full length-of-need) and also for the FEA reduced length-of-need impact points for Case 2 is shown in Table 17.

Table 17. Case 2 FEA performance characteristics for MASH T3-11 at baseline and reduced LON cases.

Case 2 - w/ VLB's: Baseline and Reduced Upstream LON

LON Upstream	Maximum Dynamic Deflection	Occupant Risk				Vehicle Stability	
		OIV	ORA	Exit Box	OCI	Max Roll Angle	Max Pitch Angle
279 ft [85 m] Baseline Test	41.4 in [1.05m]	[5.7 m/s]	11.1 g	Pass	Pass	10.9 deg	3.6 deg
Baseline FEA	40.4 in [1.03m]	[5.4 m/s]	10.6 g	Pass	Pass	21.9 deg	6.7 deg
190 ft [58 m]	43.4 in [1.10m]	18.0 ft/s [5.5 m/s]	9.3 g	Pass	Pass	23 deg	7.6 deg
125 ft [38 m]	55.8 in [1.42m]	22.6 ft/s [6.9 m/s]	13.9 g	Pass	Pass	28.7 deg	6.7 deg
92 ft [28 m]	64.8 in [1.65m]	18.4 ft/s [5.6 m/s]	9.9 g	Pass	Pass	30.5 deg	12.3 deg
59 ft [18 m]	85.8 in [2.18m]	16.4 ft/s [5.0 m/s]	15.8 g	Marginal	Pass	45.3 deg	11.8 deg
* analysis terminated prematurely							

Case 2 - w/ VLB's: Reduced Downstream LON

LON Downstream	Maximum Dynamic Deflection	Occupant Risk				Vehicle Stability	
		OIV	ORA	Exit Box	OCI	Max Roll Angle	Max Pitch Angle
190 ft [58 m]	42.9 in [1.09m]	17.7 ft/s [5.4 m/s]	12.4 g	Pass	Pass	22.7 deg	7.1 deg
125 ft [38 m]	51.2 in [1.30m]	17.7 ft/s [5.4 m/s]	13.9 g	Pass	Pass	28.8 deg	6.8 deg
92 ft [28 m]	62.3 in [1.58m]	23.9 ft/s [7.3 m/s]	14.0 g	Marginal	Pass	31.3 deg	12.7 deg
59 ft [18 m]	87.2 in [2.21m]	19.4 ft/s [5.9 m/s]	13.8 g	Marginal	Pass	58.6 deg	14.7 deg

In addition to impact performance, the maximum lateral deflection of the barrier was also of interest since it is used for determining *working width* of the barrier, which is used by roadside safety engineers to determine applicability and placement of a product for given site conditions. Figure 72 shows a summary of the maximum lateral deflection of the barrier versus impact point relative to the leading and trailing ends of the barrier for both Case 1 and Case 2 barrier systems.

When the barrier is of critical length and is struck at 85 or more barrier segments from either end (i.e., ≥ 278.9 ft from either end), the maximum lateral deflection is approximately 36 inches for Case 1 and Case 2 (showing FEA results only). For impact cases occurring within 85 barriers from either end (< 278.9 ft from either end), the maximum lateral deflection increases rapidly as the impact point gets closer and closer to the ends. For impacts on the leading end of the systems, Case 2 resulted in 12.6 percent higher maximum deflections (on average) than Case 1; and for impacts on the trailing end of the systems, Case 2 resulted in 11.1 percent higher deflections (on average) than Case 1.

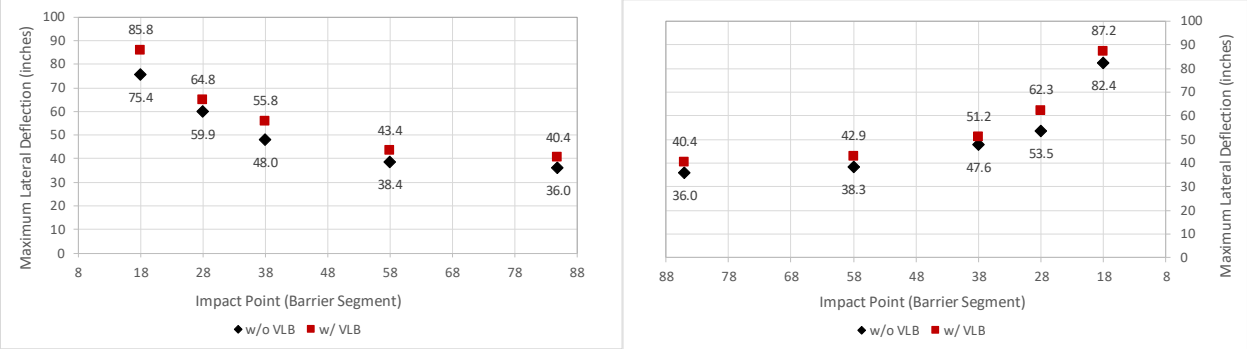

Figure 72. Comparison of maximum lateral displacement versus impact point for Case 1 (CRTS only) and Case 2 (VLBs in impact region).

REFERENCES

AASHTO09 Technical Committee for Roadside Safety, "Manual for Assessing Safety Hardware," American Association of State Highway and Transportation Officials, Washington, D.C. (2009).

Alberson16 Alberson, D.C., W.L. Menges, and D.L. Huhn, "MASH TL-2 Evaluation of the LTS Road Zipper Moveable Barrier," Test Report No. 690900-LTS1&2, Texas Transportation Institute, College Station, TX (August 2016).

FHWA00 Federal-Aid Reimbursement Eligibility Letter HSA-B69 for the CRTS and SRTS barrier system (2000). See website: http://safety.fhwa.dot.gov/roadway_dept/policy_guide/road_hardware/barriers/pdf/b-69.pdf (last accessed 11/21/2016)

LSDYNA15 "LSDYNA User's Manual" Volumes I & II, Livermore Software Technology Corporation (LSTC), Livermore, CA (2015).

Ray08 Ray, M.H., Anghileri, M., Mongiardini, M., "Comparison of Validation Metrics Using Full-Scale Automobile Crash Tests," 8th World Congress on Computational Mechanics, Venice, Italy, (June 30 – July 5, 2008).

Ray10 Ray, M.H., C.A. Plaxico and M. Anghileri, "Procedures for Verification and Validation of Computer Simulations Used for Roadside Safety Applications," NCHRP Web-Only Document 179, National Academy of Sciences, Washington, D.C. (2010).

Ray16 Ray, M.H., C. Carrigan, and C.A. Plaxico, "Guidelines for Shielding Bridge Piers," NCHRP Project 12-90, in progress (2016).

ROBUST02 Road Barrier Upgrade of Standards (ROBUST), "Deliverable 4.1.1 – Full scale test results – An analysis," ROBUST PROJECT, GRD-2002-70021 (2002).

Ross93 Ross, H.E., D.L. Sicking, and H.S. Perrara, "Recommended Procedures for the Safety Performance Evaluation of Highway Appurtenances," National Cooperative Highway Research Program Report No. 350, National Academy of Sciences, Washington, D.C (1993).

TTI98 TTI, "Test Risk Assessment Program (TRAP) Version 1.01: User's Manual," Texas Transportation Institute, College Station, TX (1998).

Wright97 Wright, A. and M.H. Ray, "Characterizing Roadside Hardware Materials for LSDYNA3D Simulations," *Report No. FHWA-RD-96-108*, Federal Highway Administration (Feb 1997).